GAS METAL ARC WELDING OF TITANIUM

by

Daniel Edward Ries

B. S., Met. Eng., Ohio State University, (1975)
M. S., Solid Mech., George Washington University, (1981)

SUBMITTED TO THE DEPARTMENT OF OCEAN ENGINEERING
IN PARTIAL FULFILLMENT OF THE REQUIREMENTS
FOR THE DEGREE OF

OCEAN ENGINEER

and

MASTER OF SCIENCE IN NAVAL ARCHITECTURE AND MARINE ENGINEERING

at the

MASSACHUSETTS INSTITUTE OF TECHNOLOGY

MAY 1983

Signature of Author: _____
Department of Ocean Engineering
May 6, 1983

Certified by: _____
Thomas W. Eagar
Thesis Supervisor

Certified by: _____
Kiochi Masubuchi, Department Reader
Department of Ocean Engineering

Accepted by: _____
A. Douglas Carmichael
Department of Ocean Engineering

TABLE OF CONTENTS

TABLE OF CONTENTS (continued)

Gas Metal Arc Welding of Titanium

by

Daniel E. Ries

Submitted to the Department of Ocean Engineering
on May 6, 1983 in partial fulfillment of the
requirements for the degrees of

Ocean Engineer

and

Master of Science in Naval Architecture and Marine Engineering

ABSTRACT

Gas Metal Arc (GMA) Welding of titanium was investigated using an analog current regulator. The current regulator has the capability of producing pulsed current wave forms up to 25 kHz of practically any shape available from a signal generator. The objective of this work was to achieve control of metal transfer so that the molten filler metal is incorporated into the weld pool in a controlled, calm, orderly fashion. Normally, with DC current conventional GMA processes, uncontrolled and unbalanced arc

forces tend to hamper controlled metal transfer when welding titanium. These unbalanced forces result in weld pool turbulance, uncontrolled droplet transfer and ultimately nonuniform weld bead formation and spatter. The use of rectangular pulsed current wave forms was investigated with respect to metal transfer control and ultimate weld bead shape uniformity.

An experimental space consisting of three independent variables including base current (I_b), peak current (I_p) and frequency (f), keeping the average current constant was investigated. Average current (I_{av}) was chosen based on the minimum DC level which produced a desired weld bead size. By changing the energy input at constant I_{av} using rectangular pulsed wave forms, changes in metal droplet transfer and resulting weld bead shape and uniformity were recorded. The experimental technique used for recording metal droplet transfer consisted of high speed photography (6,000 frames per second) using a balance of laser back lighting and arc illumination to record the size and frequency of formation of individual droplets. The current signal (high or low) was recorded on the film next to each high speed picture to allow real time analysis of droplet transfer as a function of pulsed current input. Data was taken using a multi-frequency level Box-Behnken design space grid allowing for statistical analysis of dependent

variables including weld bead width, wire feed rate, droplet transfer size, percent of droplet transfer rejected from weld pool as spatter, and droplet transfer frequency.

Thesis Supervisor: Thomas W. Eagar

Title: Associate Professor of Materials Engineering

LIST OF SYMBOLS

GTA = gas tungsten arc, tungsten electrode, filler metal added externally

GMA = gas metal arc, consumable electrode

I_b = base current

I_p = peak current

I_{av} = average current

f = pulsing frequency

SEN = Straight Polarity Electrode Positive

REP = Reverse Polarity Electrode Negative

DC = Direct Current

A = Amps

V = Volts

v = wire feed rate

ipm = Inches per minute

cfm = Cubic feet per minute

LIST OF FIGURES AND TABLES

ACKNOWLEDGEMENTS

The work presented in this thesis represents the effort of many people. Professor Thomas W. Eagar provided continued guidance and ideas. The Office of Naval Research provided funding. The MIT Welding Laboratory provided technical support. And most importantly, my wife, Nancy, and my family provided moral support. I thank them all. Finally, I thank the Lord for allowing me to see and understand.

1.0 INTRODUCTION

Titanium alloys offer a unique strength to weight combination which makes them a very attractive alternative as a pressure hull material for deep diving submersibles. As described in a paper by K. Masubuchi [1], the operating depth potential of a submersible can be increased from 2,000 to 6,000 feet with high strength steels (HY-80 to 130) to 12,000 to 15,000 feet with titanium alloys. This increase in depth potential increases the ocean floor availability of the submersible from 10% to 30%. This greater potential for resource development of the ocean floor as well as a significant strategic advantage for U.S. Navy submarines can be realized by using titanium alloys as a pressure hull material.

The deep submersible research vessel ALVIN was returned to service in 1973 with a new titanium alloy pressure hull giving it a new depth capability of 12,000 feet as opposed to its previous depth capability of 6,000 feet with an aluminum alloy hull [2]. The pressure hull consisted of two hemispherical shells welded together with the gas tungsten arc process. The SEACLIFF, a sister ship to ALVIN is currently under construction at the Mare Island Naval Shipyard, Mare Island, California, which will have a similar titanium pressure hull plus a titanium lattice for exterior

structural support. The gas tungsten arc process has proved to be reliable but slow, making only small construction jobs such as these practical with this process. Based on this experience, in order for titanium alloys to be used in a production shipyard environment for either deep ocean mining equipment or U.S. Navy submarines, a faster controllable, all position welding process that can be used in both automatic and manual modes needs to be developed for titanium.

This thesis will review the principles and past experience with the pulsed gas metal arc (GMA) welding process and discuss its applicability for use with titanium. A major problem associated with GMA welding of titanium is lack of control of weld metal transfer and spatter formation. Spatter consists of small droplets of molten weld metal which are ejected from the arc sometime between droplet formation, droplet transfer, and droplet incorporation into the weld pool. A high speed photographic technique will be described that was developed to observe the process of weld metal transfer in order to understand the origin of forces that result in spatter and nonuniform bead formation. Titanium bead-on-plate welding experiments were performed and analyzed using this technique. Changes in weld metal transfer control were recorded as a function of pulsed current parameters including base current (I_b),

peak current (I_p) and pulsing frequency (f) at constant average current (I_{av}). Results indicate that one drop per pulse weld metal transfer is possible under certain welding conditions. Thus, the achievement of controllable weld metal transfer using pulsed current GMA welding with titanium appears to be feasible and should result in a reasonable large scale production welding technique for joining large titanium structures.

2.0 ARC PHYSICS

In order to understand what conditions produce a good or bad weld with any material it is necessary to understand the physical phenomena controlling the process. In particular, in order to understand the GMA process and factors which can improve control of the process, it is necessary to understand the arc forces and metal transfer dynamics. The following section of this thesis will review work in this area.

2.1 Definition of the Arc

To understand the welding process one must understand the physics of the arc which is the media by which the energy required for fusion is transferred from the power source to the work piece, and in the case of GMA welding, transfer of weld filler metal to the weld pool. C. E. Jackson proposed the following definition of the arc [3]: "A welding arc consists of a sustained electrical discharge through a high temperature conducting plasma, producing sufficient thermal energy so as to be useful for the joining of metals by fusion." Figure 1a and 1b [3] are schematic diagrams of straight polarity electrode negative (SEN) and reverse polarity electrode positive (REP) arcs with typical voltage drops.

V_a = anode potential

V_p = plasma potential

V_c = cathode potential

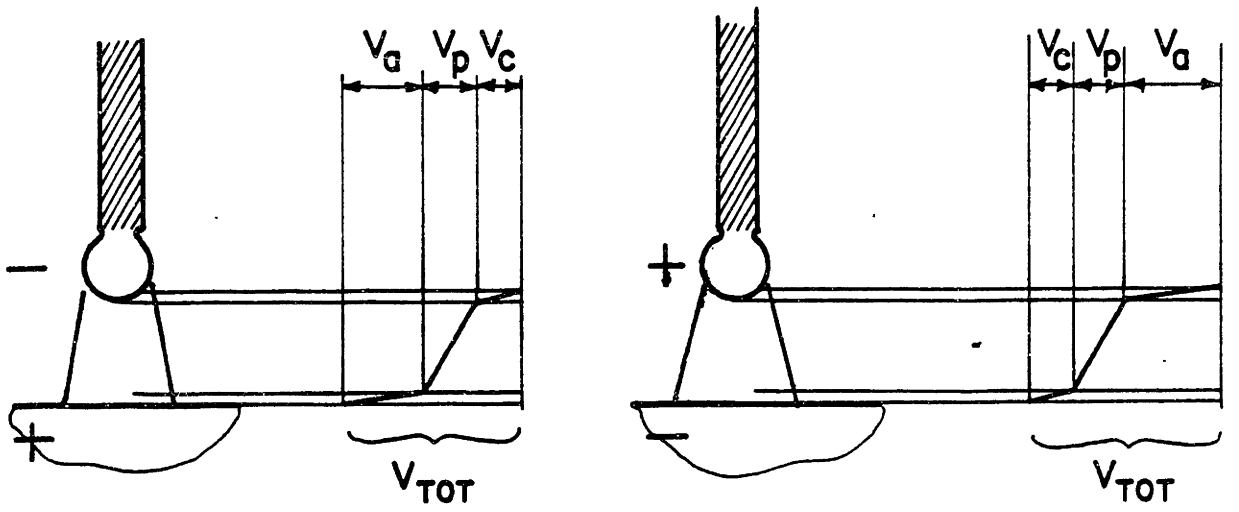

a. STRAIGHT POLARITY (SEN) b. REVERSE POLARITY (REP)

Figure 1: Straight Polarity (a), and Reverse Polarity (b) arcs with Voltage Drops [3].

P. T. Houldcroft describes three regions of an arc as follows [4]:

1. Two regions next to the electrode surfaces (anode and cathode) with a rapid drop in potential caused by electrode cooling effects.

2. A central region with a uniform potential.

These regions can be seen in Figure 1 [3]. The plasma referred to in the above definition is a column of ionized gas, electrons and highly excited electrically neutral atoms through which electrical conduction takes place [3]. In the case of GMA welding of reactive metals such as aluminum or titanium, the arc is shielded with inert gas (Ar, He or a mixture of the two) such that the Ar in the plasma displaces air thereby preventing gas-metal reactions.

As the arc is established, electrons stream from the cathode (-) and are accelerated towards the anode (+). These electrons collide with a portion of the shielding gas column resulting in excitation and ionization of the Ar gas atoms creating a mixture of neutral, excited and ionized Ar gas atoms. In addition, metal vapor can be boiled from the "spots" of highest current density on both the anode and the cathode adding neutral metal vapor to the arc plasma. These

components of the arc plasma interact with the electric and magnetic field created by the flux of current in the arc giving rise to forces that determine metal transfer characteristics [3,4]. These arc forces will be discussed in the next section.

2.2 Arc Forces

The stability of a welding arc depends on the forces present on the arc column. P. T. Houldcroft notes that the flow of current through the plasma in the arc column results in a radial temperature gradiant and magnetic field around the arc column resulting in a constricting or pinching force (Lorentz force α to I^2) on the plasma [4]. This force is a result of the cross product of the current density (J) and the magnetic flux density (B):

$$F_L = J \times B$$

When resolved in cylindrical coordinates the radial and axial directions of the consumable electrode in GMA welding, it is seen that two components of force are produced [5]. One component is radial as shown in Figure 2a and 2b as described by:

$$(F_L)r = -jz\ B$$

The other component can be either zero with no divergence in J or axially up or down when divergence in J exists as shown in Figures 2a (upward force) and 2b (downward force) as

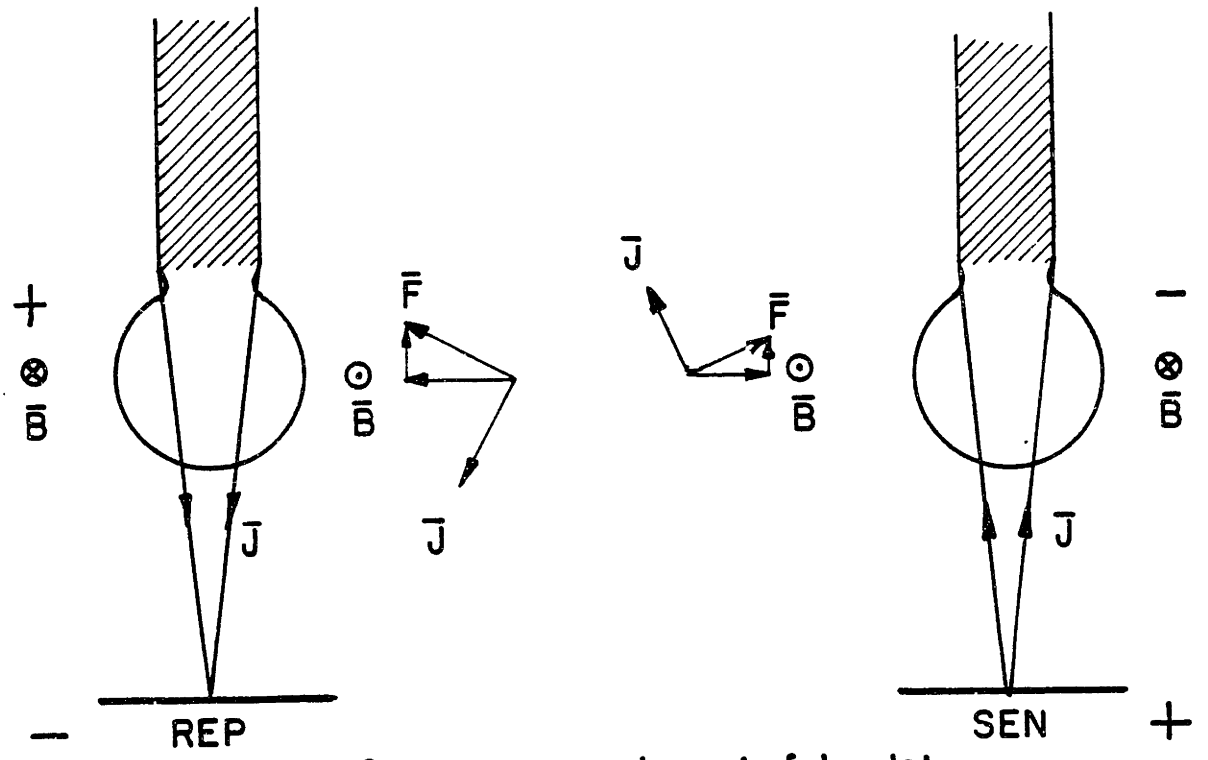

a. Current converging out of droplet.

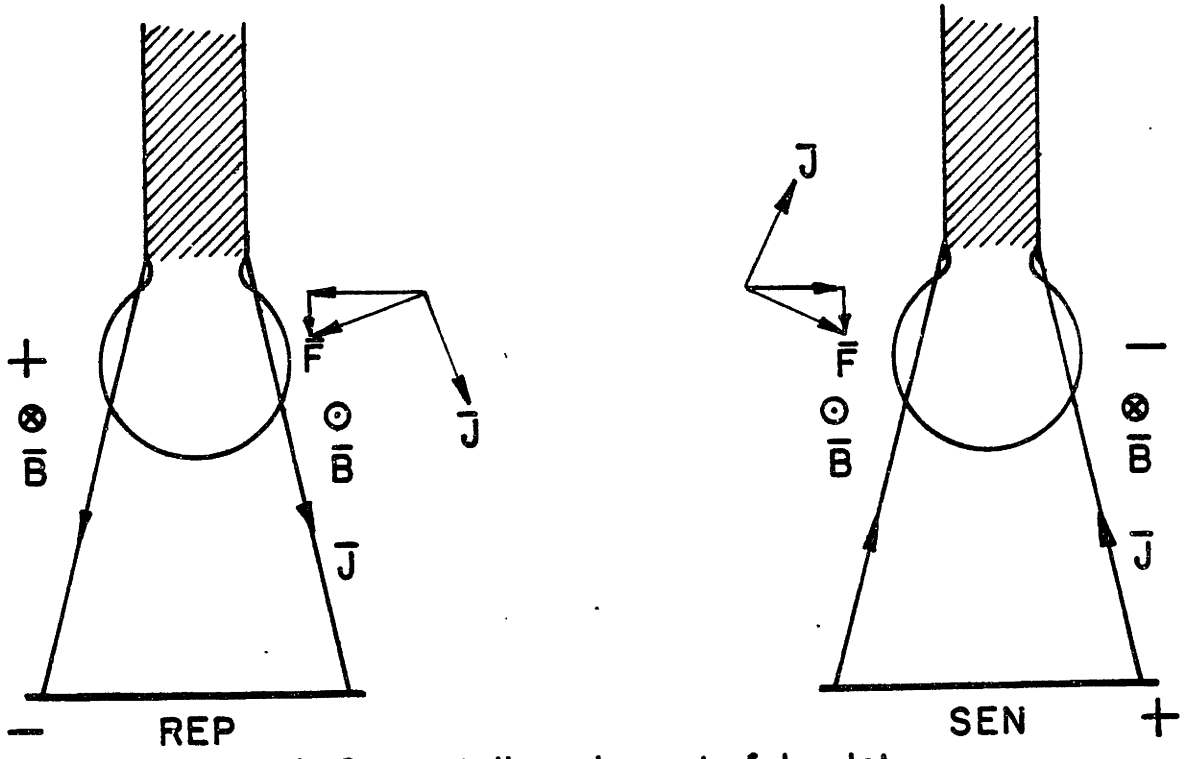

b. Current diverging out of droplet.

Figure 2: Lorentz Forces on metal droplets in Reverse Polarity (REP) and Straight Polarity (SEN) GMA welding with converging (a) and diverging (b) current density out of the droplet.

described by:

$$(F_L)z = \pm jr\ B$$

The Lorentz force gives rise to two important phenomena affecting metal transfer in GMA welding:

1. Radial and axial forces on the molten metal drop which tend to either hold the drop on the wire electrode (current converging from drop) or pinch the drop from the wire electrode (current diverging from drop).

2. The formation of high current density anode and cathode spots representing local areas of super heating of the molten metal either on the weld pool (current converging from drop) or on the droplet (current diverging from drop).

The pinching phenomena described in (1) above helps determine the nature of droplet formation and detachment. The formation of anode and cathode spots at high current density areas described in (2) above gives rise to pressure forces in an axial direction away from the high current density point setting the gases in the plasma in motion along the axis of the arc [4,6]. These flowing gases form a

plasma jet which due to its high velocity can affect arc stability and metal transfer. The velocities of plasma jets have been estimated at 10^4 to 10^5 cm/sec [4].

In straight polarity (SEN), when the arc root (area of current spread) is well defined and larger in the plate than the electrode, a bell shaped arc results as shown in Figure 3a [3] called the cathode spot mode and results in plasma jet emission due to the pressure forces on the plasma described above [4]. A second type of bell shaped arc involves a larger cathode area made up of many small cathode spots as seen in Figure 3b [3], called normal mode [4]. The normal mode arc is more stable and easier to control while the cathode spot mode results in forces on the arc away from the spot due to the plasma jet. If any asymmetries exist, the arc and metal droplets will be deflected sideways [4]. A third type of arc occurs in refractory electrodes (e.g. carbon and tungsten) where current densities over electron emitting areas are low and no spots form [4]. This type of arc is not relevant to GMA welding.

In reverse polarity (REP), both cathode and anode spots can form. Plasma jets emanating from these spots will interact. If the momentum force associated with one of these jets is small, the other will dominate and a stable jet will form. If, however, the forces from these jets are of the same order of magnitude, the interaction of these

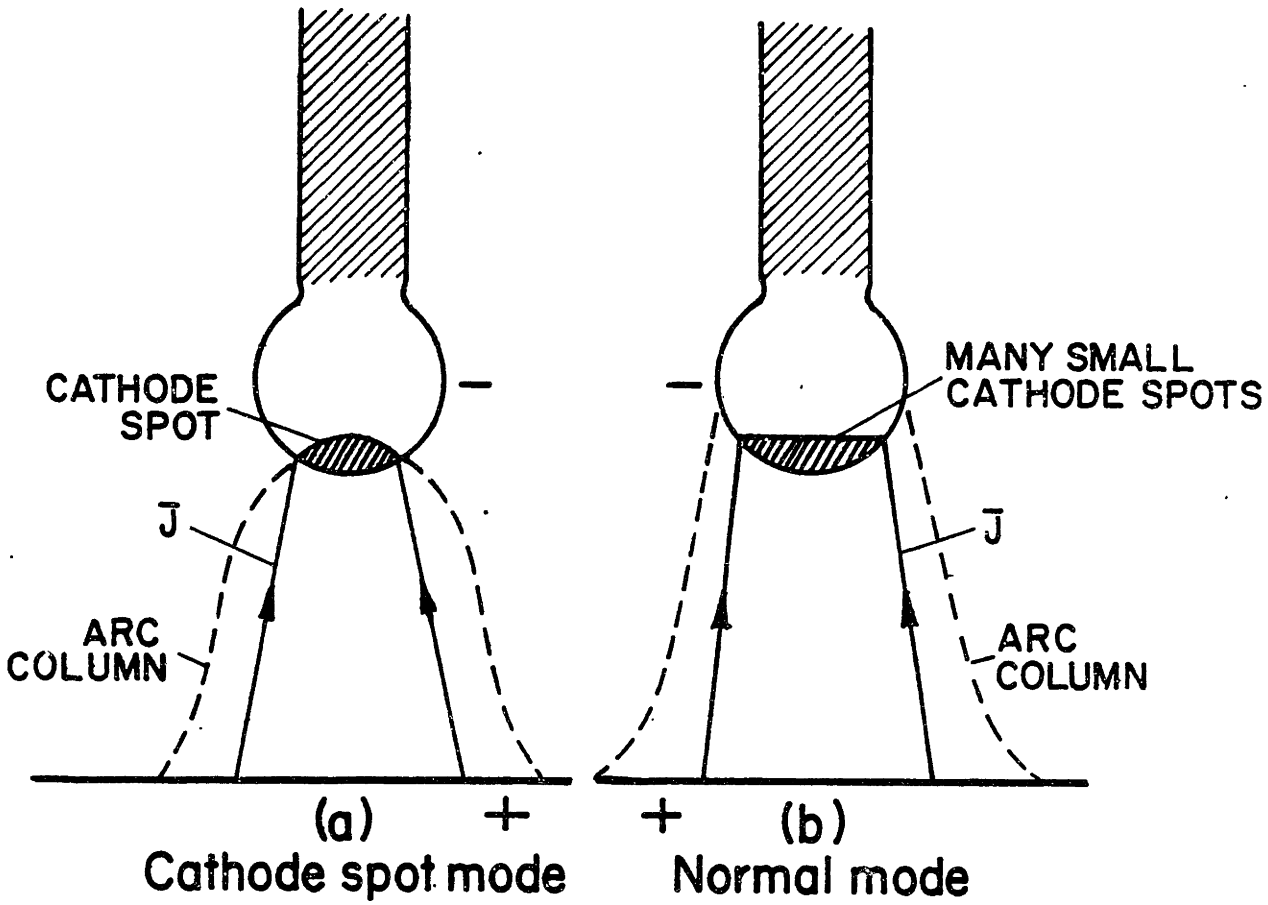

Figure 3: Straight Polarity (SEN) plasma jets forming at high current density spots on electrode in cathode (a) and normal (b) modes [3].

jets will result in plasma jet deflections which can be unstable resulting in erratic plasma jet rotations. These rotations can be obsered during welding of certain reactive metals. Figure 4 shows this interaction and resulting deflected plasma jet.

As noted by N. N. Rykalin, et al., metal vapor from molten metal on the electrode or in the weld pool can be set in motion at anode or cathode spots by the same forces creating plasma jets [7]. These metal vapor streams become a part of the plasma jet resulting in stronger plasma jet forces with magnified effects on metal transfer through stronger plasma jet reaction and hydrodynamic drag forces on droplets during transfer.

2.3 Effect of Arc Forces on Metal Transfer

One of the major obstacles in making a good GMA weld is controlling the metal transfer so that the molten filler metal is incorporated in the weld pool in a controlled, calm and orderly fashion. In order to understand how controlled metal transfer can be achieved, the effect of arc forces on metal transfer must be understood.

C. E. Jackson has described the transfer of metal in GMA welding as resulting from a net force which either [3]:

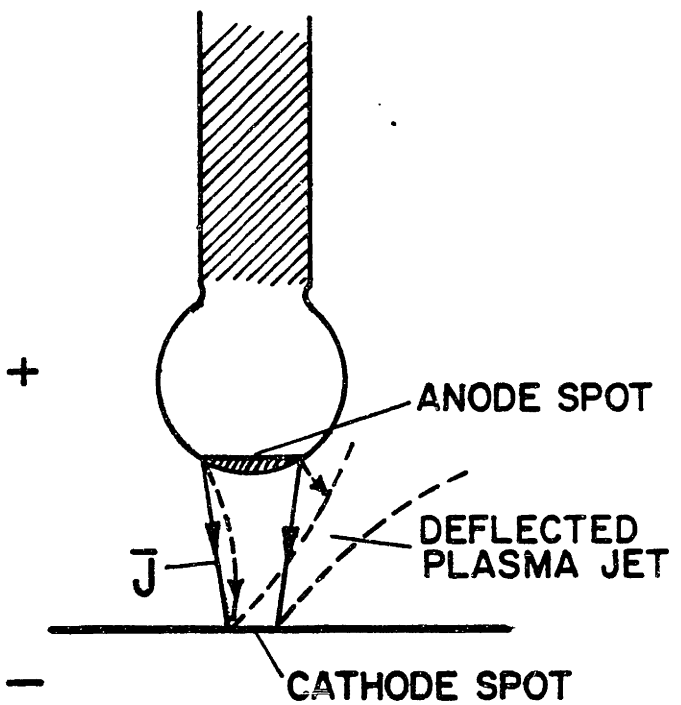

Figure 4: Reverse Polarity (REP) plasma jets forming at high current density spots on anode and cathode resulting in deflected plasma jet.

1. ejects molten filler metal drops from the electrode to the weld pool, or

2. repels the drop away from the weld pool.

C. D. Cooksey described in more detail six modes of either ejected or repelled metal transfer as follows [8]:

1. Large drops detach with little influence of arc forces. The controlling forces are gravity and droplet surface tension.

2. The drop remains spherical under surface tension forces but is detached from the electrode before gravity transfer occurs by additional force provided by the electrode plasma and Lorentz pinching forces.

3. The drop is distorted, lifted and repelled from the plate as a result of arc forces. The net repelling force comes from either Lorentz forces in the drop in an off axial direction due to anode or cathode spot instability or plasma jets from the weld pool where high current densities are concentrated at anode or cathode spots.

4. The end of the electrode is tapered and a fine spray of drops stream off due to well developed plasma jets and Lorentz pinching forces.

5. Molten metal from the electrode tip streams off in an upward direction as a result of reaction forces from metal vapor streams in plasma jets from the droplet to the weld pool or vice versa.

6. The molten metal drop and arc move sideways while the neck attaching the drop to the electrode is thrust in the opposite direction. The curvature of the current path caused by drop and arc movement gives a sideways Lorentz force and as the neck moves, the curvature, and hence the magnitude of the force, increases until separation occurs.

Cooksey indictes that the actual metal transfer for a given material can be a combination of any of the above modes depending upon the magnitude of the forces effecting metal transfer.

Figure 5 shows profiles of droplet transfer in two categories that are considered by the author of this thesis to cover the modes of transfer reported in the literature as

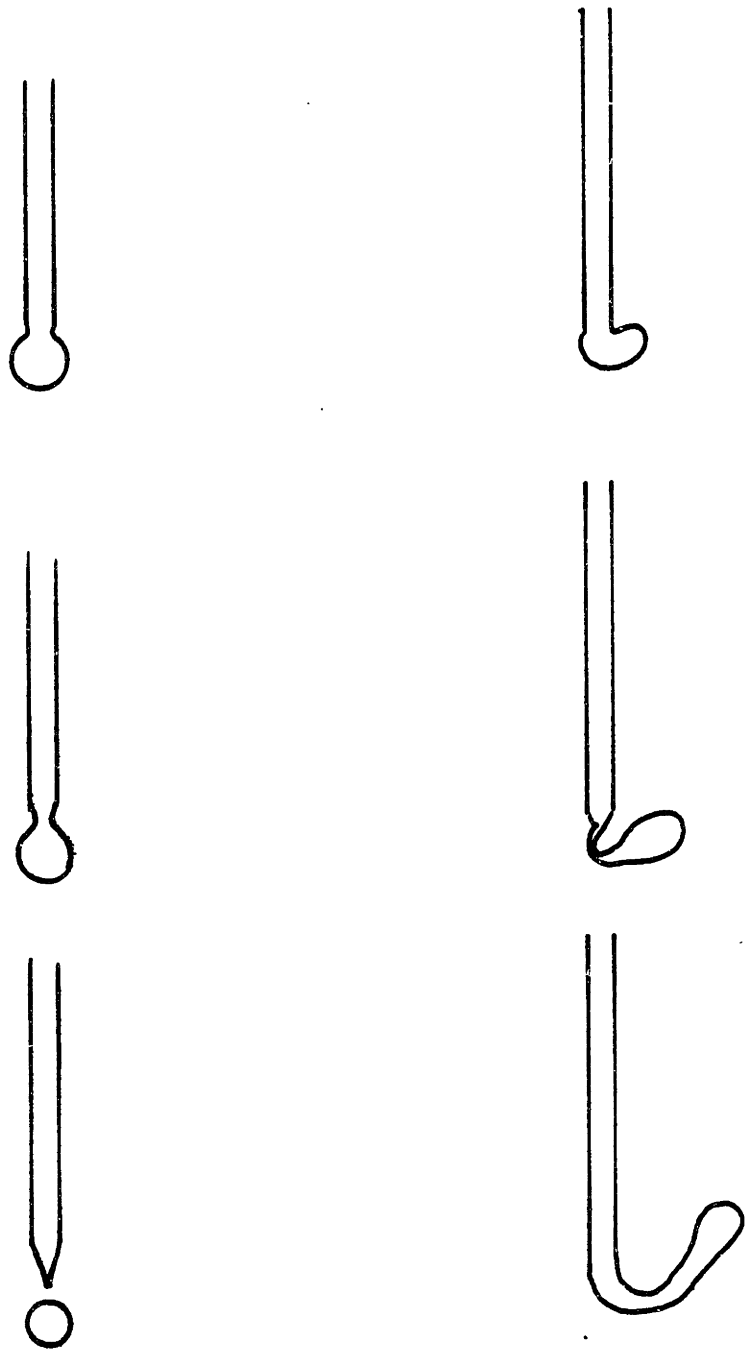

Figure 5: Varying degrees of two modes of weld metal droplet transfer, ejected (a) and repelled (b).

well as the modes of transfer observed during experimental work. The ideal type of transfer incorporates a balance of droplet ejecting and repelling forces such that droplet sizes on the order of the diameter of the electrode are formed and transferred with minimal acceleration to minimize weld pool turbulence.

Based on the above observations the forces in the arc affecting metal transfer can be classified as follows:

1. Gravity - The weight of the drop will result in a force in the direction of gravity. The direction of this force on the drop relative to the weld pool depends on the position of the electrode and work piece and its magnitude may or may not play an important role in metal transfer [5,8,9,10]. This force equals:

   Force of Gravity = $Fg = 4/3\pi r^3 \rho g$

   where

   $4/3\pi r^3$ = volume of drop

   ρ = density of molten metal

   g = acceleration of gravity

2. Electromagnetic force (Lorentz forces) - The Lorentz forces can be resolved into radial and

axial forces as shown in Figures 2a and 2b. Both the axial and radial forces affect metal transfer as follows:

a. The axial force is resolved in the direction of either retaining or ejecting the droplet forming on the end of the electrode (Figure 6) [5,8,9,10,11,12]. Assuming a conical conducting column in the drop, this force is equal to [5,10,12]:

Force due to Axial component of Lorentz Force

$$= (FL)_z = (MI^2/4\pi)(X[\alpha,\beta])$$

where:

M = magnetic permeability of arc column

I = current

$x(\alpha,\beta)$ = geometric shape factor where α and β are angles defined in Figure 8.

$$= \ln\left[\frac{\sin\alpha}{\sin\beta}\right] - \frac{1}{4} + \frac{1}{1-\cos\alpha}$$

$$+ \frac{2}{(1-\cos\alpha)^2} \ln\left[\frac{1}{1+\cos\alpha}\right]$$

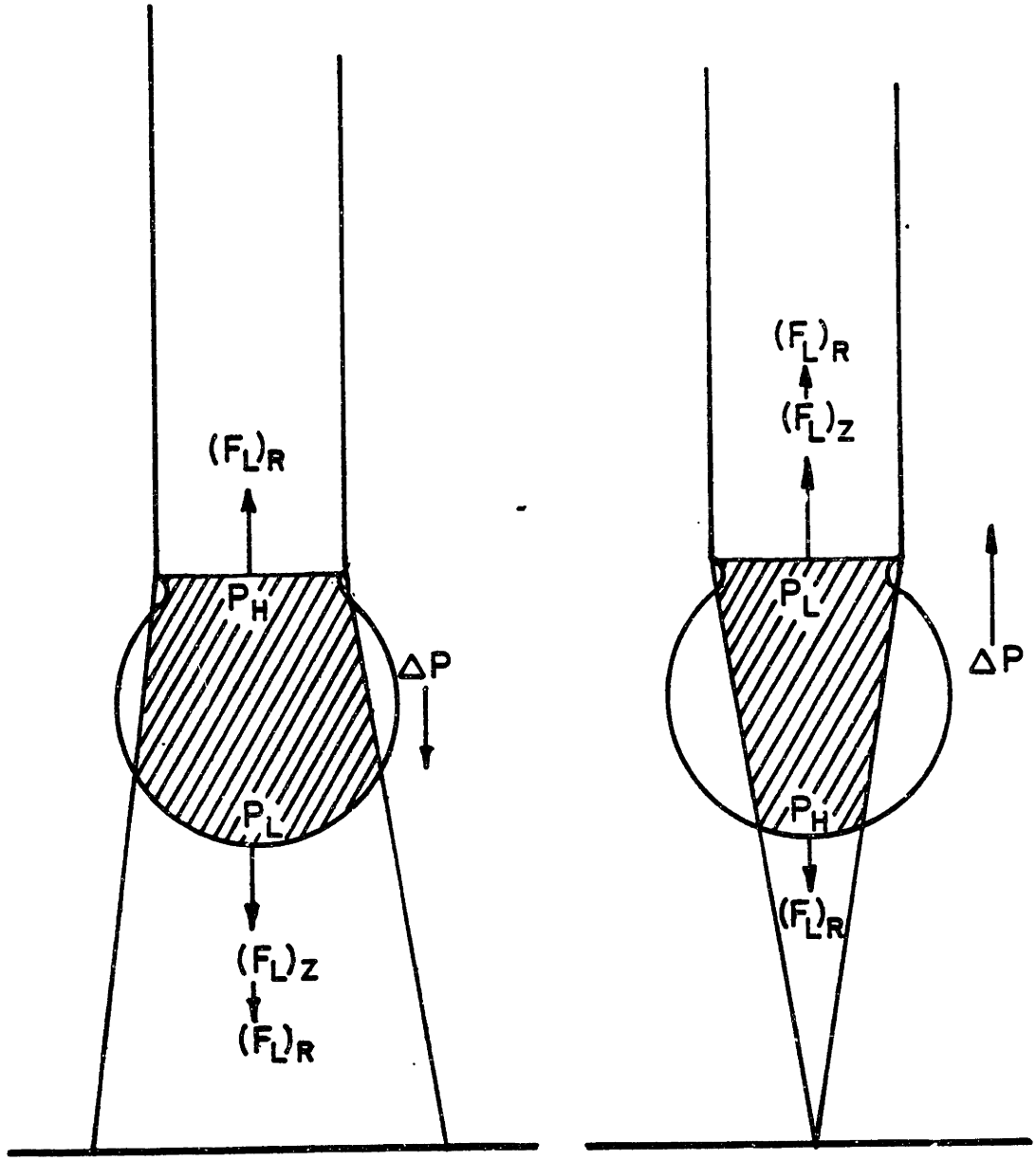

Figure 6: The effect of axial $(F_L)z$ and radial $(F_L)R$ Lorentz Forces on droplet transfer.

b. The radial force induces a constricting fluid pressure on the droplet which is resolved as a force acting along the axis of the droplet, out of both ends of the droplet [5,8,9,10,11,12]. The hydrostatic pressure created by this constricting force in the drop is [10,11,12]:

Pressure due to Radial Lorentz Force

$$= (PL)_R = (MI^2/8\pi)(1/\pi r[z]^2)$$

where:

M = magnetic permeability of arc column

I = current

r(z) = radius of the conducting column

Again, by assuming a conical conducting column in the drop, and integrating this pressure along the axis of the drop, the following equation for the force applied to the neck of the drop is:

Force due to Radial component of Lorentz Force

$$(FL)_R = (MI^2/8\pi)(r_2-r_1/r_2)$$

where:

M = magnetic permeability of arc column

I = current

r_1 = minor end radius of conical conducting column

r_2 = major end radius of conical conducting column

Both of these forces act on each cross section of the droplet, creating an internal pressure which is greatest at the smallest cross section of the conducting column in the droplet or the area of greatest current density. Thus, the change in fluid pressure caused by converging or diverging current in the droplet establishes a pressure drop, which will either tend to retain or eject the drop from the electrode as shown in Figure 6.

The ejecting pressure drop aids the constriction process which ultimately results in individual droplet formation and detachment. The retaining presure drop tends to hold the droplet to the electrode retarding droplet detachment. It should be noted that these same pressure drops are present in the droplet not only during droplet formation but also after the droplet lights on and attaches to the surface of the weld pool as shown in Figure 7. The retaining pressure drop aids in droplet incorporation into the weld pool while the ejecting presure drop retards droplet incorporation and may lead to spatter if these forces overcome gravity and surface tension forces [13].

3. Surface Tension - The surface tension driven forces consist of an internal pressure tending to eject the drop and retention force at the drop neck. The internal pressure force results from the pressure difference across the surface caused by the droplet surface tension. This pressure acts over the

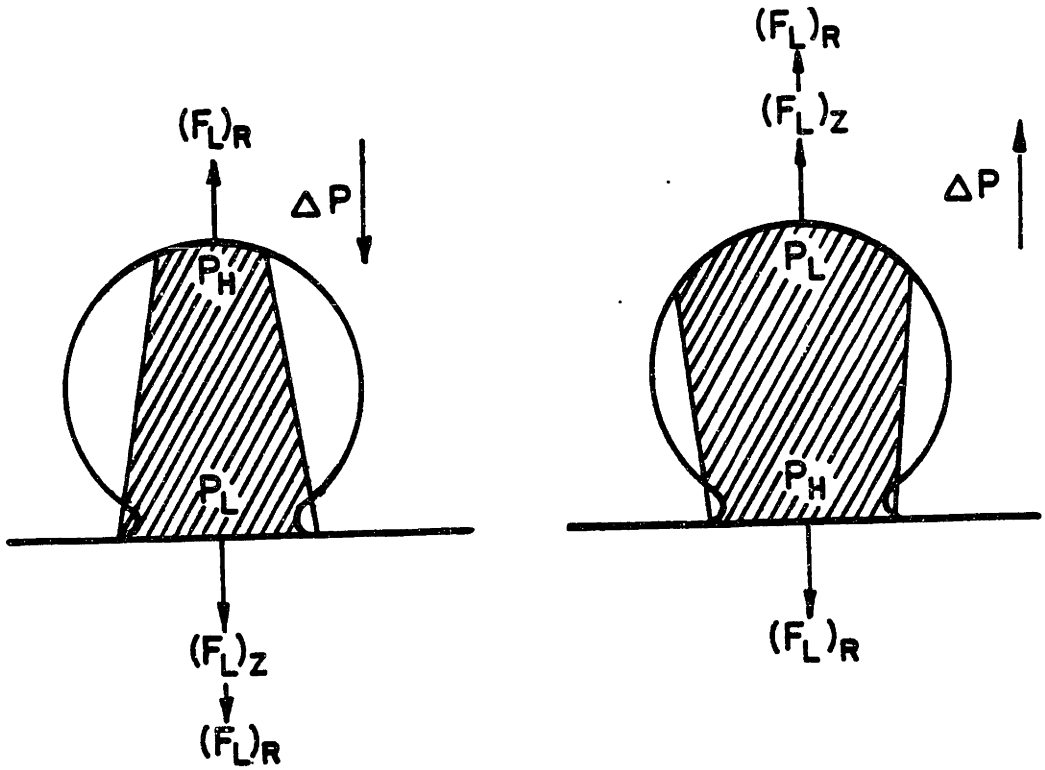

Figure 7: The effect of axial $(F_L)z$ and radial $(F_L)R$ Lorentz Forces on droplet incorporation into the weld pool.

base of the droplet as a detaching force. The retention force is the result of surface tension forces acting along the perimeter of the droplet base as a force per unit length which tends to retain the droplet until surface tension is overcome and droplet detachment occurs. The forces are shown in Figure 8. The internal pressure force is equal to [10]:

Internal Pressure Force from drop Surface Tension

$$= F_{s_1} = \gamma [1/r_1 + 1/r_3] \pi r_1^2$$

where:

γ = surface tension

r_1 = inside drop neck radius of curvature shown in Figure 8.

r_3 = outside drop neck radius of curvature shown in Figure 8.

The droplet neck retension force is equal to [10]:

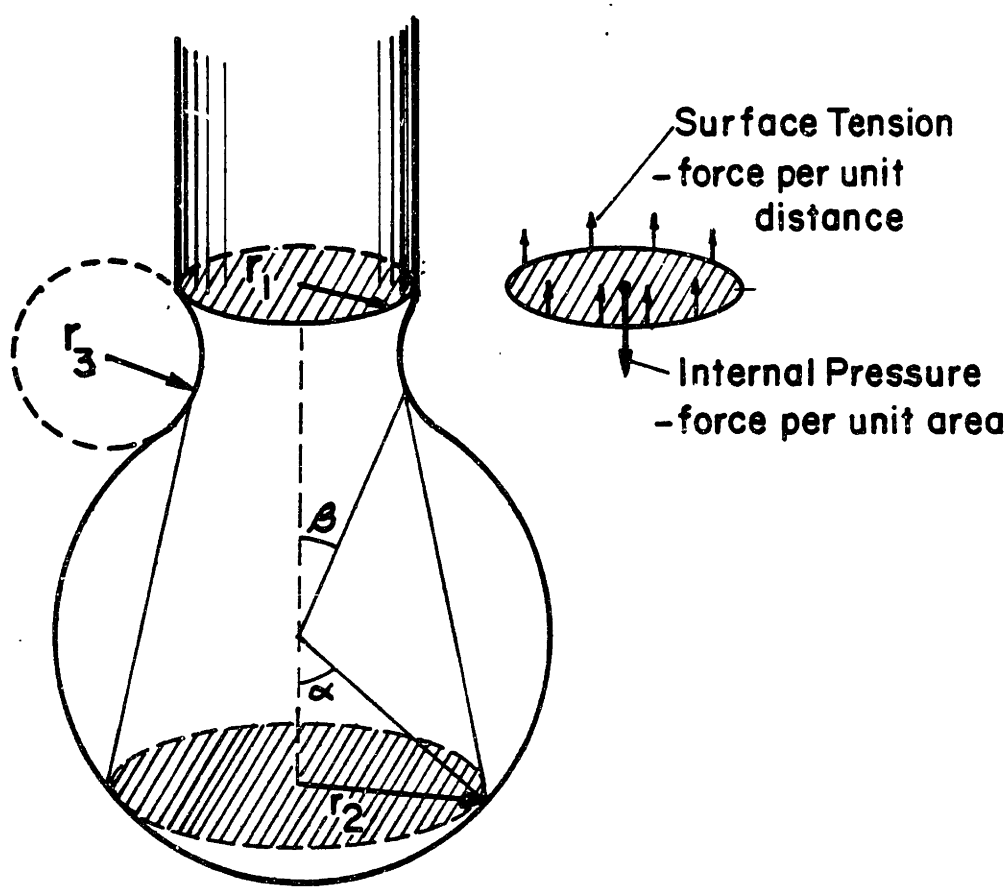

Figure 8: Surface Tension driven forces in a droplet.

Droplet Neck Retension Force from Surface Tension

$= F_{s_2} = 2\pi r_1 \gamma$

where:

γ = surface tension

r_1 = inside drop neck radius of curvature shown in Figure 8.

4. Hydrodynamic Drag Force - The hydrodynamic drag force is a result of plasma and metal vapor flow around the drop creating a force which tends to drag the drop along with the gas flow. This force is shown in Figure 9. The force is equal to [5,10]:

Hydrodynamic Drag Force

$= Fh = 1/2\ \rho\ v^2\ A\ Cd$

where:

ρ = density of plasma

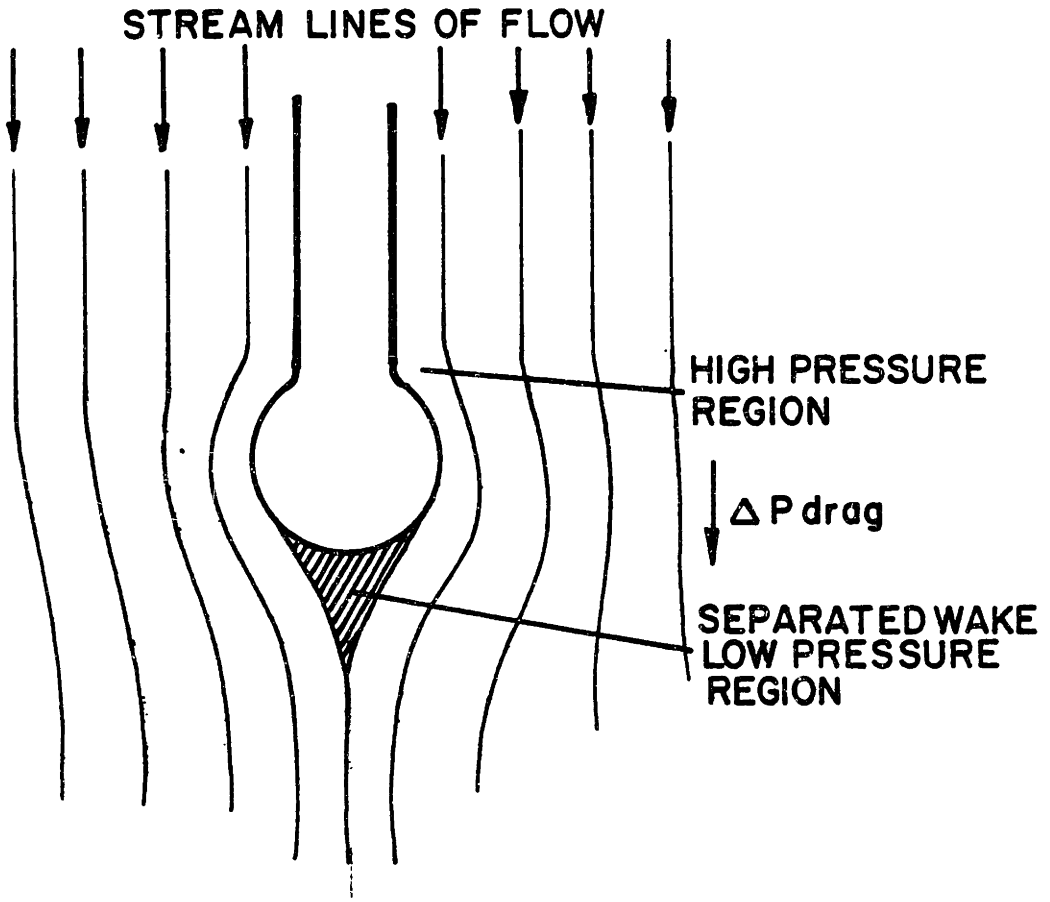

Figure 9: Hydrodynamic Drag force on droplet resulting in ΔP in direction of flow velocity.

V = velocity of plasma

A = frontal area of drop exposed to plasma flow

Cd = drag coefficient which is a function of the Reynolds Number of the plasma

5. Reaction and Momentum Transfer Forces - The transferring metal droplets experience reaction and impingement forces resulting from high velocity plasma jets forming at anode and cathode spots which transfer momentum to the droplet. The reaction force acts opposite in direction to the flow of plasma when plasma jets form on the droplet surface. The impingement force acts in the same direction as the flow of plasma when plasma jets emanate from the weld pool surface or from the electrode surface immediately after droplet detachment. These forces are equal to [11]:

Plasma Jet Momentum Transfer Force

$$= Fm = f(d/dt)(m_p V_p)$$

where:

$d/dt\ m_p$ = mass flow rate of plasma

V_p = velocity of plasma jet

f = fraction of momentum transferred which is a function of the geometry of the momentum exchange

The summation of the above forces gives the net force on the droplet during droplet formation and incorporation into the weld pool. During actual droplet transfer or flight in the arc, only the forces not depending on the droplet/electrode or weld pool interface are active, e.g. gravity, hydrodynamic drag and momentum transfer from plasma jets. This force summation is given mathematically for the cases of droplet detachment and incorporation, as follows:

Force Balance During Droplet Detachment and Incorporation

$$F_{net} = Fg + F_{s_1} + F_{s_2} + (FL)_z + (FL)_R + Fh + Fm$$

For droplet transfer or flight in the arc, the force summation becomes:

Force Balance During Droplet Transfer or Flight

$F_{net} = Fg + Fh + Fm$

It should be noted that the magnitude and sometimes even the direction of these forces can change during the life of the droplet, making the dynamic modeling of droplet transfer a formidable task and one which greatly depends on the properties of the material being welded.

3.0 CONVENTIONAL GMA PROCESS

This section will describe present day experience with GMA welding and the problems associated with control of the process to obtain a good weld. The equipment used in GMA welding will also be described.

3.1 Principles of Operation

The results of the conventional GMA process, i.e., the production of a good or bad weld, is a function of a multiplicity of interacting variables, all of which affect weld quality [14]. According to P. T. Houldcroft, the GMA welding process is operated on knife edge conditions causing small local variations to have a major effect on weld quality [14].

The knife edge operating conditions can be seen by examining the effect of different weld parameters on metal transfer. J. C. Needham describes two modes of metal transfer in GMA welding of aluminum [15]:

1. Normal - Rapid spray transfer of small drops on the order of the electrode diameter (most desirable mode),

2. Subthreshold - Infrequent transfer of large globules (used sometimes for short circuiting transfer).

The transition between these modes of metal transfer is shown in Figure 10a and 10b [16,17] where drop transfer rate (drops per second) and drop volume are plotted versus current for steel and aluminum. Since these two modes represent two different weld bead formation modes with varying penetration, the inadvertant transfer from one mode to another caused by only small changes in current, can have a devastating effect on weld qualtiy. To better quantify the mode of transfer occuring throughout the normal and subthreshold ranges, J. C. Needham and A. W. Carter define the ranges of metal transfer in Figure 11 [18] according to the length of wire per droplet [18]. According to J. F. Lancaster, subthreshold transfer for aluminum occurs by gravity where the droplet temperature is well below boiling whereas spray transfer occurs by injection of the droplet into the arc stream by pinch forces at temperatures ranging from the melting point during drop formation to the boiling point before transfer [19].

The voltage versus current characteristics of GMA welding with aluminum, established by J. C. Needham and A. A. Smith for a constant wire feed rate shown in Figure 12

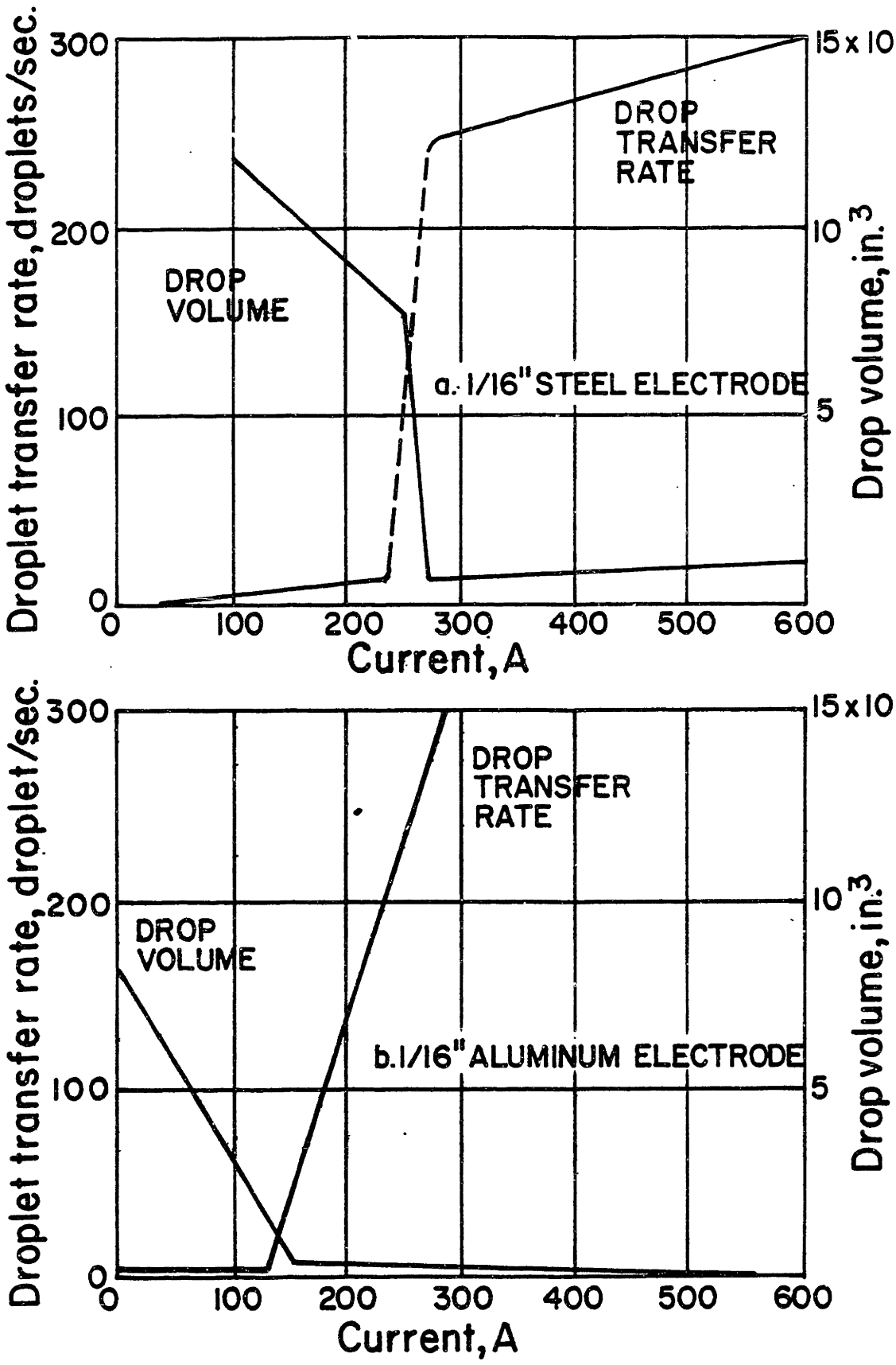

Figure 10: Drop transfer rate and drop volume versus current for steel (a) and aluminum (b) showing transition in transfer mode [16,17].

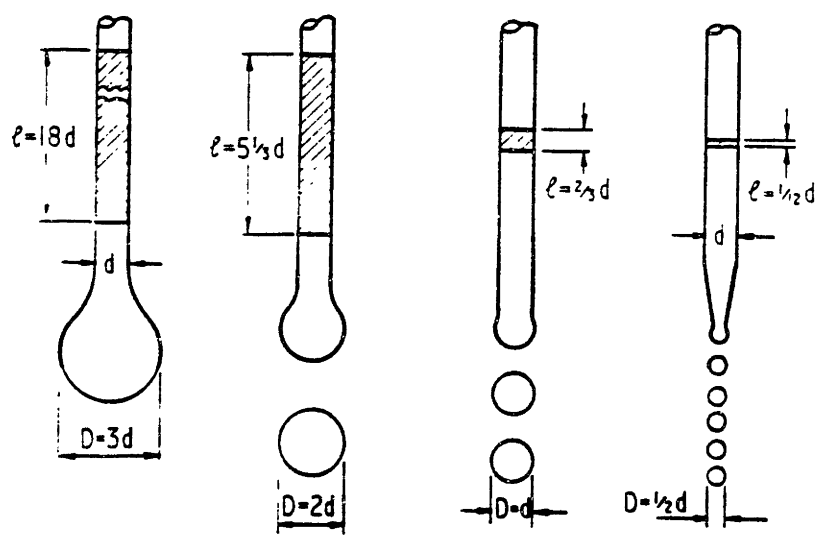

Figure 11: Range of metal transfer according to length of wire per drop [18].

Modes of transfer include
a) subthreshold
b) globular
c) spray
d) jetting or streaming

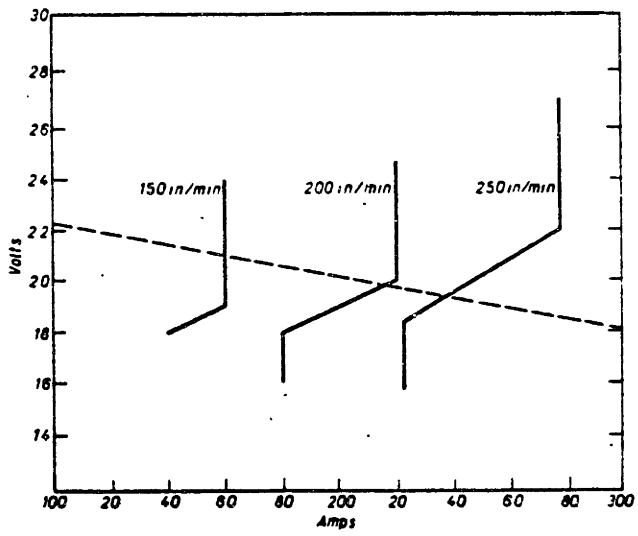

Figure 12: Voltage versus current relationship for constant wire feed rates in GMA welding. Dashed line represents power supply characteristic [14].

[14], appears applicable to other metals [14]. This Z relationship is characterized by modes of transfer previously described:

1. Free flight or normal spray transfer,
2. globular or short circuiting transfer, and
3. a mix of modes 1 and 2.

A three-dimensional representation of the regions of these modes as a functin of voltage, current and penetration further demonstrates the knife-edge operating zone for free flight spray transfer at the edge of the cliff on the "MIG mountain". Operation as near to the edge as possible is desirable to reduce arc and metal transfer instabilities caused by high velocity plasma jets and unfavorably high Lorentz forces. Figure 13 [14] illustrates this mountain.

P. T. Houldcroft states that due to the knife-edge character of GMA welding better controls on conventional equipment are needed along with feedback controlled power sources and precision wire feed devices to eliminate the human element [14]. Pulsed GMA provides a means to obtain better control of the welding process.

3.2 Conventional GMA Equipment

Before discussing the benefits of current pulsing with

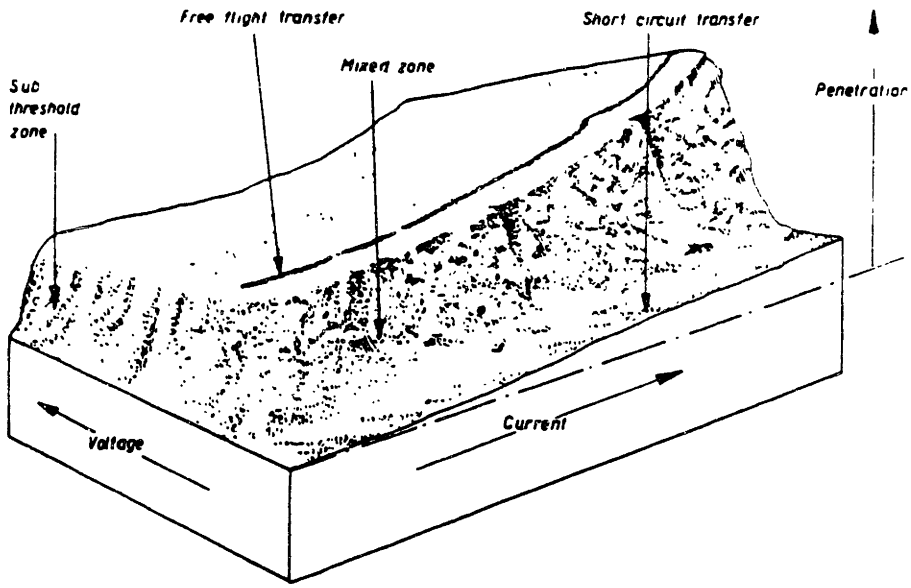

Figure 13: "Mountain" of possible operating parameters for GMA welding with resulting metal transfer mode from Houldcroft [14].

GMA welding, it is first logical to describe the equipment used for conventional GMA welding so that changes or additions made to the equipment to incorporate current pulsing can be understood.

Two basic types of GMA direct current welding power supplies are available. They are [20]:

1. Constant current (CC) power supplies with variable speed wire drive controlled by arc voltage, and
2. Constant potential (CV) power supplies with self-adjusting arc length.

Schematic diagrams of these systems are shown in Figure 14 [21]. The output characteristics of both of these types of power supplies are shown in Figure 15 [22].

As noted above the constant current system requires a feedback loop whereby arc voltage controls the wire feed rate by means of a variable speed wire drive. This system is limited by the sensitivity of the variable speed wire drive and for this reason is not commonly used for GMA welding. However, J. Reynolds reports that this system has an advantage compared to the constant potential system of a closed feedback loop control system and does not require a high degree of operator skill to maintain control of the arc

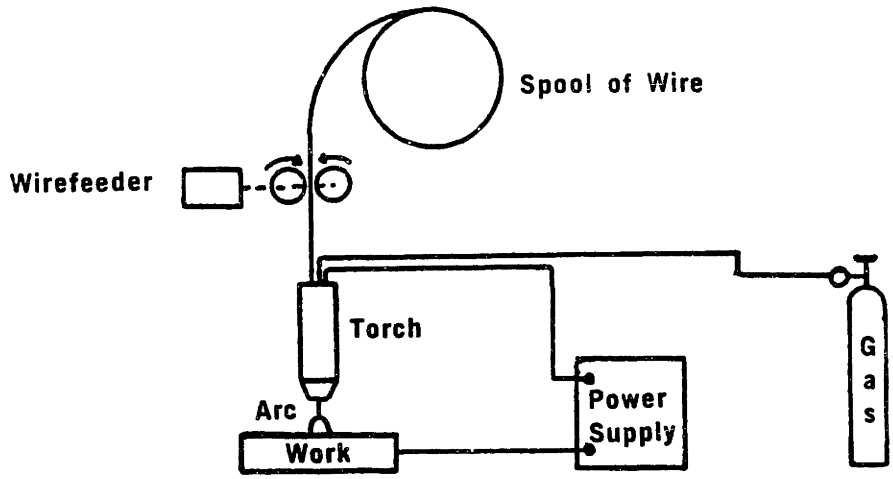

a) Constant potential power supply

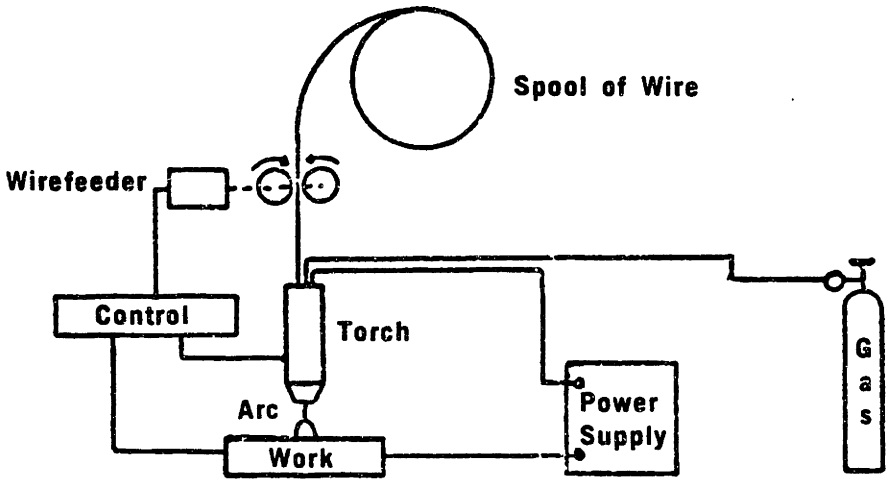

b) Constant current power supply

Figure 14: GMA welding systems with constant potential (a) and constant current (b) power supplies [21].

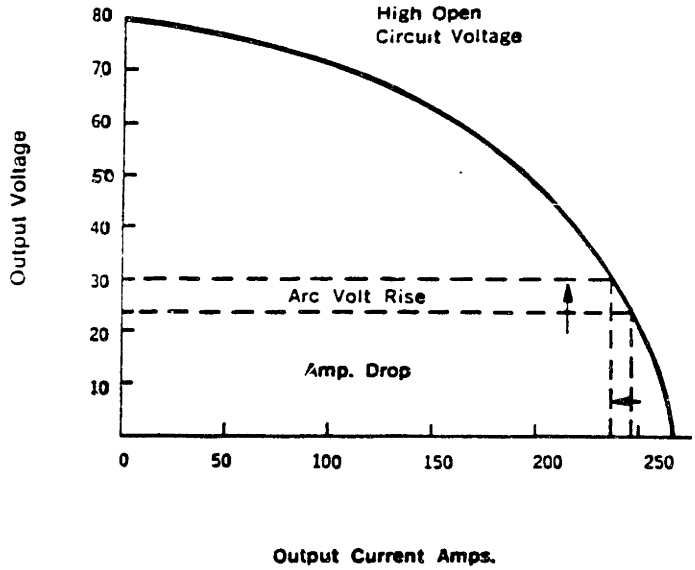

a) Constant current

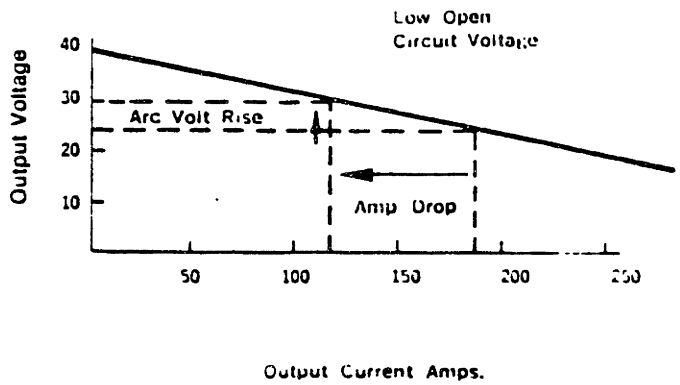

b) Constant potential

Figure 15: Output characteristics for constant current (a) and constant potential welding (p) power supplies [22].

[17].

The constant potential power supply has the advantage of arc length self regulation. The principle of self regulation is based on the fact that an increase (or decrease) in arc length will increase (or decrease) arc voltage and move the operating point to a higher (or lower) current which will cause increased (or decreased) melting rates which forces the arc length back to the equilibrium position [21]. This feature of constant potential power supplies makes them the most desirable power source for GMA welding.

The GMA torch (electrode holder or gun) can be automated [23] for machine welding or can be incorporated into a flexible hand held gun [24] for semi-automatic or manual welding. The gas shielding is provided by argon, helium or a mixture of the two gases to provide optimum arc stability and penetration. For welding highly reactive metals such as titanium, it has been found necessary to provide a gas backing shield and a trailing shield to protect the hot weld bead from atmospheric contamination. Details of backing and trailing shield designs used successfully to weld titanium are given in Reference 25. The wire drive system consists of motor drive rollers by which the wire is either pushed or pulled through the welding torch. If the torch contact tube material and weld

wire are not a compatible wear couple, contact tube wear can become limiting and reduce the productivity of the welding process due to excessive downtime while changing contact tubes. This has been reported to be a problem at the Mare Island Naval Shipyard during hot wire GTA and GMA welding of titanium. Appendix discusses this problem in greater detail.

4.0 PULSED GMA PROCESS

In summarizing the history of GMA welding, A. Laesnewich states that while conventional GMA process has many advantages it was not accepted universally since the minimum current needed to produce spray transfer is relatively high creating a hard to control, very penetrating arc which can only be operated at very high deposition rates making out-of-position welds difficult, if not impossible [26]. Decreasing deposition rates with conventional GMA requires very high wire feed rates while increasing deposition rates increases the transition current for spray transfer to levels where arc control becomes difficult. This is clearly shown in Figure 16 [26]. The following section will describe the development of pulsed GMA as a means to better control metal transfer and penetration.

4.1 Principles of Operation

J. C. Needham of the British Welding Research Association noted in 1962 that a quasi-equilibrium mode of operation can be achieved by using a pulsed current whereby the background current produces sufficient melting to form a drop while an enhanced current pulse detaches the drop by pinch forces [15]. Figure 17 [15] shows the modulated current described by Needham with associated effects on weld

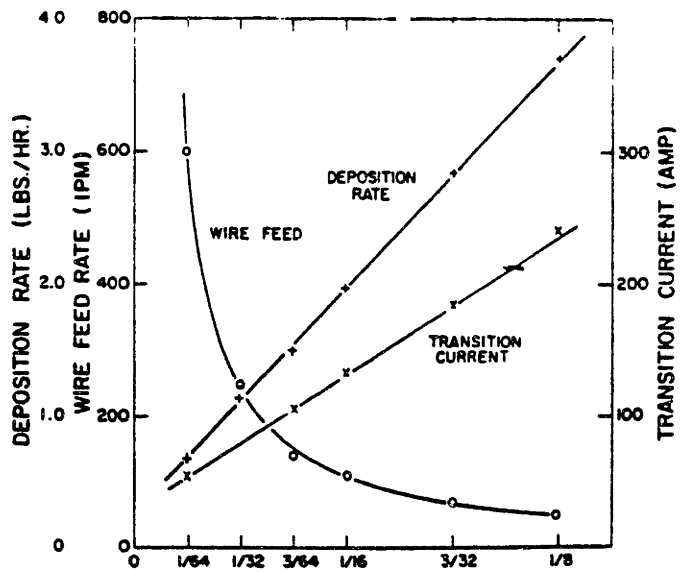

Figure 16: Deposition rate, transition and wire feed rate versus wire diameter for conventional GMA welding [26].

I_p = Peak current

I_b Base current

I_{av} = Average current

T_p = Peak current time

T_b = Base current time

$f = \frac{1}{t_b + t_b}$ = frequency

$x = T_p f$ = fraction of period high

$I_{av} = (I_p - I_b)T_p f + I_b$

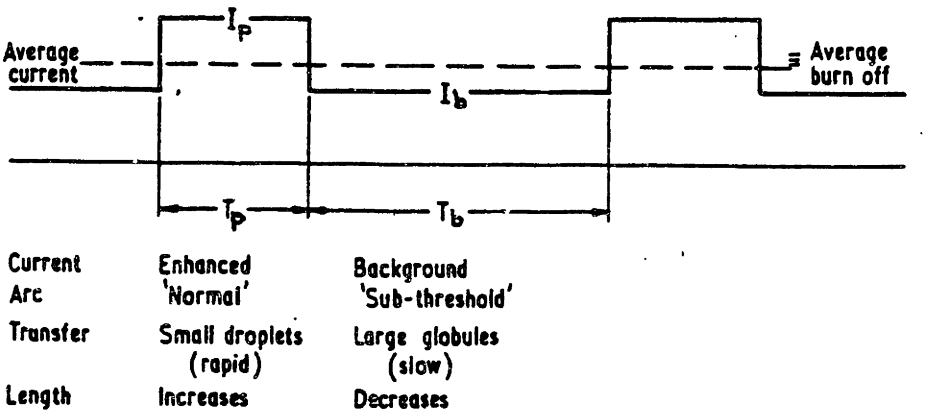

Figure 17: Rectangular pulsed modulated current used for pulsed GMA welding showing effects on weld metal transfer [15].

metal transfer. In 1964, B. E. Paton et al. of the Paton Welding Institute, Soviet Union, described similar use of pulsed current for controlled GMA welding [27]. Needham later noted that the pinch forces causing droplet transfer were proportional to I^2 and that spray metal transfer (drop diameter wire diameter) could be obtained at background current levels much lower than the transition current (minimum DC current required for spray transfer) by imposing a periodic current pulse of magnitude greater than the transition current [16] as shown in Figure 18a [16]. The concept of one drop per pulse transfer is illustrated in Figure 18b [16]. For a given pulse amplitude controlled spray transfer can be achieved over a wide range of average operating current levels with varying weld bead size depending on pulse width and frequency. Detailed arc voltage and current oscillograms of the work by Needham and Carter showed that the actual metal transfer was signalled by a sharp pip near the end or just after each current pulse providing a signal for a possible feedback control system [18].

The work by Needham and Carter on aluminum which established the principles of pulsed GMA is summarized as follows [16,18]:

1. Spray transfer induced by pulse current can be

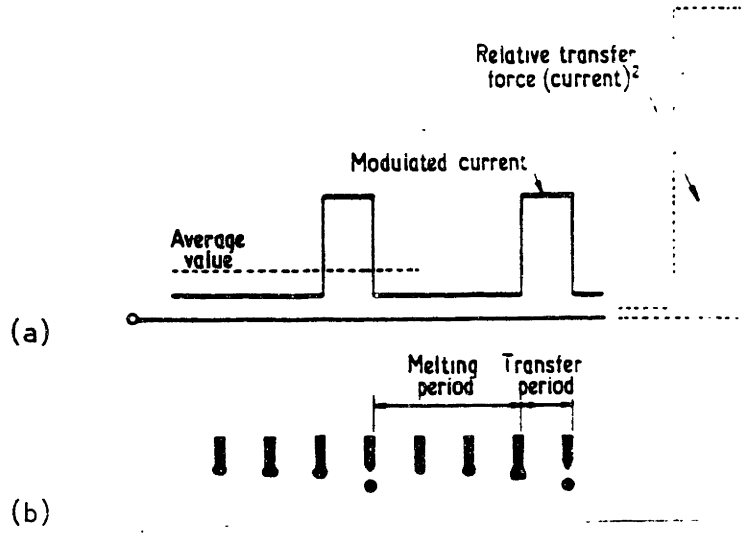

Figure 18: Pulsed current waveform (a) resulting in one-drop-per-pulse transfer (b) [16].

obtained over a very wide range of current extending from 260 to 300 Amps down to about 125 Amps without any change in the mechanism of transfer or break in the current range. This versatility allows for the close control of deposition rates (proportional to average current) and penetration making out-of-position welding and welding of very thin sheet possible. Figure 19 [14] shows the range of penetration possible by changing pulse current and duration for thin aluminum plate.

2. Pulsed current control of the spray transfer process results in a highly reproducible droplet transfer mode with the size and velocity of the drops controlled independently of the mean current and wire speed. The drop size is directly controlled by wire feed speed and pulse frequency while the transfer velocity is controlled by the ratio of pulse to background current level.

3. By using pulse currents just greater than the minimum required for normal spray transfer, droplet detachment takes place towards the end or after the pulse period such that the current is

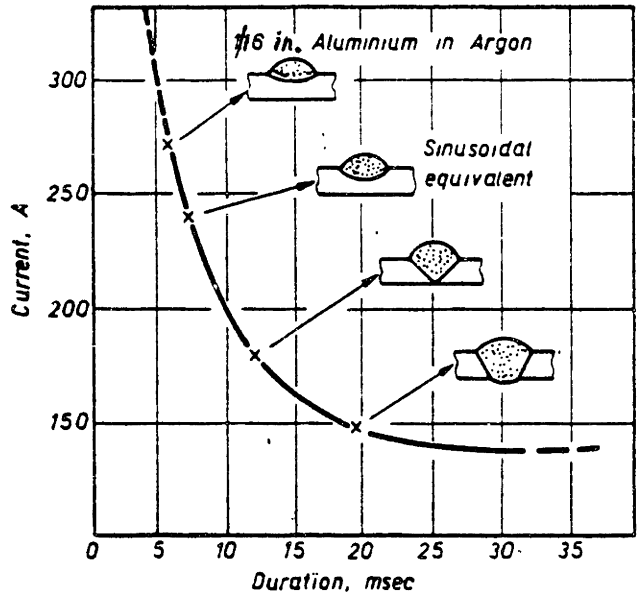

Figure 19: Range of penetration possible in GMA welding of aluminum by changing peak current and peak current duration [14].

well below the peak pulse current allowing for a relatively smooth spatter-free transfer.

4. In all cases investigated with pulsed current control molten droplets are transfered axially along the electrode providing an easily controlled metal transfer process.

In addition to controlled transfer of molten weld metal with pulsed GMA welding in all welding positions, V. A. Lenivkin of the Soviet Union reports that formation of the weld pool also occurs in a controlled fashion [28]. Movement of liquid metal in the weld pool occurs from the head to the tail of the pool. By changing the pulsed current weld parameters, weld pool dimensions can be changed presumably by changing the circulation of molten metal in the weld pool. These observations were made based on welding experiments with aluminum alloys. Thus, enhanced control of both molten weld metal transfer as well as weld pool formation appears to be possible with pulsed current GMA welding.

There are four independent variables in pulsed GMA welding that can be controlled at the power supply:

1. Base Current - Provides enough energy to maintain

the arc during the time current is at I_b and provides sufficient melting at the electrode tip by electron and I^2R heating for formation of the desired droplet size.

2. Peak Current - Must exceed the transition current for the material being welded in order to achieve spray transfer drop sizes and so that one-drop-per-pulse transfer is approached or achieved.

3. Pulse Current Duration - Needs to be long enough to provide sufficient energy to overcome surface tension and other arc forces tending to hold the drop to the electrode, e.g. sufficient energy to form and transfer one drop.

4. Pulse Frequency - Must be synchronized with melting rate at I_b so that pulsing occurs with sufficient molten metal present at the tip for drop formation and transfer.

The relation between I_b and I_p at constant I_{av} and f is shown in Figure 20. Lesnewich described a criteria for the minimum power required for droplet formation and transfer.

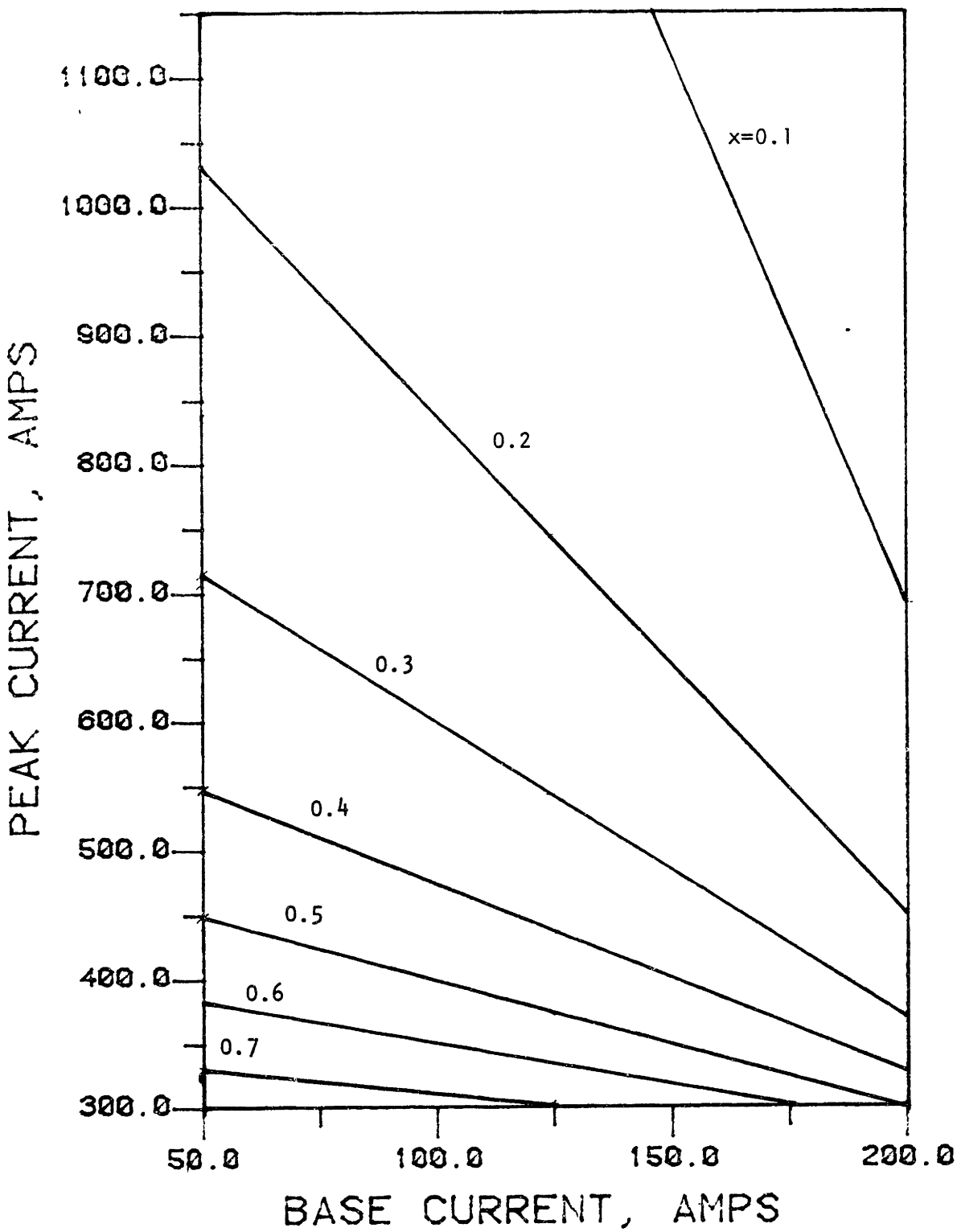

Figure 20: Change in pulsing parameters I_p and I_b at constant x (fraction of period high) and I_{av} for any frequency f.

This relation is shown below [26]:

$$P_{min} = (I_p - I_t)t_p \qquad \text{(A - sec)}$$

where:

P_{min} = minimum power

I_p = peak current

I_t = transition current

t_p = peak current duration

The best transfer is reported to occur when the droplet is released just beefore the pulse is completed. If the drop is detached at the peak of the pulse, fragmentation of the drop occurs causing spatter.

4.2 Pulsed GMA Equipment

Conventional present day pulsed GMA power supplies provide a continuous background current from a conventional constant potential GMA power source in parallel with a pulsed current power source. Conventional GMA power sources were discussed in Section 3.2. The principle behind the pulsed current power source is the modification of line current to provide pulses with the desired Amplitude, width and frequency. With this conventional equipment, amplitude is controlled with transformers, pulse width with mechanical or solid state switches, and frequency with solid state

rectification or mechanical commutation as follows [29]:

1. Half wave rectification of single phase line current,
2. Full wave rectification of single phase line current,
3. Rectification of multiphase line current, and
4. Commutation of recitified line current for reducing pulse frequency.

Two major manufacturers of welding equipment in the U.S. market pulsed current GMA welding power supplies that are based on half or full wave rectification of 60 cycle line current. These power supplies include the Pulstar 450 made by Miller Electric Manufacturing Company [30] and the Pulsed-Arc Model PA-3A made by Airco [31]. Both of these power supplies offer current pulsing at either 60 or 120 Hz.

As shown in Figure 21, the pulse amplitude is controlled by switching the pulsed current using SCRs fired at different times during the sinusoidal pulse. Thus, setting peak current also defines pulse width with these supplies.

Discussions by the author with welders experienced in GMA welding of steel, aluminum and titanium alloys at the Lockheed Missile and Space Company, Sunnyvale, California

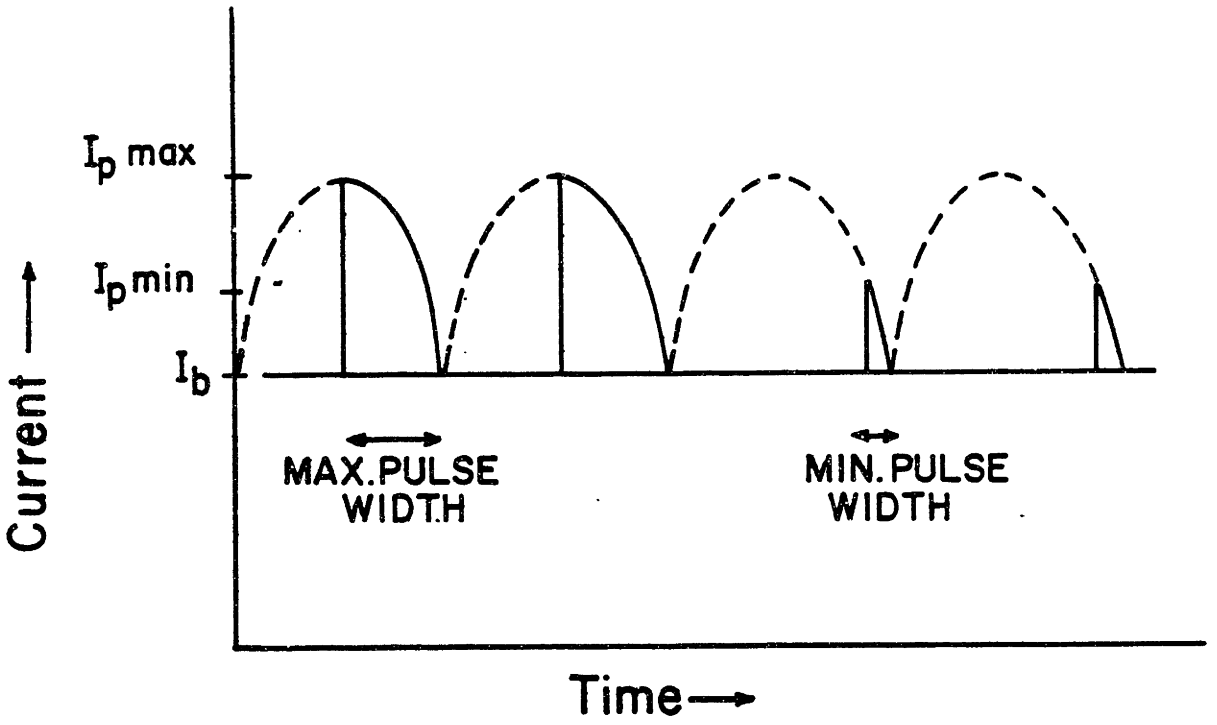

Figure 21: Wave form from typical conventional commercial pulsed current GMA welding power supplies [31].

[32], and the Mare Island Naval Shipyard, Mare Island, California [33], indicated that these conventional pulsed current power supplies provided added arc and metal transfer control when welding steel and aluminum, but that little or no additional control was achieved when welding titanium. This particularly applied to out-of-position welds including vertical up and overhead where experienced welders could not produce acceptable titanium welds in these positions using either pulsed current or DC GMA welding power supplies. Two problems associated with welding of titanium identified by these welders included soot and spatter formation. It was noted that use of conventional pulsed current power supplies had little if any effect on these problems. It appears that for some metals like titanium, the limited additional flexibility offered by current pulsing at only two set frequencies, with constraints on either pulse height or width, is not sufficient to provide controlled weld metal transfer.

Researchers in the Soviet Union have reported the use of a similar rectified (or commutated for frequencies lower than the base AC signal) pulsed power supply where 50 Hz line current is rectified or commutated and superimposed on a DC base power supply [27] as shown in Figure 22. Results of pulsed current GMA welding experiments with steel, aluminum and limited results with titanium have been

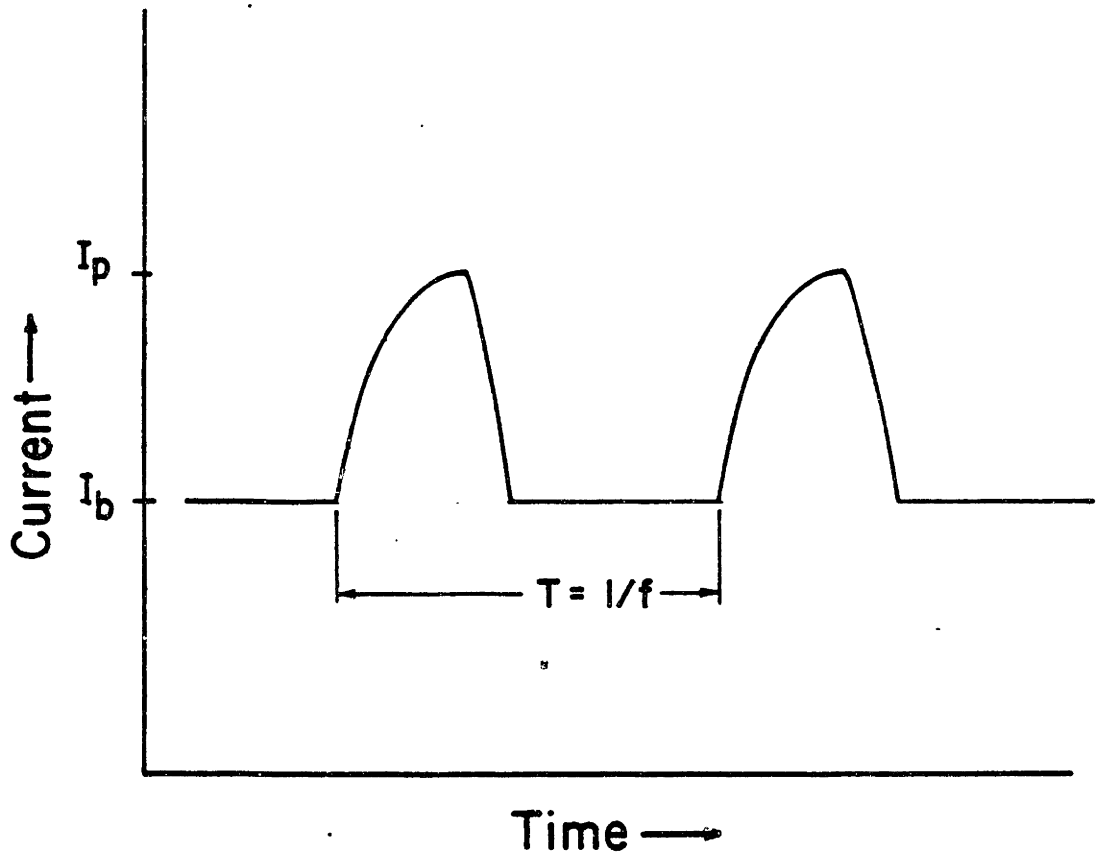

Figure 22: Pulsed current signal used in Soviet GMA welding work where pulse frequency is controlled by commutation or rectification of 50 Hz line current.

reported with pulsing frequencies between 2.5 and 500 Hz. This type of work was first reported by B. E. Paton of the E. O. Paton Welding Institute, Ukraine SSR Academy of Sciences, Soviet Union [27]. A later paper reports the addition of voltage controlled SCRs to the above power supply to provide limited control of pulse duration by controlling the firing time of the solid state device [34], similar to the technique used in conventional pulsed current GMA welding supplies previously described.

Results of Soviet research with the above described pulsed current GMA welding power supply have been published. A comparison of weld quality in flat, vertical and overhead positions with pulsed GMA welding of aluminum alloys was reported by V. P. Lapchinskii et al. [35]. V. A. Lenivkin et al. reported the development of empirical relations for minimum and maximum current pulse amplitude defining a region of peak current versus frequency for controllable transfer in welding aluminum alloys [36,37]. The upper limit on peak current is the value where a slight increase in current peak causes breaks in the arc and is a function of the pulse decay characteristics of the power source. The lower limit on current is the value which results in a transition from uncontrollable to controllable metal transfer which was found empirically to be a function of the metal surface tension and drop diameter. F. Z. Tenenbaum

established regions of mean welding current versus welding speed for a pulse amplitude of 600 to 700 Amps which will minimize the formation of lack of fusion and burn through defects in welding aluminum alloys with various electrode sizes in vertical and horizontal welding positions [38]. Another Soviet study by V. N. Buchinskii, et al. reported the development of empirical relations of pulsed current welding parameters defining a region for controllable transfer in welding steel alloys [39].

The policy for pulsed GMA welding research in the Soviet Union appears to be the establishment of acceptable regions of parameters for pulsed GMA welding using conventional pulsed current power supplies. As noted by B. E. Paton the pulsed GMA process is being widely adopted by Soviet industry as evidenced by the wide variety of welding studies of this process in Soviet literature [27].

Modern state of the art welding incorporates transistorized pulsing power supplies which can provide a multitude of wave forms defined by a signal generator with adjustable frequency, pulse amplitude and pulse width over wide welding parameter ranges. A number of welding power supply companies and welding research laboratories are currently engaged in developing transistor controlled pulsed current GMA welding power supplies. A summary of systems being developed or curently available will be given below

according to country:

1. Japan - The Hitachi Mechanical Engineering Resarch Laboratory has produced a prototype transistor controlled pulse current GMA welding power supply. Based on information received by T. W. Eagar during a visit to Hitachi, this power supply has been operated at frequencies of up to 500 Hz [40]. The independent welding parameters appear to be base current, peak current, and pulse duration with pulsing frequency apparantly tied to wire feed rate. A similar power supply is produced by Mitsubishi called the Clean Mag 350 which operates in a "synergic" mode [41]. This power supply operates with three phase 60 Hz current and provides 350 Amps max output at a duty cycle of 50%. Again the independent weld parameters set on the machine include base current, peak current and pulse duration which are adjusted based on the material being welded while frequency control is linearly tied to wire feed rate which is changed to produce a desired weld bead size. Results of GMA welding of steel using the Clean MAG 500 are reported in Reference 42. During a visit by M. Kobayashi of Matsushita Electric Industrial

Company to MIT in April of 1983, it was noted that Matsushita also markets a pulsed current welding power supply [43]. However, details of this power supply were not available in time for incorporation into this thesis.

2. Great Britain - The Welding Institute of Great Britain has devloped the Synergic Pulse GMA welding system and is the origin for the term "Synergic" mode of operation [44]. As in the power supplies manufactured in Japan, the "synergic" mode of operation establishes base current and peak current based on wire size and material being welded. The pulse frequency and pulse duration are both tied to wire feed rate by means of a solid state mixing system whereby at one extreme, frequency is constant with pulse duration dependent on wire feed rate, while at the other extreme the pulse duration is constant with frequency dependent on wire feed rate. It should be noted that the "synergic" system requires precise sensing and control of wire feed rate requiring large feed rolls and very precise variable speed wire feed motors. Such equipment can easily be accommodated for automatic welding

in a laboratory, but application of this system to semi-automatic welding, for example in a shipyard environment requirng long flexible wire feeds and hand held torches, may not be practical. Results of welding mild steel with the "synergic" system are reported in Reference 44.

3. U. S. A. - The NU-Weld division of Dimetrics, Inc., Diamond Springs, California, currently markets the Metal Beam Power Source and Servo Controls [45,46]. This system uses a pre-programmed 16.5 KHz current signal produced by providing DC current to a transistorized chopping system with the capability of modulating the pulse width of the 16.5 KHz chopped signal. The pulse amplitude is controlled by providing 300 ADC inputs in parallel to achieve the desired peak current. This system can modulate the 16.5 KHz signal from 50 to 1000 Hz. The baseline high frequency signal was chosen to provide optimum arc stability and the modulation of this signal provides an effective base and peak current level to achieve controlled metal transfer. Figure 23 shows schematically how the above decribed 16.5 KHz signal is modulated to provide effective

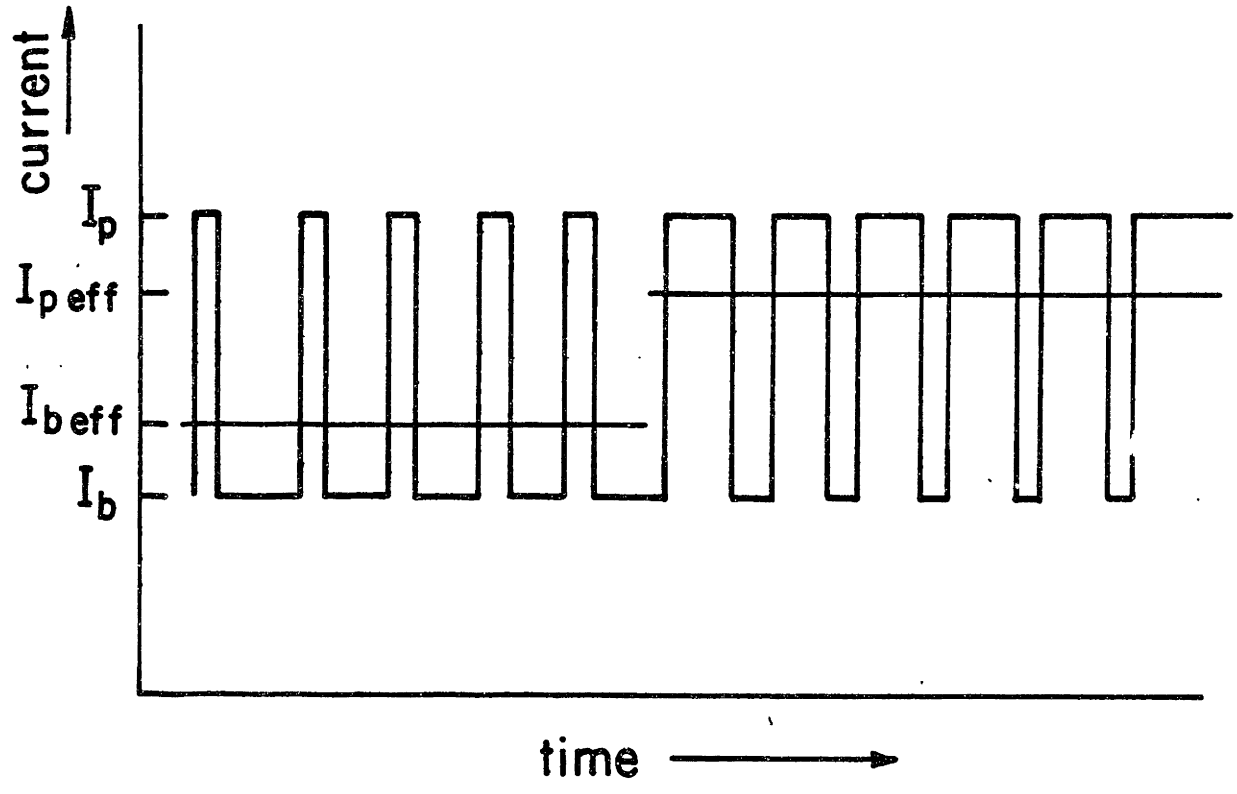

Figure 23: Pulse Width modulated 16.5 KHz current signal giving an effective pulsed current signal.

current pulsing. The maximum current level for the 16.5 kHz signal is fixed by the maximum capability of the DC current source. The modulation rate and effective base current is programmed into the machine while the effective peak curent is preset and detemined by the output of the 16.5 kHz signal at maximum possible pulse width. During a visit by the author to Dimetrics [45], a series of welds were performed on a 3/4-inch thick titanium plate with the Metal Beam Power Source over a range of modulated frequencies. Results of evaluations of these welds will be discussed in Section 8.3.3. The power supply used in the experiments for this thesis consisted of two commercial DC power supplies connected in parallel to a specially built 20 kW current regulator designed and made by Alexander Kusko, Needham Heights, Massachusetts [47]. This current regulator was produced as a tool for welding research. It is a series-pass transistor power supply that provides a current signal based on an analog input signal from a signal generator. This system will be described in greater detail in Section 6.2.2.

Based upon a review of available literature, there appear to be three common ways to produce pulsed current signals for welding [48].

1. Voltage controlled SCRs or phase controlled three-phase thyristors which modify an alternating current input to provide pulsed current wave forms. This method can provide pulse frequencies of a few hundred Hz limited by the firing time of the solid state device.

2. Transistor choppers using a DC input where the output voltage and current signal is controlled by the duration of the on and off times of the transistor switch. Frequencies of up to 40 kHz are common with this type of device.

3. Linear series-pass transistor power supply where water cooled power transistors are used as adjustable resistors to dissipate the difference in energy between input and output. This system provides the cleanest and most accurate output signal with frequencies as high as 100 kHz. However, this system requires water cooling which may make it unacceptable for some type of

production welding.

The shielding gas equipment and wire feed system for pulsed GMA welding are similar to those described in Section 3.2 for conventional GMA welding. As noted by P. T. Houldcroft, as the power supply systems for pulsed GMA welding are upgraded, the auxiliary equipment, including gas shielding systems, wire feed systems and welding parameter gauges and monitors, must also be upgraded in order to obtain the full potential of the power source [14].

5.0 EXPERIENCE WITH PULSED GMA

This section will summarize experience in the literature pertinent to pulsed GMA welding of titanium. Specifically, past experience with conventional GMA welding and more recent experience with pulsed GMA welding of titanium will be discussed. Information covering welding parameters used, metal transfer characteistics and quality of the welds including appearance, soundness and mechanical propeties will be summarized where available. It should be noted that a wealth of information exists concerning pulsed gas metal arc welding of aluminum alloys and steel, but relatively little information exists with titanium. Almost all of the information on gas metal arc welding of titanium plate originates with work done by or for the following laboratories and companies:

1. David Taylor Research and Development Center, Annapolis, Maryland, or its predecessor, the U.S. Naval Applied Science Laboratory, Brooklyn, NY,

2. The National Aeronautics and Space Administration Laboratories,

3. The British Welding Institute, Cambridge, England,

or its predecessor, the British Welding Research Association, Cambridge, England,

4. The E. O. Paton Welding Institute, Ukraine SSR Academy of Sciences, Soviet Union, and

5. Reactive Metals Products, Niles, Ohio, a U. S. producer of titanium products.

5.1 U.S. and British Experience

L. E. Stark, et al. reported for Reactive Metals Products the results of welding 1" thick Ti-6Al-4V plate with conventional GMA process [23]. Single V-groove joint preparation was used with the following optimum weld parameters to minimize spatter: direct current reverse polarity, 320 to 350 Amp DC, 35 to 38 volts, wire feed speed at 380 ipm and Ar shielding. Cross sections of welds indicate a relatively rough weld bead profile. The conclusions state that conventional GMA welding can be used for thick section titanium, but weld bead contours and uneven penetration indicate that better control of the process would be desirable. Furthermore, it is desirable to reduce the current level and thereby reduce the burnoff rate and wire feed speed to levels which could be accommodated by conventional wire feed motors (i.e., 200 to 300 ipm).

R. J. Wolfe, et al. reported results of conventional GMA welding of 1" thick Ti 721 alloy for the U.S. Naval Applied Science Laboratory [49]. Both spray and short circuiting (globular) transfer were used and typical weld parameters for each mode of transfer are:

1. Spray transfer - 330 Amps DC reverse polarity, 36 volts, 270 to 400ipm wire feed rate, and

2. Short circuiting transfer - 155 to 160 Amps DC straight polarity, 16 to 17 volts, 350 to 425 ipm wire feed rate.

Results from this work show that spray tranfer can only be performed in the flat welding position with reverse polarity while short circuiting transfer in straight polarity is prone to lack of fusion defects. Again, additional control of the weld process is needed.

G. R. Salter and M. H. Scott of the British Welding Research Association reported results of pulsed GMA welding of 1" thick Ti 721 alloy plate again for the U.S. Naval Applied Science Laboratory [25]. Initial weld trials with conventional GMA welding equipment exhibited the following arc and metal transfer characteristics.

1. Reverse Polarity - A cathode plasma jet formed at the arc root in the weld pool. At low currents this jet dominated the arc being much stronger than the jet from the filler metal. Metal transfer occurred by gravity with large drops breaking up upon entering the weld pool. Drop fragments were ejected away from the weld pool by the strong cathode jet. Upon increasing current, the anode jet from the filler metal began to dominate the jet from the weld pool partly due to the breaking of the strong cathode spot into a number of weak spots. The strengthened anode jet caused increased metal transfer frequency until transfer in the form of individual droplets occurred. In the conclusion section of this thesis, an alternate explanation for the above observations will be given.

2. Straight Polarity - Only one plasma jet was present at the cathode, and this jet was unstable. At low currents the cathode jet rotated around the filler metal causing droplet deflection. Metal transfer occurred when droplet size overcame surface tension. At high currents the arc rotated rapidly around the electrode, and droplets were

shattered at the electrode tip resulting in spatter. These observations and conclusions are supported in the conclusion section of this thesis.

It was concluded that pulsed GMA welding should offer increased metal transfer control with reverse polarity since a stable spray transfer mode could be achieved at high current. Pulsed GMA welding with straight polarity was considered impractical due to arc instability and spattering.

The weld parameters used to investigate pulsed GMA welding in this study include:

(1) I_p = 330 Amp, I_{av} = 150 Amp, 120 imp wire feed rate, and

(2) I_p = 180 Amp, I_{av} = 78 Amp, 420 ipm wire feed rate.

All pulsing was done at 50 Hz. The background current was provided by a 200 Amp transformer rectifier, while a transformer rectifier connected in half wave mode provided the pulse current. Droplet transfer occurred regularly after each current pulse with droplets landing in the weld

pool. The use of either Ar or Ar/25% He had no apparent effect on metal transfer although globular transfer occurred with He alone.

Short circuiting GMA welds were prone to lack of fusion defects while spray transfer required excessive filler metal feed speeds. Pulsed GMA welds showed good fusion and a large weld pool, however metal could not be pushed into position in a narrow joint and arc stability was disturbed by the side wall. Furthermore, good fusion was only obtained when the arc was directed at the position of interest indicating high current density concentrations on the work piece.

In summary, pulsed GMA welding required fewer passes to complete the joint, showed no tendency for lack of fusion defects, reduced total arc time, resulted in less spatter and produced acceptable mechanical properties.

G. R. Salter notes that the use of He shielding gas with high voltage equipment may reduce the cathode flame and improve weld pool wetting and that higher pulse frequencies may improve metal transfer characteristics [25].

The David Taylor Naval Research and Development Center, Annapolis, Maryland, reported results of pulsed current GMA welding of thick section titanium using conventional pulsed current welding power supplies [50] similar to those described in Section 4.2. This work was performed at 60 and

120 Hz pulsing frequency. Typical welding parameters included peak currents of about 300 Amps with 280 ipm wire feed rate. The report indicates that spray mode pulsed GMA welding can be used in all welding positions. A weld demonstration model consisting of a seven foot diameter, five foot long, 2 1/8 inch thick titanium alloy stiffened cylinder was fabricated using state of the art technology. All vertical welds were made using short circuiting transfer. Spray mode GMA welding was used only in the flat position. This report includes an extensive list of references regarding thick section titanium GMA welding development work performed by the National Aeronautics and Space Administration Laboratories.

5.2 Soviet Experience

S. M. Gurevich of the E. O. Paton Welding Institute, Ukraine SSR Academy of Sciences, Soviet Union, reported results of pulsed current GMA welding of a high tensile strength titanium alloy [51]. This work was performed with the Soviet conventional pulsed current power supply previously described at 50 Hz. Base current levels were reported at 150-300 Amps with on peak current level or pulse duration given. It was noted that straight polarity resulted in less spatter than reverse polarity, but that vertical welding with straight polarity could not be done

satisfactorily. These results appear to contradict those of Salter, et al. who reported that no control over metal transfer was possible using straight polarity [25]. The results of this thesis reported in Section 8 agree with Salter, et al.'s conclusions.

6.0 EXPERIMENTAL WELDING TECHNIQUE

The following section will describe the experimental welding technique used to study the gas metal arc (GMA) welding of titanium alloy Ti-6Al-4V.

6.1 Goals

A major problem associated with GMA welding of titanium is lack of control of weld metal transfer and spatter formation. Spatter consists of small droplets of molten weld metal which is ejected from the arc sometime between droplet formation, droplet transfer, and droplet incorporation into the weld pool. A high speed photographic technique will be described that was developed to observe the process of weld metal transfer in order to understand the origin of forces that result in spatter and nonuniform weld bead formation. Titanium bead-on-plate welding experiments were performed and analyzed using this technique. Changes in weld metal transfer control were recorded as a function of pulsed current parameters including base current (I_b), peak current (I_p) and pulsing frequency (f) at constant average current (I_{av}). Results were evaluated to determine if one drop per pulse weld metal transfer is possible under controlled welding conditions.

6.2 Description of Welding Experiment

A unique combination of conventional constant current DC gas metal arc welding equipment commercially available plus a research analog current regulator was used to provide pulsed current welding power. The following sections will describe this equipment and how it was interfaced to operate as a system.

6.2.1 Welding Power Supply

Two Gold Star 600 SS 600 Amp constant current welding power supplies manufactured by Miller Electric Manufacturing Company, Appleton, Wisconsin, were connected in parallel to provide 1200 Amp capability at 60% duty cycle. These power supplies were connected through a Miller TIG-RIG control unit. Since this power supply was intended for straight polarity GTA welding, the output leads were switched to provide reverse polarity current e.g., on the power supply, the work lead represented the positive lead which was connected to the electrode for reverse polarity electrode positive welding. These DC power supplies are represented schematically in Figure 24. These power supplies were each connected to a standard 30 Amp 480 volt three-phase bus in the MIT Welding Laboratory.

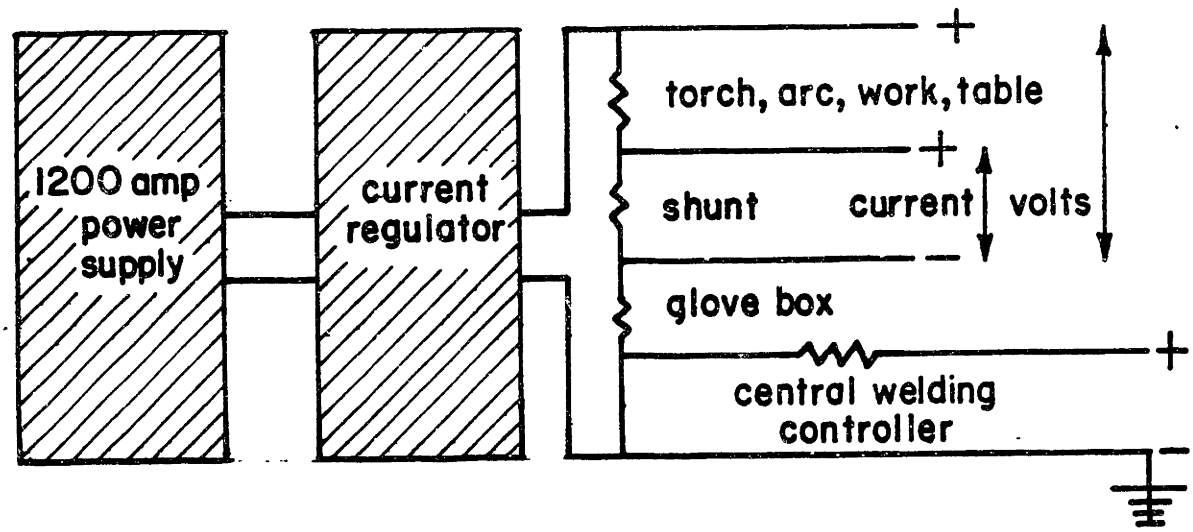

Figure 24: Schematic of GMA pulsed current welding system.

6.2.2 Current Regulator

A specially designed analog current regulator designed and made by Alexander Kusko, Inc., Needham Heights, Massachusetts, produced the desired current waveform from the DC current provided by the parallel Miller power supplies. This current regulator consisted of four modules of 48 water cooled power transistors that produced a current waveform output, by dissipating the energy from the DC input not needed for the output. Thus, connecting this current regulator in series with the parallel Miller power supplies as shown in Figure 24 produced a very flexible pulsed current welding power supply of the linear series-pass transistor type discussed in Section 4.2.

Each power module consisted of one driver circuit heatsink and four output power circuit heat sinks as shown in Figure 25a and 25b. A block diagram of the current regulator showing the interaction of power output circuits, protection and sequencing circuits and control circuits is shown in Figure 26. This current regulator will operate at pulsing frequencies of up to 20 kHz with 600 Amp RMS output

A Wavetek model 166 50 MHz pulse/function signal generator provided the analog current reference signal to the current regulator. A Tektronics Oscilloscope provided a visual display of the analog current reference signal and output current signal measured across an internal shunt.

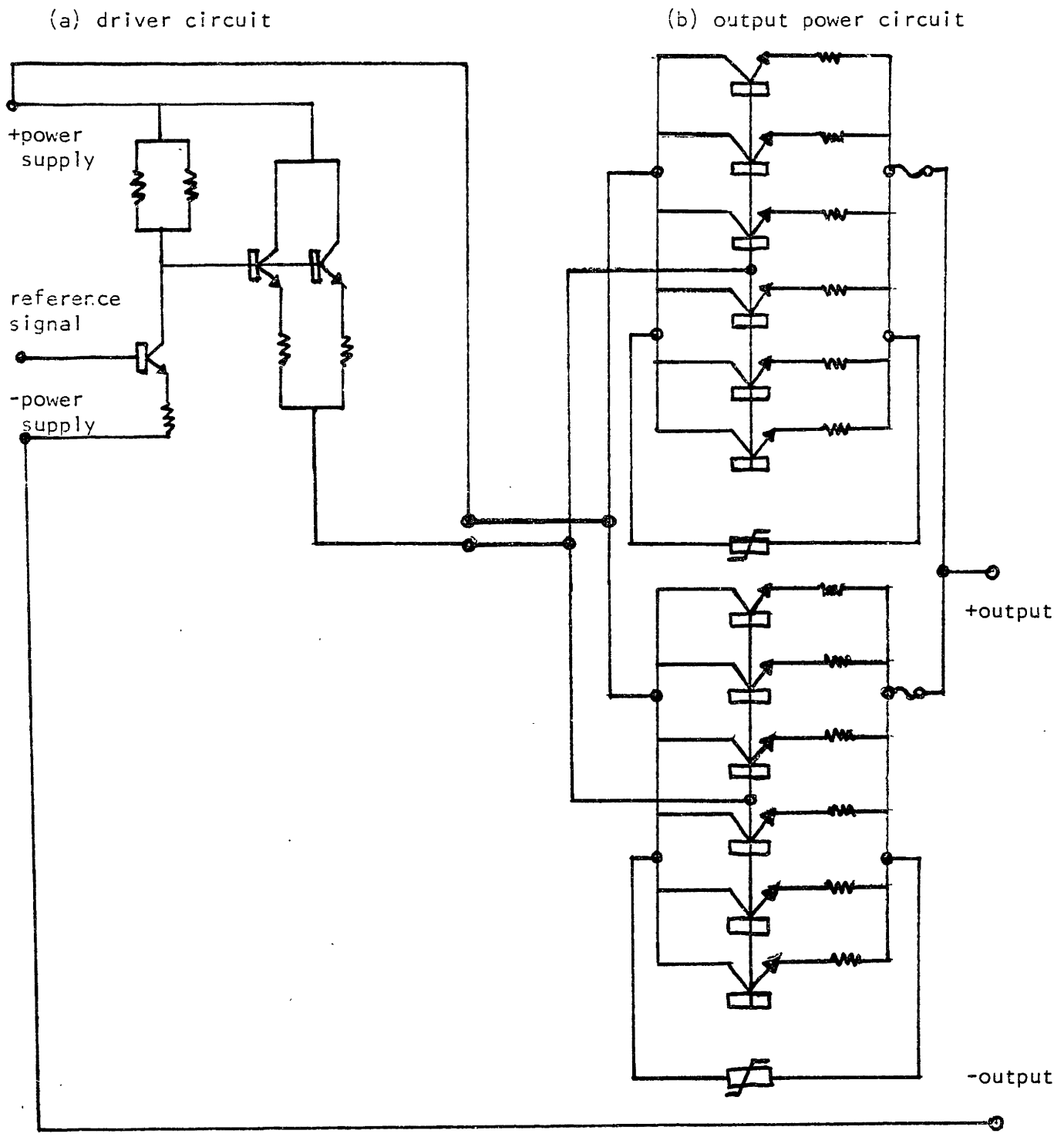

Figure 25: Schematic of power module circuit in each of four current regulator power modules including driver circuit (a) and output power circuit (b).

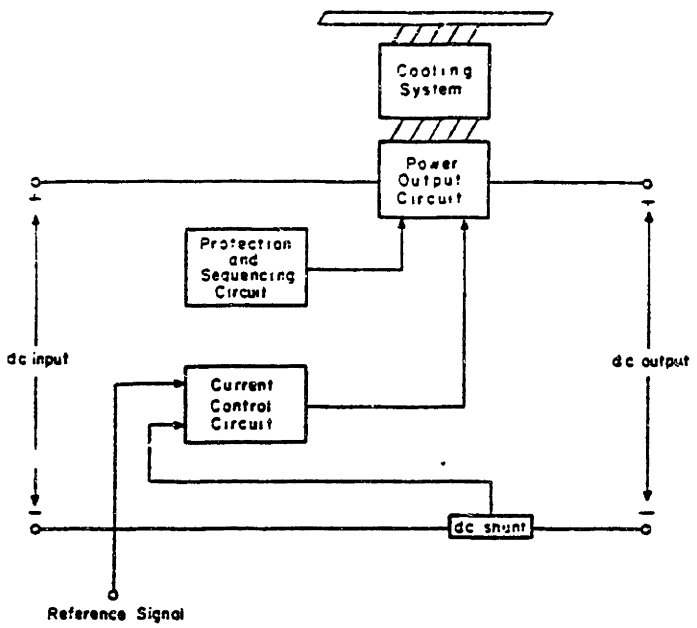

Figure 26: Block diagrams of current regulator [48].

This equipment is shown in Figure 27.

6.2.3 Purged Containment

All welding was performed inside an argon purged glove box Drilab produced by Vacuum Atmospheres. Figure 27 shows the glove box with a 25 cubic foot capacity. The glove box was equipped with the following features:

1. Windows - The glove box had two 30"x40" lexan windows each with two handholes for rubber gloves and one optical port with a glass window.

2. Welding Power Connections - Two weld cable electrical feed throughs for positive and negative welding leads were installed on the glove box side.

3. Cooling Water - Two water feed through ports for welding table cooling water were installed.

4. Over Pressure Protection - One pressure relief oil bubbler was installed to prevent damage to windows and gloves from Argon over-pressure.

5. Auxiliary Power - One 120V AC line current box (4

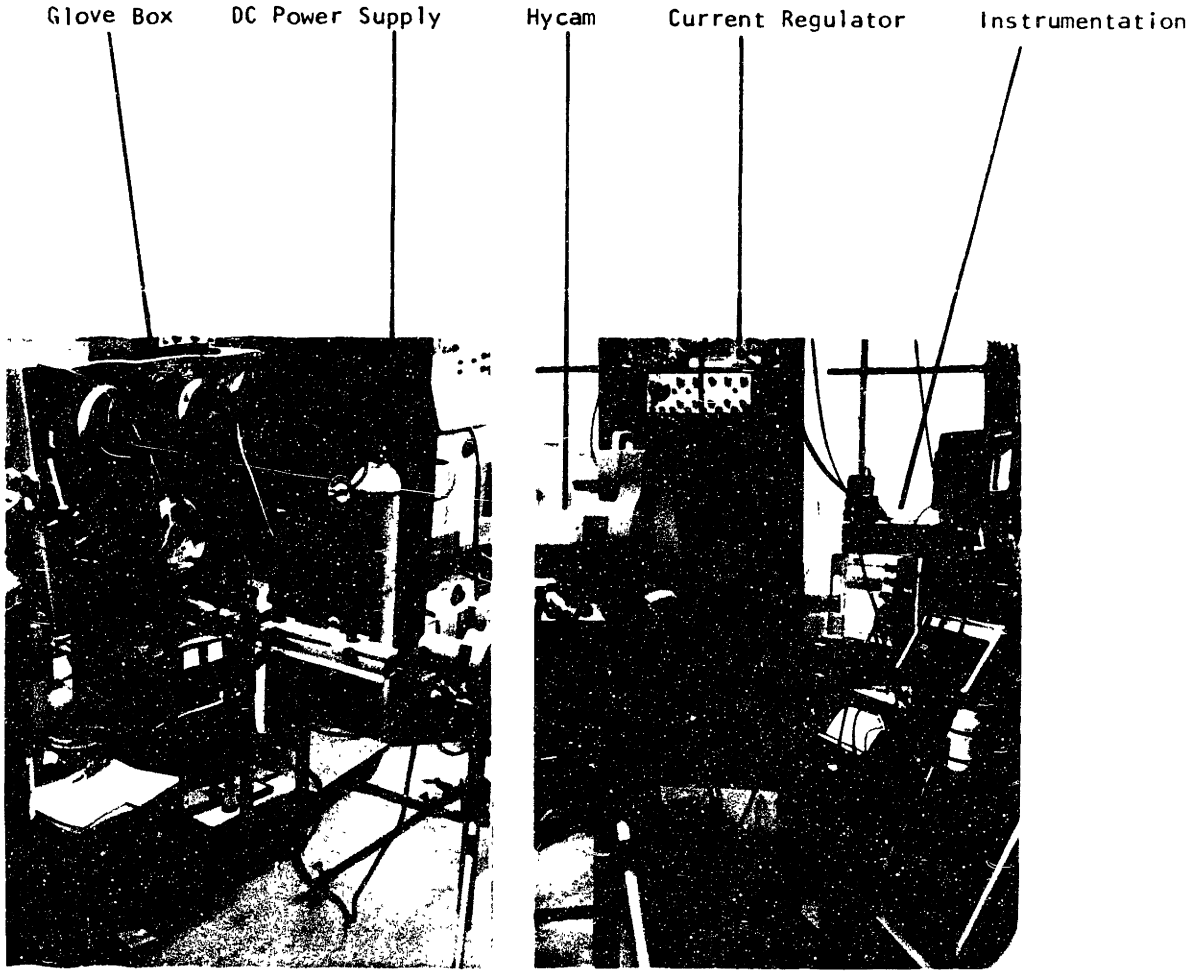

Figure 27: Glove box Dri-lab with 25 ft^3 capacity with DC power supply, current regulator and instrumentation.

outlets) was located inside the glove box for auxiliary power along with 24V DC connections for table translator power.

6. Antichamber - An antichamber with roughing vacuum pump, pressure gauge, and Ar refill connections for evacuation and refill was located on the glove box side to allow welding samples and tools to be passed into and out of the box without contaminating the atmosphere.

7. Pressure Maintenance System - A photohelic pressure maintenance system for set point pressure control by solenoid valve activation of gas supply (low pressure) or evacuation (high pressure) was installed to allow operation at slightly positive pressure to minimize leaks into the glove box.

8. Vent Valve - A vent valve was installed on the top of the glove box to allow for glove box purging and continuous feed-and-bleed operation at low Argon flow rates.

9. Electrical Penetrations - Two electrical penetrations were installed in the glove box for

wire feed motor power and for instrumentation as follows:

(a) Box Penetration, Electrical -1 (BPE1)

1. Wire feed motor power (3 leads)
2. Digital tachometer (2 leads)

(b) Box Penetration, Electrical -2 (BPE2)

1. Wire feed control arc voltage measure high and ground (2 leads)
2. Instrumentation arc voltage measure high (2 leads)
3. Instrumentation arc current measure high (1 lead)
4. Instrumentation common ground (1 lead, same point for 1, 2 and 3)

10. Gas Supply System - The argon gas supply system consisted of a 4000 ft^3 liquid argon bottle connected for gas use and fitted with an argon gas regulator and dual range flow meter.

11. Gas Cleansing and Recirculation System - A gas cleansing and recirculation system was installed for recirculating the atmosphere through a particulate filter in either atmosphere cleansing mode through a getter furnace or in bypass mode.

This system includes:

(a) Particulate filter,

(b) Diaphragm gas circulating pump with a 1 cfm capacity,

(c) Titanium getter furnace atmosphere cleansing system and O_2 analyzer made by Centorr Associates, Inc., for stripping gas O_2 content to less than 10^{-8} ppm O_2. This system also removes C, H_2, N_2 and H_2O contamination from the atmosphere.

Figures 28a, b, and c show schematic diagrams of glove box atmosphere control systems including antichamber, gas supply, and gas cleansing and recirculation systems respectively.

The above described system allowed the contamination-free welding of titanium plate samples while observing the welding process and recording metal transfer with high speed photography using laser back lighting (see Section 6.3) through the optical ports.

6.2.4 Wire Feeder and Control System

Welding was performed in an automatic mode with wire feeder attached to x, y translators mounted on a frame with casters translatable in the z or welding direction. A

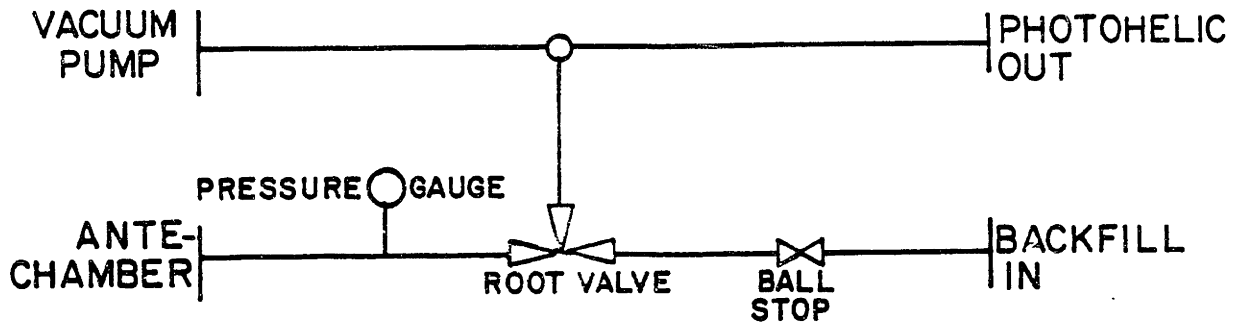

a) Anti chamber system

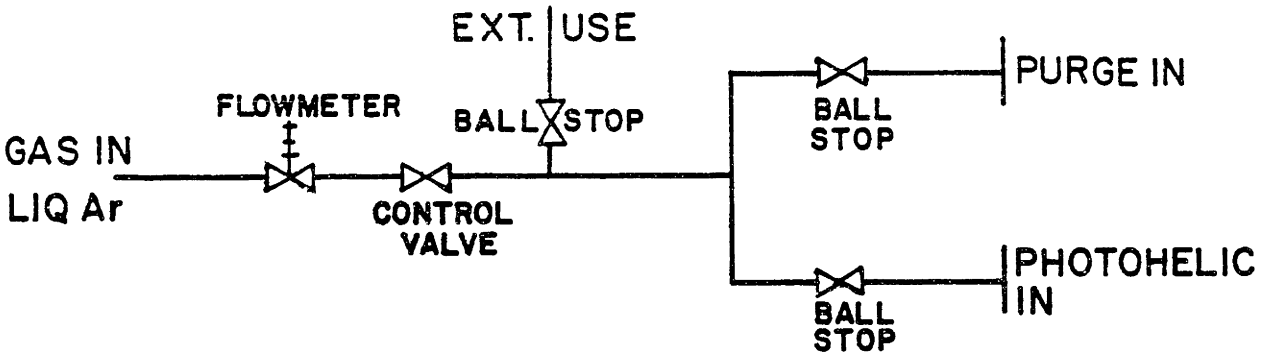

b) Gas supply system

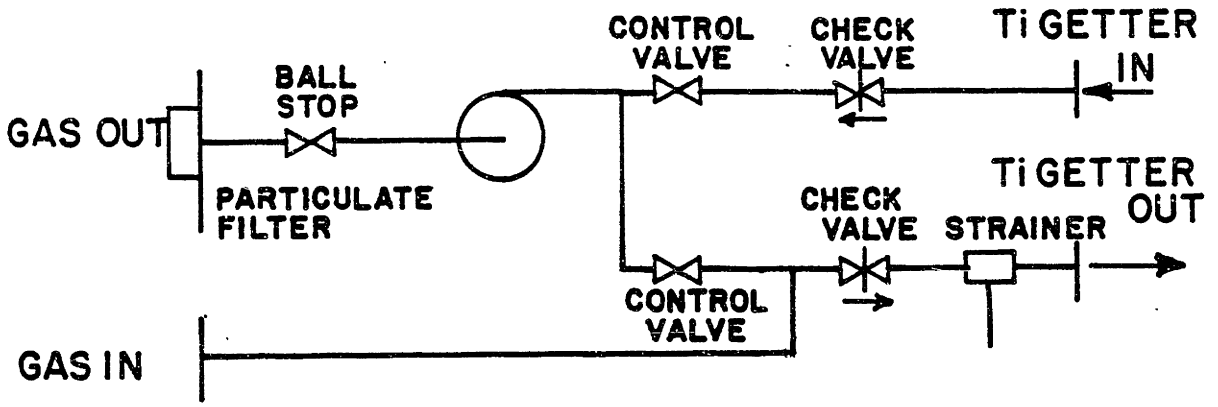

c) Gas cleansing and recirculation system

Figure 28: Glove box atmosphere control systems.

welding table was located under the wire feeder mounted on free wheeling casters for translation in the x, z directions. Initiation of wire feed, table translation and welding current was synchronized by a central controller with single switch operation. The wire feeder, table translator and control system are described below:

1. Wire Feeder - A permanent magnet variable wire feed speed motor model EH-11 made by Linde Division of Union Carbide was used with the following attachments:
   (a) Digital tachometer with a one-inch circumference drive wheel for ipm readout,
   (b) wire straightener,
   (c) feed rolls,
   (d) insulated brass bus for torch/weld cable connection,
   (e) torch with contact tube and optional gas cup.

   The wire feed system was rated for 250 ipm maximum, but operated at 300 ipm satisfactorily for short periods of time.

2. Table Translator and Carriage Control - The welding table consisted of a 3/8" x 12" x 18"

aluminum plate mounted on Thompson ball bushings riding on steel rods mounted on a base plate with Thompson pillow blocks. The table was translated by means of an electric lead screw actuator model 15D Electric Cylinder made by Industrial Devices. The linear speed of the lead screw was controlled by controlling input voltage from 0 to 24V DC and the direction of travel was controlled by input polarity. The DC power to operate the lead screw motor was provided by a 120V AC to 24V DC recitfied and filtered variable transformer carriage control power supply. The carriage control allowed for variable speed operation in either direction in manual or automatic welding modes.

3. Central Welding Controller - The central welding controller Model UEC-8 made by Linde, Division of Union Carbide, synchronized the operation of wire feeder, table translator and carriage controller, and welding current contactor. Of the following items, (a) through (d) are outputs, and (e) and (f) are inputs to the welding controller:

(a) Wire feed motor power

(b) Carriage controller power

(c) Welding power supply contactor relay control

(d) Voltage control potentiometer for fine current adjust

(e) 120V AC power for central controller

(f) Voltage sense.

The voltage sense input to the central welding controller provides a feedback signal to internal logic which adjusts wire feed speed to maintain a steady arc voltage. Arc length could be separately adjusted with the wire feed speed conrol on the UEC-8. With all systems set in automatic, welding can be initiated and stoped with a single switch. The wire feeder and translating table are inside the glove box while the carriage controller and central welding controller are outside. Figure 29 shows drawings of the welding torch with and without a gas cup.

6.2.5 Instrumentation

Instrumentation included three means to record arc voltage and current as a function of time. All instrumentation measurements were made with respect to a common ground (i.e., the low side of the shunt attached to

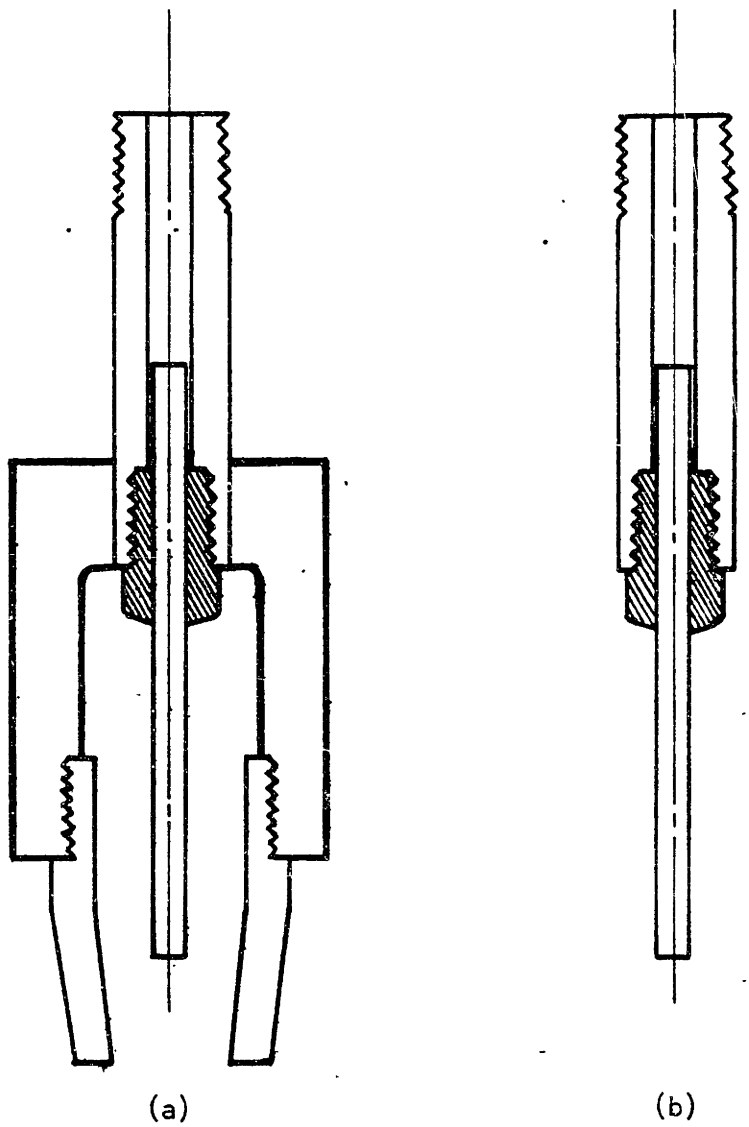

Figure 29: Drawings of GMA welding torch with (a) and without (b) gas cup.

the translating table as shown schematically in Figure 24). Average voltage and current were measured with a Hewlett Packard Strip Chart recorder model 7132 A, while high speed oscillographs of voltage and current were recorded on a Honeywell Visicorder model 1858 with 1883 differential input amplifiers. A Tektronics storage oscilloscope was also used to record single voltage and current traces. A bank of three switches controlled data acquisition during welding from:

1. strip chart recorder
2. visicorder and high-speed camera
3. digital tachometer

The welding and data acquisition system described above can be operated easily by a single person by operating one welding control switch and a bank of three data acquisition switches.

6.3 Description of High Speed Photography Equipment

The experimental technique used for recording metal droplet transfer consists of high speed photography (6000 frames per second) using a balance of laser backlighting and arc illumination to record formation, detachment, time-of-flight, and incorporation of droplets into the weld pool. The current signal (high or low) was recorded on the film next to each high speed picture to allow real time

analysis of droplet transfer as a function of pulsed current input. The following section will describe the optics, high speed camera, and film used for high speed photography of GMA weld metal transfer.

6.3.1 Optics

The original goal of early work in high speed photography of weld metal transfer performed in the MIT Welding Laboratory consisted of developing a laser backlighting system to provide a shadow image of droplet transfer in GMA welding. A low power (2mW) He-Ne laser Model 145-02 produced by Spectra Physics with spatial filter and beam expander provided a large diameter beam of laser light as shown in Figure 30. This expanded beam of light was then directed through one glove box optical port at the arc gap, between the consumable welding electrode and base plate, and out the other optical port on the other side of the glove box. The expanded beam was then focused by an objective lens through a pin hole aperture and a 6328A band pass filter blocking out all arc light and leaving a laser shadow picture of the electrode/base plate arc gap. A field lens then converged the image to the proper size at the high speed camera. Figure 31a shows this optical train. Initial work with this technique showed good results with black and white film.

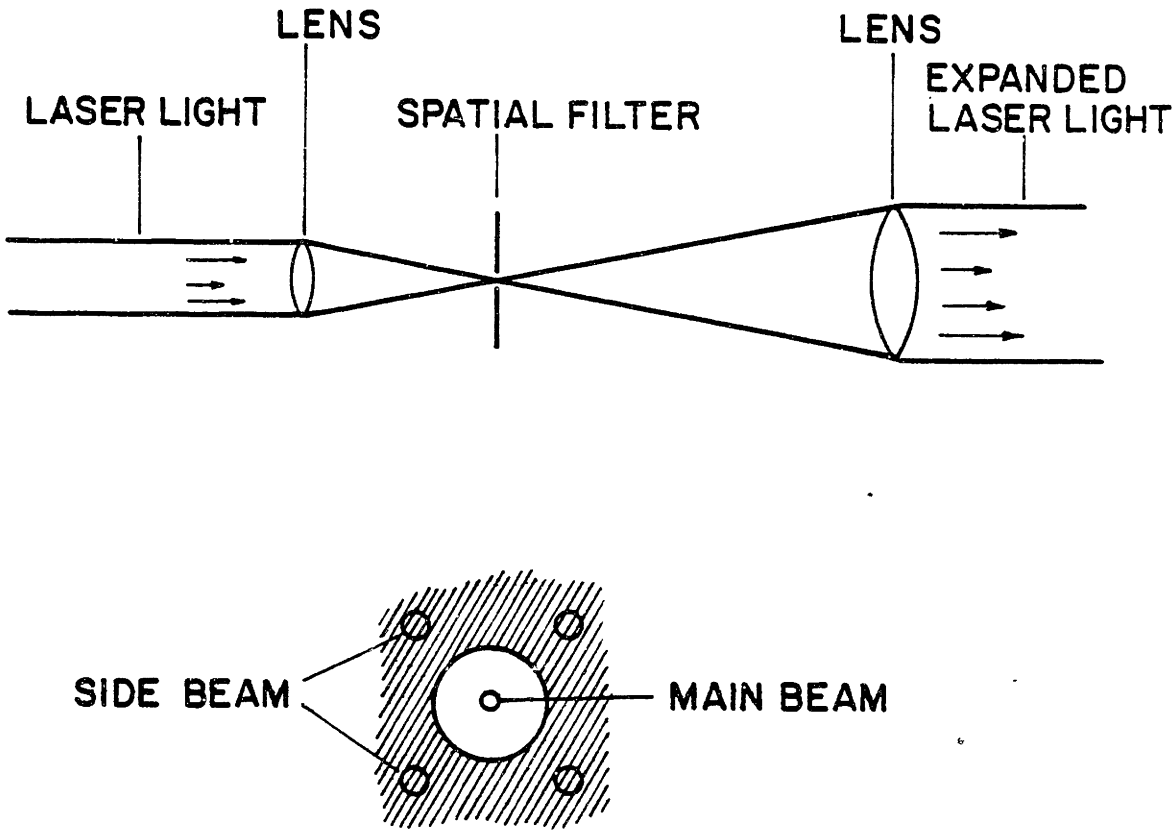

Spatial filter blocks side beams so interference fringes are minimized.

Figure 30: Spatial filter and beam expander.

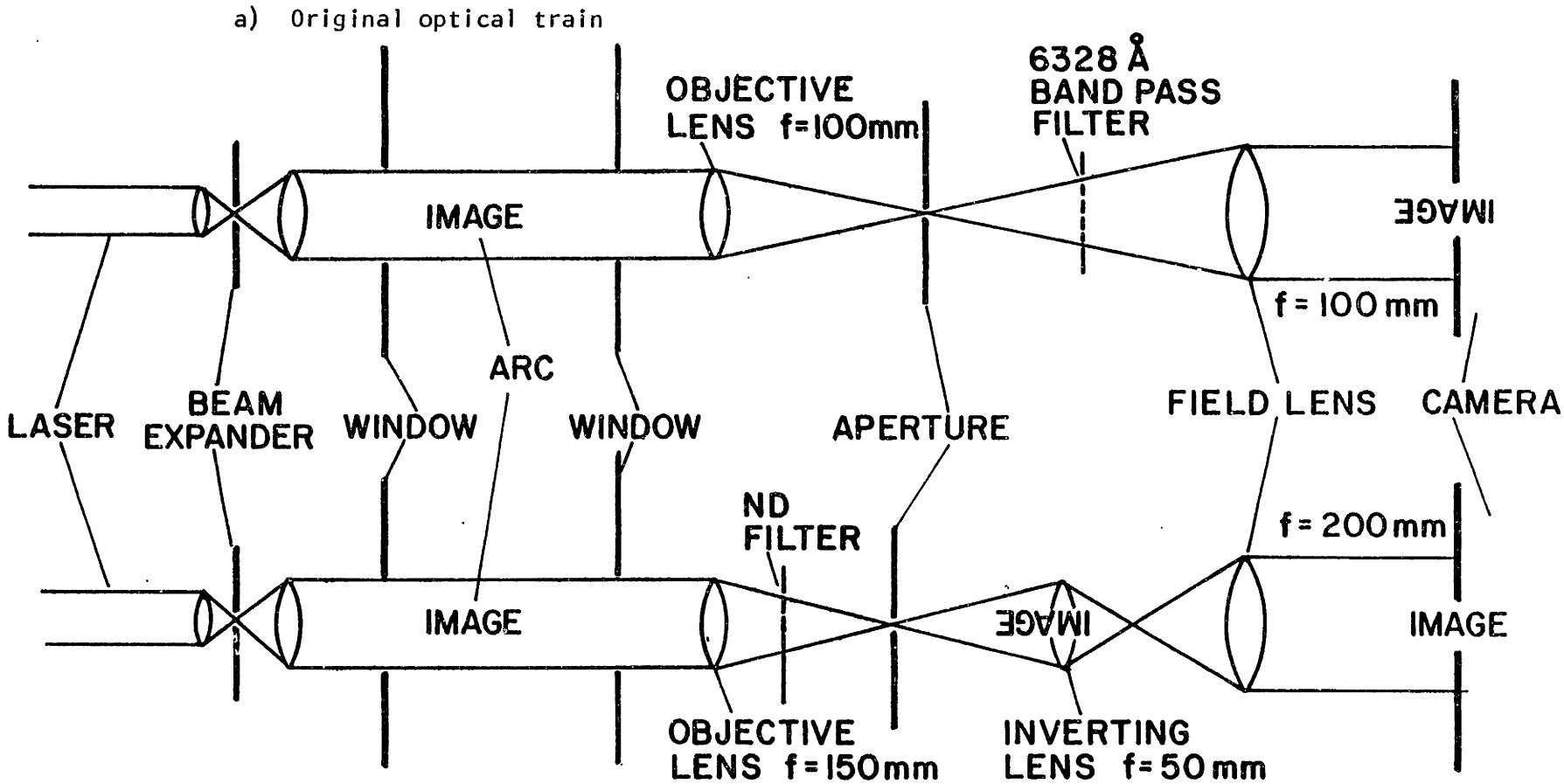

Figure 31: Original and improved optical trains for high speed photography of weld metal transfer.

The above described system was improved by replacing the band pass filter with a neutral density filter to allow limited arc light illumination and eliminate interference fringes introduced by the band pass filter. In addition, an inverting lens was added to turn the image right side up on the film. When used with color film, this optical train, shown in Figure 31b, provided an excellent balance of arc light illumination and laser backlight shadowing, giving a three-dimensional effect to the image of droplets forming and detaching from the electrode.

The procedure used to align the optical system consisted of the following steps:

1. Adjust high intensity expanded laser beam spot between electrode tip/base plate gap as shown in Figure 31.
2. Level the laser in the optical bench.
3. Adjust objective lens and field lens to get proper elevation of image at camera.
4. Adjust inverting lens to provide for proper magnification of image and sharp focus.
5. Adjust camera fore and aft tilt to obtain a plane image on the film in the camera with tripod base adjustment screws.
6. Align optical train left and right for alignment

with aperture when closed down to a pin hole.

The improved optical train was used successfully for over 50 high speed movies with only minimal optical train and laser realignment necessary. Figures 32 and 33 show the laser plus beam expander and optical train aligned with the arc gap respectively.

6.3.2 Camera

A 16mm Hycam high speed camera made by Redlake Corporation was used to take high speed movies of GMA weld metal transfer. This camera is a shutterless high speed rotating prism camera capable of speeds up to about 10,000 frames per second. Figure 27 shows the Hycam mounted and aligned with the optical train for use. The Hycam used for this work was equipped with LED timing lights for illumination of the portion of film outside of the sprocket holes by switching an external 5 volt DC supply with a TTL reference signal as shown schematically in Figure 34. The reference signal used for timing purposes was the TTL output of the signal generator providing the current reference signal to the current regulator. This film marking technique was used to record peak and base current time (corresponding to high and low in the TTL signal) next to each frame so that weld metal droplet formation and transfer

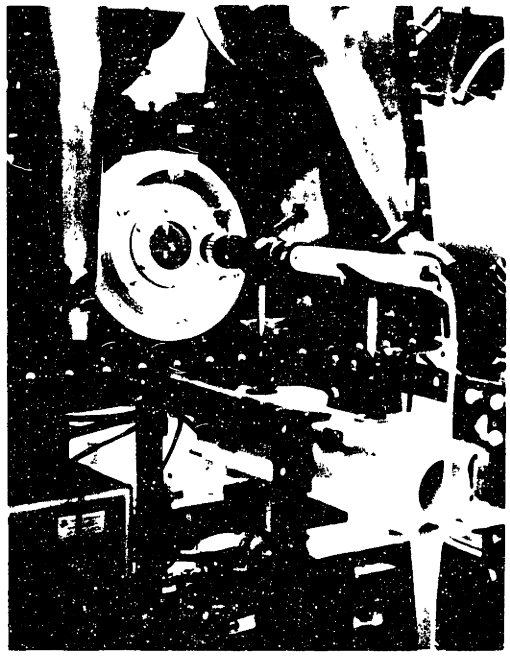

Figure 32: Laser plus beam expander aligned with the arc gap

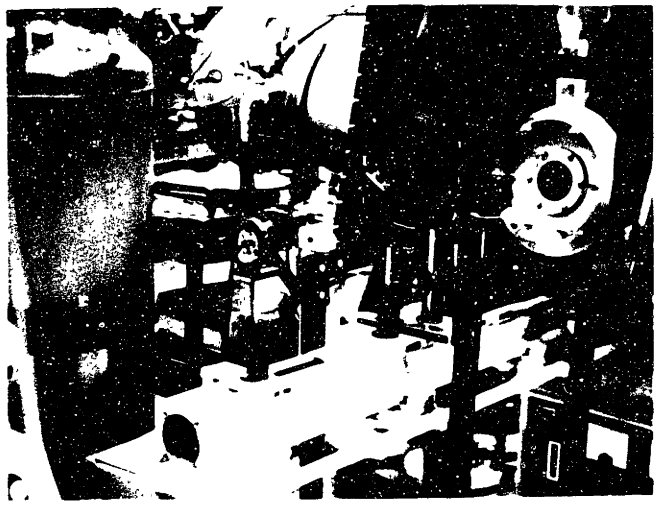

Figure [illegible]

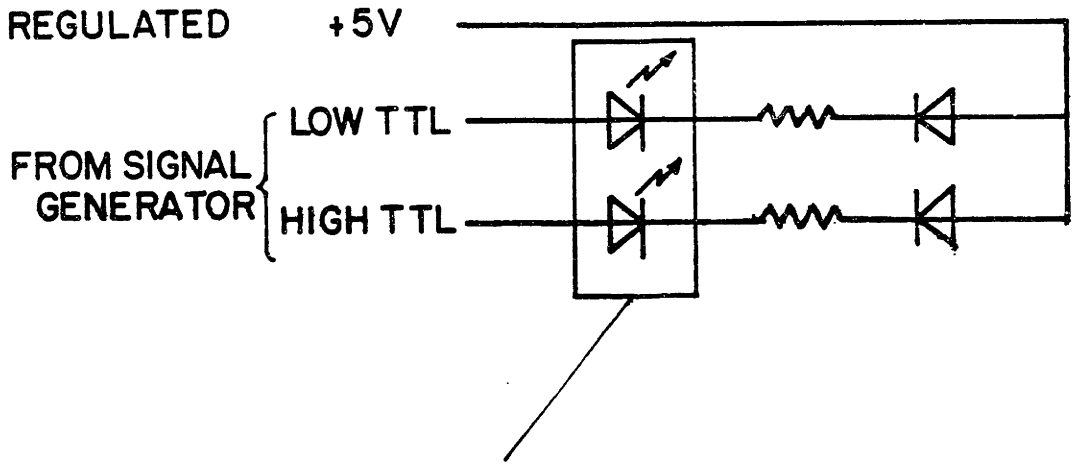

Timing blocks in Hycam with LEDs for marking film outside sprocket holes.

Figure 34: Power Supply for LED film markers with switching provided by TTL and $\overline{\text{TTL}}$ output from signal generator.

could be correlated to the pulsed weld current signal. This Hycam was also equipped with a lens at the back of the camera which could be focused on an oscilloscope screen operating in the spot mode as a volt meter to mark the film with actual current or voltage signals as opposed to high or low only. However, this system required a special oscilloscope tube phosphor (P11 type) which was not available at the time of this work.

6.3.3 Film and Film Analysis

Three types of 16mm film were evaluated for use with the laser backlighting system for high speed photography. The film types evaluated included:

1. Kodak Tri-X reversal 7278, ASA 160, Black and White
2. Kodak Ektachrome 7241, ASA 40, Color
3. Kodak Video News Film High Speed 7250, Tungsten, ASA 400, Color

The Video News Film provided the easiest attainable balance of laser backlighting and arc illumination by using a neutral density filter ND = 0.5. The Ektachrome color film proved to be too slow to attain this balance of lighting. The Tri-X black and white film worked

satisfactorily for laser backlighting but was dropped in favor of the balance of light attained with color Video News Film. All high speed photography was performed with 100 ft. rolls of film at a speed of 6000 frames per second. The first 50 ft. of film was expended while the camera reached the desired speed. The last 50 ft. of film, when the camera had reached the set speed, was analyzed for droplet size, droplet frequency of formation and transfer, and percent of droplet transfer resulting in spatter, i.e., portion of droplet ejected from the weld pool. The predominant mode of droplet transfer was also evaluated (see Figure 5). All films were analyzed with a Selectra Frame 53 16mm projector made by Visual Instrumentation equipped with side film marker illumination to alow for analysis of when the drops detached with respect to high or low (peak or base) in the current signal.

7.0 PULSED GMA WELDING OF ALUMINUM

Three eights inch thick aluminum plate (1100 alloy) and a 1/16 inch diameter electrode was used for practice bead-on-plate welds in operational testing of the welding, data acquisition and high speed photography systems. This section will discuss notable results obtained when welding aluminum with this welding system.

7.1 Goals

The major goal of welding performed with aluminum was the shakedown and operational testing of the welding system. Aluminum (1100) plate and wire are readily available at low cost and provide an easy-to-weld practice material for this purpose.

7.2 Experimental Design

The experimental design for this portion of the research consisted mainly of operating the welding system in DC and pulsed current modes in various controlled glove box environments to test the operation of each system and to determine the optimum optical system for high speed photography. The following specific areas were evaluated during operational testing of the welding system:

1. Aluminum weld metal transfer was evaluated with high speed photograpy with constnt DC current and square wave pulsed current at 50 and 500 Hz.

2. The effet of argon shield gas flow rate and oxygen content on weld porosity and cathodic cleaning was evaluated using the controlled argon shielded glove box atmosphere.

To provide easy handling inside the glove box, all samples were cut into 3" x 12" pieces. Each weld sample contained either one 10" long weld or two 6" long welds, each starting at the center and extending to both ends of the plate. All weld samples were mechanically wire brushed shortly before welding to remove surface scale.

7.3 Results

This section will discuss results obtained from welding experiments performed during operational testing of the welding system.

7.3.1 Aluminum Weld Metal Transfer

Good quality welds were made using both DC and pulsed current wave forms with average current inputs of about 250 Amps. High speed movies of weld metal transfer

were taken using the technique described in Section 6.3. Droplet formation, detachment, transfer, and incorporation into the weld pool occurred in an orderly, spatter-free manner in both pulsed and DC current welds. At low frequencies (50 Hz), drops slightly larger than the electrode diameter are formed, and detachment and transfer were achieved when the current signal was high. During the high part of the current signal, several small drops were formed and detached with diameters slightly smaller than the electrode diameter. At higher frequencies (500 Hz) regular droplet transfer was achieved with droplet detachment frequencies and droplet diameters similar to those achieved with the average current in DC welding. Figure 35, 36, and 37 show typical aluminum weld metal transfer using DC and pulsed current wave forms along with droplet detachment time, droplet transfer frequency and droplet diameter. The formation of very small secondary drops upon primary drop detachment is observed in these figures. These secondary drops were formed from the filament of liquid metal left after drop detachment and were incorporated into the weld pool.

The transfer mode in each case is such that the droplet is ejected without deflection from the electrode as shown in Figure 5. The operative or overriding force in transfer appears to be always in the direction of droplet transfer

Figure 35: Aluminum weld metal transfer with DC.

I = 260ADC, V = 28.5 V, v_{wire} = 252 ipm
Avg droplet detach time = 2.6 msec.
Avg droplet detach frequency = 380 Hz
Avg drop diameter = 0.050 in.
frame time = 0.167 msec.

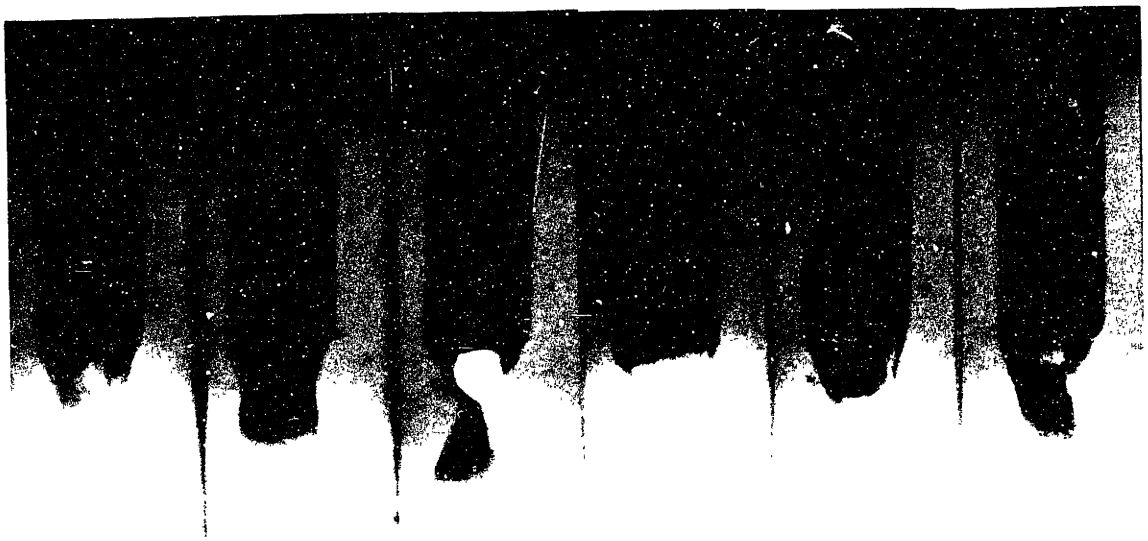

Figure 36: Aluminum weld metal transfer with f = 50 Hz

I_b = 200 A, I_p = 300 A, I_{av} = 250 A, V = 28 V, v_{wire} = 245 ipm

Avg droplet detach time = 10.0, 4.6, 2.5, 2.5, 2.5, 2.5, msec. (recurring pattern)

Avg droplet detach frequency = 100, 220, 400, 400, 400, 400 Hz

Avg drop diameter = 0.07 in.

frame time = 0.167 msec.

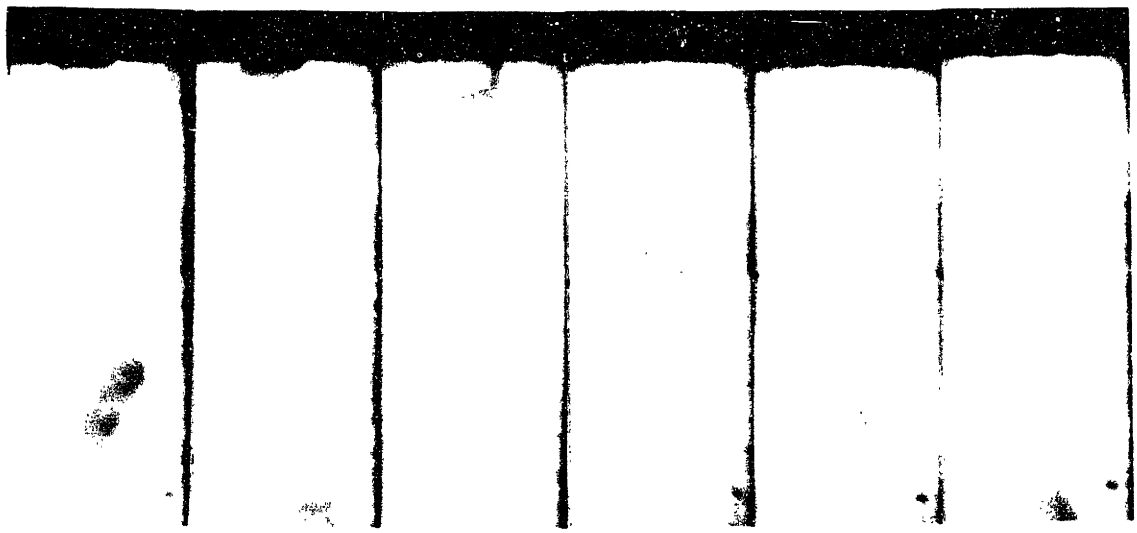

Figure 37: Aluminum weld metal transfer with f = 500 Hz
I_b = 200 A, I_p = 300 A, I_{av} = 250 A, V = 2.90, v_{wire} = 249 ipm
Avg droplet detach time = 2.5 msec.
Avg droplet detach frequency = 400 Hz
Avg drop diameter = 0.05 in
frame time = 0.167 msec.

from the electrode to base plate with no significant plasma jet or metal vapor deflecting forces present. This conclusion is supported by the fact that even the small secondary drops are transferred without spatter formation due to plasma or metal vapor jet deflection. The anode spot (area of high current density) on the electrode covers almost one half of the droplet surface as the drop forms, while the cathode spot is large and spread out at the base plate. The large areas of both anode and cathode spots result in stable arc formation at both high and low current during pulsed current welding as well as during DC welding. This type of arc is indicative of the normal mode arc discussed in Section 2.2. Apparently, the current carrying area of the droplet is spread out and stable, i.e., made up of many small anode spots, resulting in steady low magnitude plasma and metal vapor jet forces. This is contrary to experience with titanium where one or two high intensity anode and cathode spots form resulting in strong plasma and metal vapor jet forces.

Both DC current and base pulsed current levels were well above the transition current for aluminum of 124 Amps [52]. The mode of transfer in all cases was observed to be spray mode as shown in Figure 11 [18]. These results are consistent with results of high speed movies of aluminum reported in Reference 52. It was concluded that metal

vapors were present in the arc column during metal transfer due to the abundance of black oxide soot forming next to the weld. The source of vaporization was probably the anode spot area on the surface of the droplet.

Pulsed current GMA welding of aluminum appears to offer the advantage over DC GMA welding by providing the means to achieve single drop-per-pulse transfer. As reported in the literature (see Section 4.1), this type of weld metal transfer control allows the use of lower heat inputs, making out-of-position welding and welding of thin sheet easier to control.

7.3.2 Effect of Shield Gas Flow Rate and O_2 Content on Porosity and Cathodic Cleaning

It is a well known effect that the surface ahead of the arc in reverse polarity welding of aluminum is cleaned of oxides. This same effect is not present on the base plate in straight polarity welding. Thus, this phenomena has been termed cathodic cleaning. W. Mantel describes this phenomena as resulting from the preferential formation of cathode spots at the edges of the arc column due to the superior electron emitting power of oxides compard to pure metal [53]. The spots formed on these oxides reach sufficient temperatures to cause evaporation of metal underneath the oxides which expand and blow the oxides

from the surface [53].

H. E. Pattee, et al., provide an alternate explanation based on argon sputtering of the oxide film [54]. This explanation is based on observations that the cleaning effect on aluminum in reverse polarity welding occurs only with argon shielding gas. Argon sputtering is simply the blowing away of surface material due to an exchange of momentum from an impinging ionized gas stream on the surface of the material being sputtered [55]. These explanations appear to be compatible in that it would be expected that areas of high current density such as cathode spots forming on oxide films would attract a high velocity stream of ionized gas, i.e., plasma from the arc column.

Regardless of the mechanism, this self-cleaning action provides a cleaned metal surface for welding. H. E. Pattee notes that the phenomena applied to metal surfaces of aluminum with a plasma torch may provide an efficient method of surface cleaning before welding [54].

This phenomena was observed in the experimental work for this thesis to be a function of both argon flow rate and oxygen content of argon at low flow rate. Figure 38 shows the width of cleaned surface that extends in front of the weld pool as a function of argon shielding gas flow rate. It is seen that at stagnant or low flow rate <0.125 cfm, little or no cleaning occurs, and nonuniform and porous

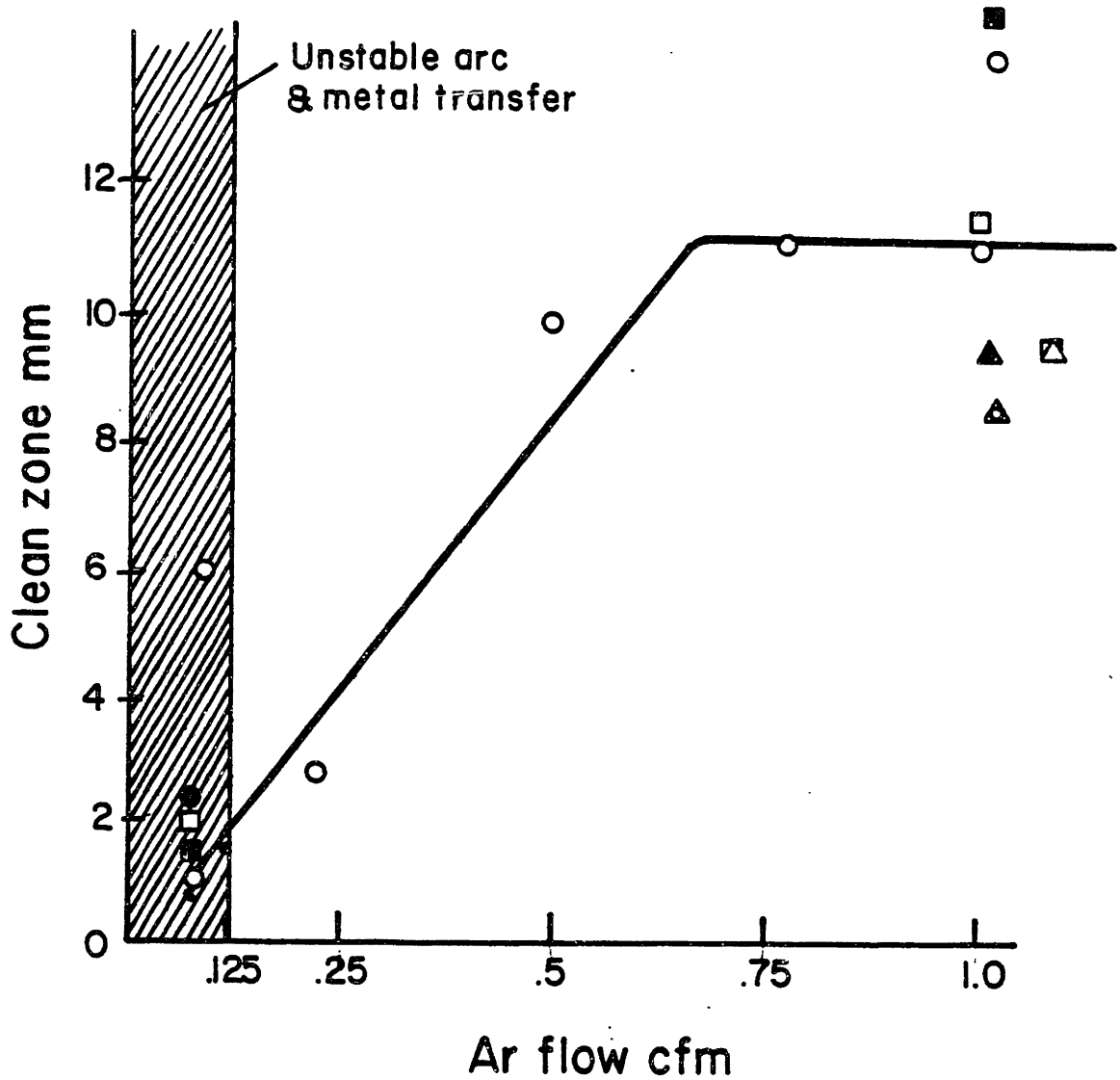

o 0.0 O_2 added

x 80 cc/min O_2 added to shield

\+ 80 cc/min O_2 added around shield

Y 80 cc/min O_2 added to shield and 80 cc/min O_2 added around shield

o, x, + condition with hydrocarbon contamination of surface (oil)

Figure 38: Cathodically cleaned zone width versus Argon flow rate.

welds with a drossy appearing surface result. As argon flow rate is increased, the width of the cleaned zone increases and the weld bead surface appears clean and shiny. Finally, above a flow of about 0.5 cfm, the width of the cleaned zone remains constant and black oxide soot from weld metal vaporization in the arc column is carried away from the weld bead by the flow of shield gas. Figure 39 shows increasing cleaned zone widths on samples welded with increasing shield gas flow rate. It should be noted that the other points on the graph representing argon with various additions of O_2 in the shield gas also follow the trends described above.

These observations are consistent with Pattee et al.'s explanation of cathodic cleaning in that the efficiency of the sputtering increase as the flux of ionized gas atoms hitting the plate surface increases, i.e., higher flow rates [54]. Furthermore, the result that stagnant or low flow rates result in nonuniform welds with porosity and a drossy surface appears to be consistent with no cleaning action, thereby leaving the oxide film to contaminate the weld bead. The nonuniform appearance may stem from poor wetting of the molten weld pool due to surface oxide contamination. Hydrocarbons and moisture entrained in the film can explain the occurrence of porosity. According to Martuknitz, et al., the source of porosity in aluminum welds is hydrogen contamination from either the weld rod or base metal [56].

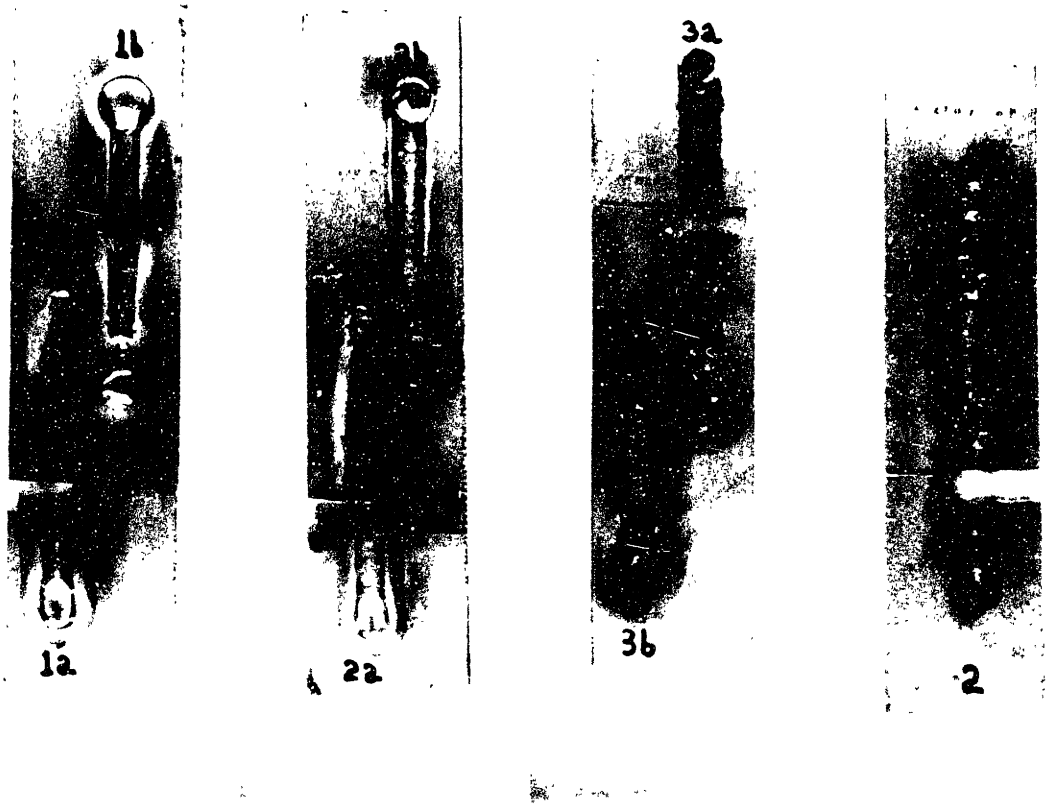

Figure 39: Increasing cleaned zone width on weld samples with increasing shield gas flow rate.

I_b = all A, I_p = 300 A, I_{av} = 250 A, square wave, 500 Hz

2 = 0.0 cfm Ar

3b = 0.063 cfm Ar

3a = 0.125 cfm Ar

2b = 0.25 cfm Ar

2a = 0.50 cfm Ar

1b = 0.75 cfm Ar

1a = 1.00 cfm Ar

It appears that argon shield gas flow is necessary for good quality welds in aluminum in an argon purged containment. Since welding of aluminum is normally done in the air, sufficient argon flow rates, normally provided to keep air from the molten weld pool, are present to provide adequate cathodic cleaning for good weld pool wetting and minimal porosity formation.

Figure 40 provides a further insight into the nature of the cathodic cleaning phenomena in reverse polarity welding of aluminum. This figure shows that the width of the clean zone at low flow rates is a functin of argon shield gas oxygen content. As increasing levels of O_2 are added to the shield gas, the width of the cleaning zone increases to a threshold level. Figure 41 shows increasing cleaned zone widths on samples welded with low shielded gas flow rate and increasing O_2 shield gas content. This effect can be explained by the fact that O_2 is commonly added to argon atmospheres in analytical tools using sputtering such as Secondary Ion Mass Spectroscopy (SIMS) to increase the sputtering yield of argon [57]. Furthermore, the presence of O_2 at the site of sputtering may result in chemical reactions at the surface which result in enhanced or reactive sputtering. Under normal GMA welding conditions, the air around the arc column would provide a ready source of O_2 for enhancing argon sputtering yields.

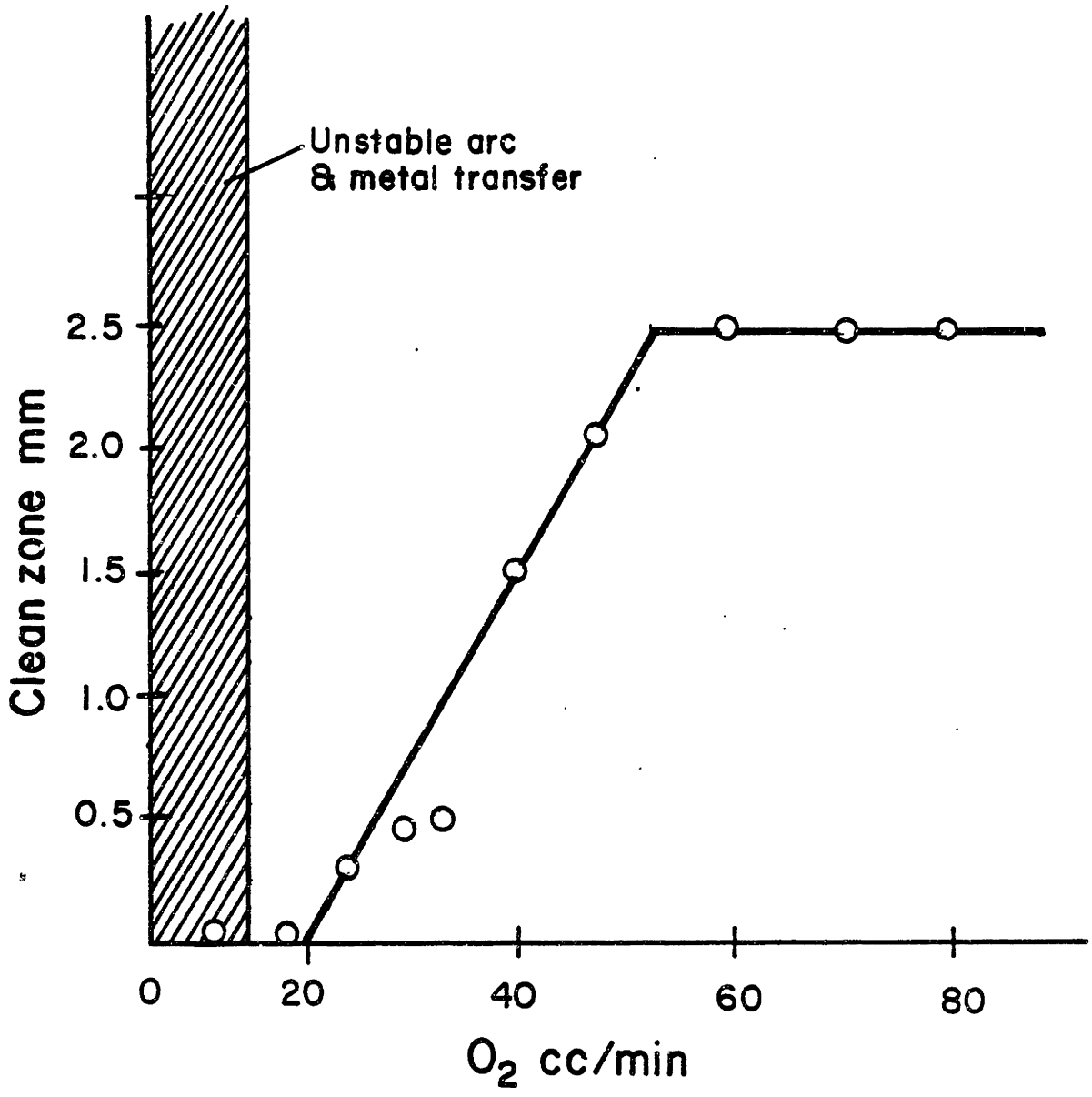

Figure 40: Cathodically cleaned zone width versus shield gas O_2 at low flow rate.

Figure 41: Increasing cleaned zone width on samples welded with low shield gas flow rate (0.125 cfm) and increasing O_2 shield gas content.

1a = 25 cc/min O_2

1b = 30 cc/min O_2

3a = 50 cc/min O_2

3b = 60 cc/min O_2

7.4 Conclusions

The following conclusions were made regarding the above described work:

1. Controlled uniform spray transfer with no spatter is achieved with GMA welding of aluminum at 250 ADC or with pulsed current with I_{av} = 250 A. As the frequency increaes, the frequency of metal transfer approaches that of DC welding at the corresponding average current.

2. In an argon purged environment at zero flow rate, GMA weld metal transfer is unstable, weld pool wetting nonuniform, and gross weld porosity is present with no cathodic cleaning. As flow rates are increased, the cathodically cleaned zone width increases and porosity is eliminated. A threshold flow rate is reached where no further increase in the cleaned zone width occurs.

3. Adding 0_2 to the argon shielding gas at low flow rate appears to stabilize metal transfer and increase the width of cathodic cleaning. This may be the result of either or both of the following

phenomena:

(a) Increased sputtering yield from argon shield gas due to small amounts of O_2.

(b) Surface reaction of O_2 with hydrated oxide species and/or hydrocarbon contaminants removing oxides and contaminants from the surface.

8.0 PULSED GMA WELDING OF TITANIUM

Thus far, this thesis has reviewed the principles and past experience with the pulsed gas metal arc (GMA) welding process and discussed its applicability for use with titanium. A major problem associated with GMA welding of titanium is lack of control of weld metal transfer and spatter formation. Spatter consists of small droplets of molten weld metal which are ejected from the arc sometime between droplet formation, droplet transfer, and droplet incorporation into the weld pool. A high speed photographic technique was described that was developed to observe the process of weld metal transfer in order to understand the origin of forces that result in spatter and nonuniform bead formation. Titanium bead-on-plate welding experiments were performed and analyzed using this technique. This section will describe and discuss the results of these experiments.

8.1 Goals

Gas metal arc (GMA) welding of titanium was investigated using an analog current regulator. This current regulator has the capability of producing pulsed current wave forms of practically any shape available from a signal generator. The objective of this work was to achieve control of metal transfer so that the molten filler metal is

incorporated into the weld pool in a controlled, calm, orderly fashion. Normally, with DC current conventional GMA processes, uncontrolled and unbalanced arc forces tend to hamper controlled metal transfer when welding titanium. These unbalanced forces result in weld pool turbulance, uncontrolled droplet transfer and ultimately nonuniform weld bead formation and spatter. The use of rectangular pulsed current waveforms was investigated with respect to metal transfer control and ultimate weld bead shape uniformity.

8.2 Experimental Design

An experimental space consisting of three independent variables including base current (I_b), peak current (I_p) and frequency (f), keeping the average current (I_{av}) constant was investigated. Average current was chosen based on the minimum DC level which produced a desired weld bead size and upon an average current level above the reported transition current of 215 Amps required for spray transfer [52]. By changing the energy input at constant I_{av} using rectangular pulsed wave forms, changes in metal droplet transfer and resulting weld bead shape and uniformity were recorded. The experimental techniques used for recording metal droplet transfer consisted of the high speed photographic technique (6000 frames per second) described in Section 6.3 which recorded the size and frequency of formation and detachment

of individual droplets. The current signal (high or low) was recorded on the film next to each high speed picture to allow real time analysis of droplet transfer as a function of pulsed current input.

Data was taken using a multi-frequency level Box-Behnken design space grid allowing for statistical analysis of dependent variables including droplet transfer size, droplet spatter size, percent of droplet transfer rejected from weld pool as spatter, and droplet transfer frequency [58]. In addition, wire feed rate, spatter per square inch and weld bead width were also analyzed. The geometry of the Box-Behnken experimental design space is shown in Figure 42 [58] with three levels. The axes of this design space are peak current (I_p), base current (I_b), and frequency (f). Both I_p and I_b extend three levels (or one box) along each axis, respectively. Frequency, however, extends seven levels along its axis at increments of about half decades from 5 Hz to 5000 Hz forming three connected Box-Behnken design spaces. The base and peak limits of the experimental space were chosen to cover the range in pulsed current parameters that were possible with the available equipment. The bounds of each experimental space are defined in Figure 42 [58].

The Box-Behnken experimental design space provides two distinct advantages in data analysis. The first advantage

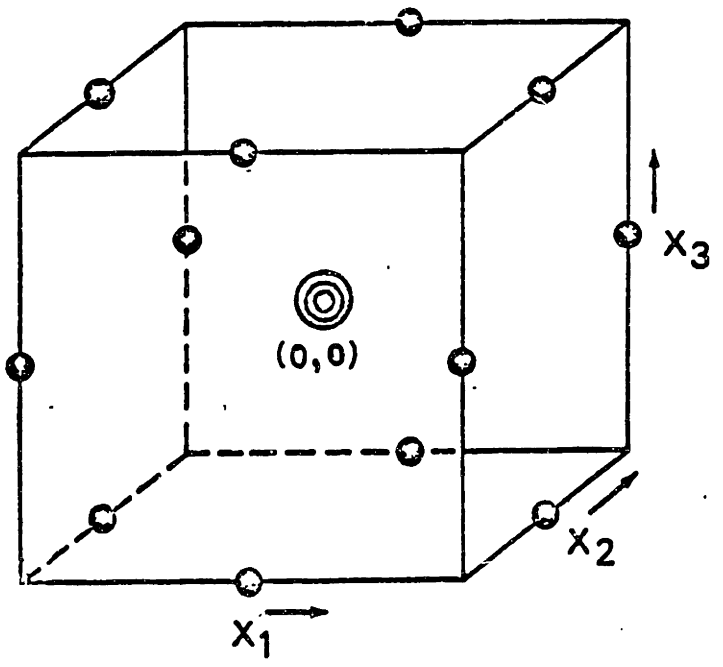

Figure 42: Box-Behnken experimental design space with ranges of independent variables for three adjoining design spaces [58].

	Scale Value		
	-1.0	0	+1.0
Independent Variable			
I_b Amps all design spaces	50	125	250
I_p Amps all design spaces	300	725	1150
f Hz design space a	5	15	50
design space b	50	150	500
design space c	500	1500	5000

is that it is a symmetric, as well as rotatable, design space with all points lying equal distance from the center point [58]. The second advantage is that the center points are replicated to provide an indication of experimental error and are sufficient in number to give a relatively constant prediction variance as a function of distance from the center within the design space [58]. Thus, this experimental design maximizes the information attainable with the least number of data points required. To ensure that systematic error due to experimental order was not introduced, the order of experimental trials was randomized.

A multiple regression analysis routine available on MIT's computer system called MINITAB was used to evaluate the response of each dependent variable with respect to the three independent variables defining the experimental space [59]. This routine provides coefficients to allow prediction of a dependent variable as a second order polynomial function of the independent variables as follows:

$$y=ax_1^2+bx_1+cx_2^2+dx_2+ex_3^2+fx_3+gx_1x_2+hx_1x_3+ix_2x_3+j$$

where

y = dependent variable or response

x_1, x_2, x_3 = independent variables

a,b,c,d,e,f,g,h,i,j = multiple regresion coefficients.

A plotting routine was then used to evaluate the isoresponse of each dependent variable as a function of I_b and I_p. By extending the lines of isoresponse in the frequency dimension, the response surface behavior of each dependent variable was defined within the experimental space.

All welds were performed on 7/8" thick titanium alloy Ti-6Al-4V plate (Reactive Metals heat no. HT-295 426-01-00) with 1/16" titanium weld wire (Astro Metallurgical Corp. heat no. F248). Weld samples were cut into 3" x 12" pieces to allow for easy handling inside the glove box. Each weld sample contained two welds, approximately 5 to 6 inches long. Welds were started at the center of the plate and extended to near the plate end so that the starting portions of each weld overlapped. This left about 5 inches of weld for evaluation relatively free from effects of spatter and soot from the prior weld. All weld samples were grit blasted to remove mill scale from the surface. Each sample was then skim ground using a pneumatic grinder with abrasive belt. Skim grinding was performed shortly before welding (same day) and care was taken to ensure that burning of the sample surface did not occur. Microscopic and chemical analysis of the surface of a plate sample prepared according to the above procedure showed no significant transfer of grinding belt contamination from the skim grinding

operation. To ensure that the weld wire used in these experiments was not contaminated with hydrocarbons, the wire spool was vapor degreased in trichloroethylene.

All welds were performed in the glove box drilab environment. Argon gas was fed into the glove box at 0.125 cfm and bled from the glove box by a vent valve at a slightly lower rate to maintain a slight positive pressure. The argon supplied by a liquid argon tank contained a nominal oxygen content of 100 ppm. It was found that high argon torch gas flow rates resulted in contaminated weld beads as evidenced by a straw colored appearance of the weld bead and the formation of white oxide soot (probably TiO_2). With no argon torch gas flow rate, clean silvery weld beads were produced when a stable argon atmosphere was maintained in the glove box by feed and bleed at 0.125 cfm as noted above. Therefore, since torch gas flow rate was not required, a torch with no gas cup similar to that shown in Figure 29b was used.

The torch contact tube was adjusted to provide a 5/8" gap with the weld sample. Standard copper contact tubes were used with an inside diameter of 0.071 inches. Contact tubes lasted on the average of 8 to 10 welds until either arc instability or contact tube tip erosion and wear caused burn back. The subject of contact tube erosion and wear is discussed in Appendix.

All welds were performed with a travel speed of 18 ipm. The wire feed speed adjustment on the central weld controller was adjusted after the arc was started to provide a reasonable arc gap without causing contact tube arcing and burnback. After a stable arc was achieved, the data acquisition system was actuated by a bank of three switches as described in Section 6.2.5.

8.3 Results

The baseline behavior of weld metal transfer in GMA welding of titanium was established by evaluating high speed movies (6000 frames per second) of direct current welds in both reverse and straight polarity. With the baseline behavior established, pulsed current waveforms in reverse polarity were evaluated with the same high speed photographic technique to determine changes in weld metal transfer characteristics due to the pulsed current waveforms. Finally, welds performed using a commercial pulsed current power supply made by Dimetrics and described in Section 4.2, were evaluated. The following section will discuss the results of each of these areas.

8.3.1 Reverse Polarity versus Straight Polarity

The baseline behavior of weld metal transfer in

GMA welding of titanium was established using direct current in reverse and straight polarity. The following sections describe the baseline weld metal transfer behavior:

Reverse Polarity

Weld beads produced with direct current in reverse polarity at 250 and 300 Amps are shown in Figure 43a. The weld metal transfer is characterized by a large fraction of the transferred metal resulting in spatter around the weld bead. At 300 Amps the spatter appears less severe but the wire feed rates at currents in this range begin to fall outside the capability of most commercial equipment, i.e., wire feed rates greater than 300 ipm.

Figure 44 shows the weld metal transfer sequence as seen with high speed photography that leads to the observed uncontrolled weld metal spatter at 250 Amps. Droplets about 1.3 times larger than the wire diameter are formed at the electrode tip. One or two stable cathode plasma jets form on the weld pool, creating hydrodynamic drag and momentum transfer forces in the direction opposing metal transfer. A weaker anode plasma jet forms on the drop surface and appears to interact with the cathode jets creating at times a deflected plasma plume off the axis of the weld wire. The droplet necks down and finally breaks off due to surface tension and Lorentz constricting forces from the high

Figure 43: Titanium weld beads produced with direct current in reverse polarity (a) and straight polarity (b).

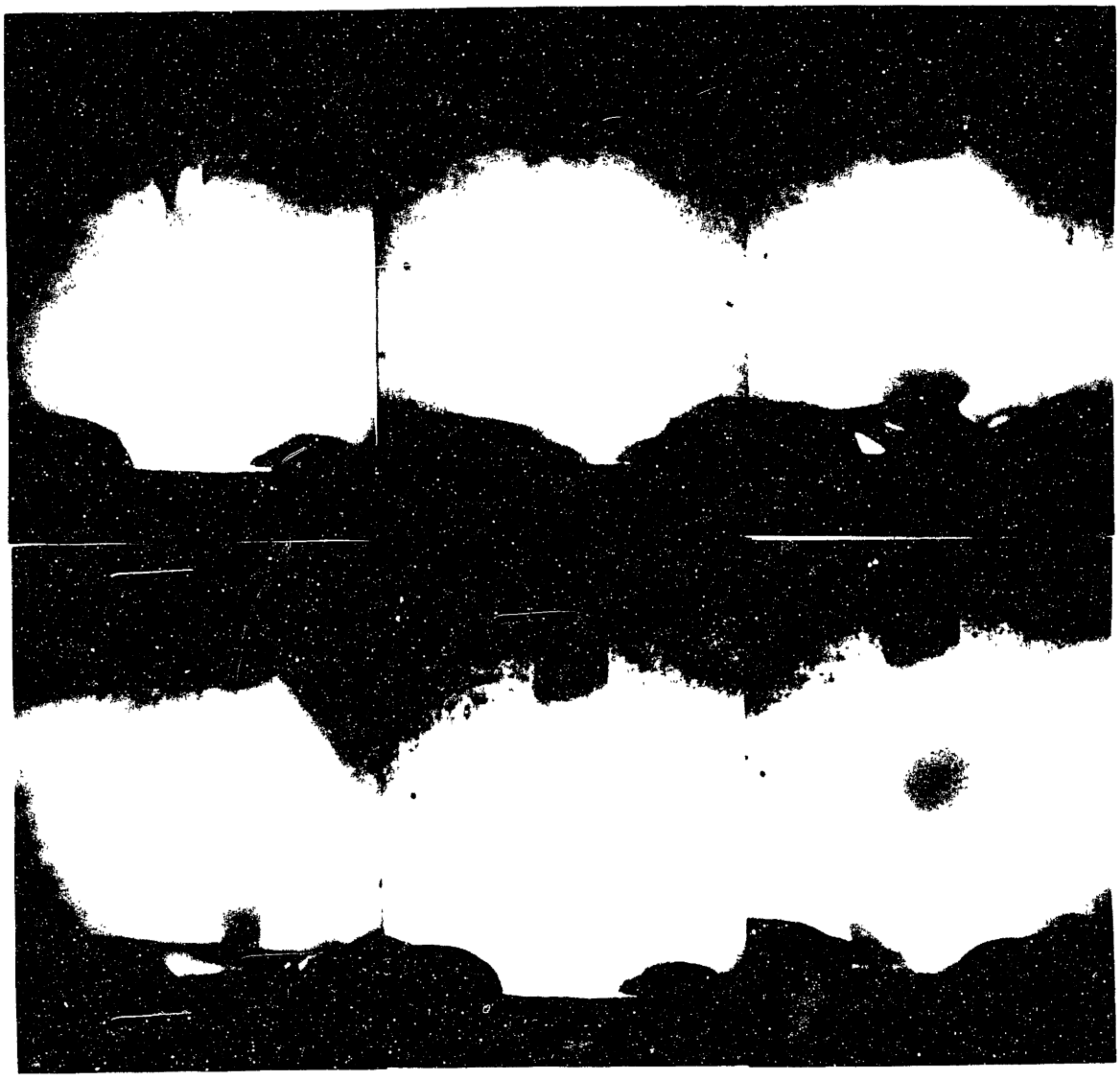

Figure 44: Titanium weld metal transfer with DC in reverse polarity.
I = 250 ADC REP, V = 27.5 V, v_{wire} = 229 ipm
Avg drop detach time = 27.5 msec.
Avg drop detach frequency = 36.4 Hz
Avg drop diameter = 0.0854
Avg spatter diameter = 0.0458
Percent of transfer as spatter = 15.4
Frame time = 0.167 msec.

current density at the anode spot.

The droplet appears to transfer from the electrode to the weld pool with occasional deflections from cathode plasma jets. The droplet then lands on the weld pool. Up to this point, no spatter has formed. The droplet appears to anchor on the weld pool due to surface tension forces. The droplet size decreases as the molten metal in the drop is consumed by the weld pool. When the drop has been reduced to about 0.5 times the original diameter, Lorentz constricting forces break the droplet from the weld pool (see Figure 7). As the droplet breaks off, a cathode plasma jet forms at the droplet/weld pool interface which accelerates the droplet up and away from the weld pool, creating spatter. It appears reasonable to assume that spatter formation can be decreased or eliminated by reducing the magnitude of the Lorentz forces that forms and ejects the spatter droplet from the weld pool. Since the Lorentz forces are proportional to I^2, reducing the current by pulsing during droplet incorporation into the weld pool should reduce or eliminate spatter.

Straight Polarity

Weld beads produced with direct current in straight polarity at 250 and 300 Amps are shown in Figure 43b. The weld metal transfer is completely uncontrollable and little

if any weld metal is transferred to the weld pool. Figure 45 shows the weld metal droplet formation and detachment sequence that leads to the observed uncontrolled weld metal transfer at 250 Amps. A strong cathode plasma jet forms on the droplet surface. This plasma jet deflects the droplet away from the weld pool by means of a momentum transfer reaction force from the high velocity gas jet. The droplet eventually breaks off but is immediately deflected away from the weld pool due to the plasma jet reaction force.

Controllable GMA welding of titanium appears to be unfeasible in straight polarity unless very low current levels are used to reduce the magnitude of the Lorentz forces creating the cathode plasma jet. These observations are consistent with those of Salter, et al. [25].

Observations of titanium GMA weld metal transfer in both reverse and straight polarity indicate the formation of strong cathode plasma jets that create forces affecting weld metal transfer. These plasma jets form in one spot and wander or rotate around the arc column at a rate on the same order of magnitude as the frequency of droplet transfer. This strong cathode plasma jet formation is not observed with aluminum. The explanation for these different behaviors may lie in a balance of driving forces which result in plasma jet formation. The Lorentz forces in the arc column are the initial driving force for formation of a

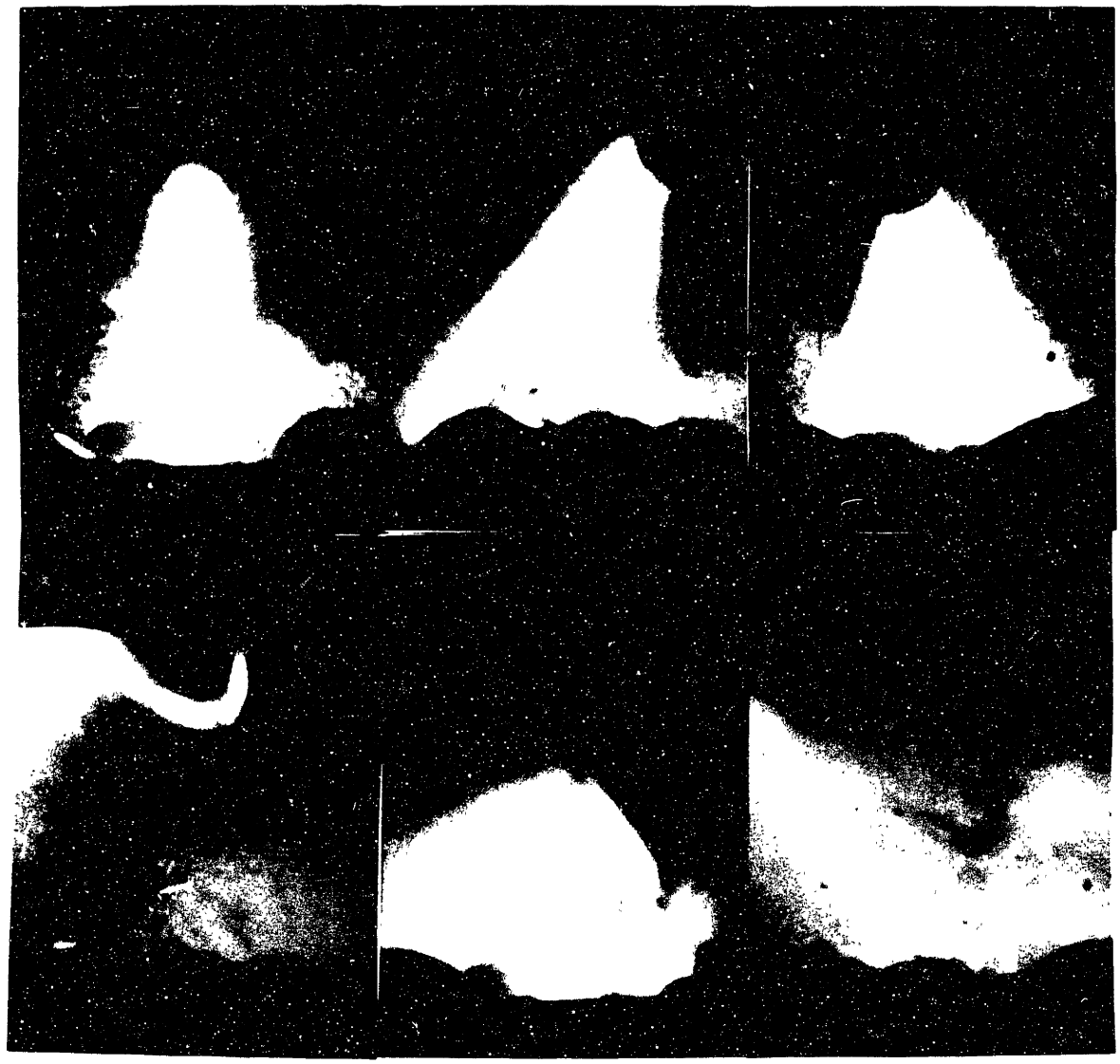

Figure 45: Titanium weld metal transfer with DC in straight polarity.
I = 250 ADC SEN, V = 23.0 V, v_{wire} = 177 ipm
Percent of transfer as spatter ≃ 100
frame time = 0.167 msec.

plasma jet at the region of high current density on the drop or weld pool surface. These forces cause a differential pressure in the plasma creating a high speed jet of plasma emanating from the high current density spot. This differential pressure can be represented as a stable energy well. A second driving force determines whether or not this high current density spot remains stable in the well, or whether it breaks up into many small spots over a larger area. This second driving force results from energy minimization of the arc column by choosing the path of least resistance for current flow. For materials such as aluminum where oxides float on the surface of the weld pool and molten droplet, the anode and cathode spots spread out into many small spots which follow the oxides floating on the weld pool surface. This lowers the energy of the arc column since oxides are more efficient electron emitters than liquid metals. This driving force can be represented by an unstable energy peak. The result is a distribution of small spots randomly following oxides floating on the liquid metal. The plasma jet forces from these small weak plasma jets distributed over a large area have a small but steady effect on weld metal transfer.

For materials such as titanium where oxides dissolve in the molten metal, no driving force exists to break the strong anode or cathode spot into many small spots. The

result is the formation of a strong stable plasma jet which wanders slowly over the molten metal creating unstable metal transfer by imposing unbalanced forces on the metal droplet during transfer. A schematic of this driving force theory for plasma jet formation is shown in Figure 46.

8.3.2 Results of Dependent Variable Multiple Regression Analysis

Titanium bead-on-plate weld tests were performed with various rectangular pulsed current waveforms according to the experimental points defined in Section 8.2 for the Box-Behnken experimental spaces. High speed pphotography was used to record metal transfer characteristics including droplet transfer size, droplet spatter size, percent of droplet transfer rejected from weld pool as spatter, and droplet transfer frequency. In addition, wire feed rate, spatter per square inch, and weld bead width were recorded. Each of these dependent variables were analyzed as a second order polynomial of the three independent variables. A multiple regression routine was used to define the response behavior at the center of each design space and the standard deviation of the response was calculated. Lines of isoresponse were then plotted at each design space center frequency, i.e., 15, 150 and 1500 Hz.

These plots were then evaluated to determine specific

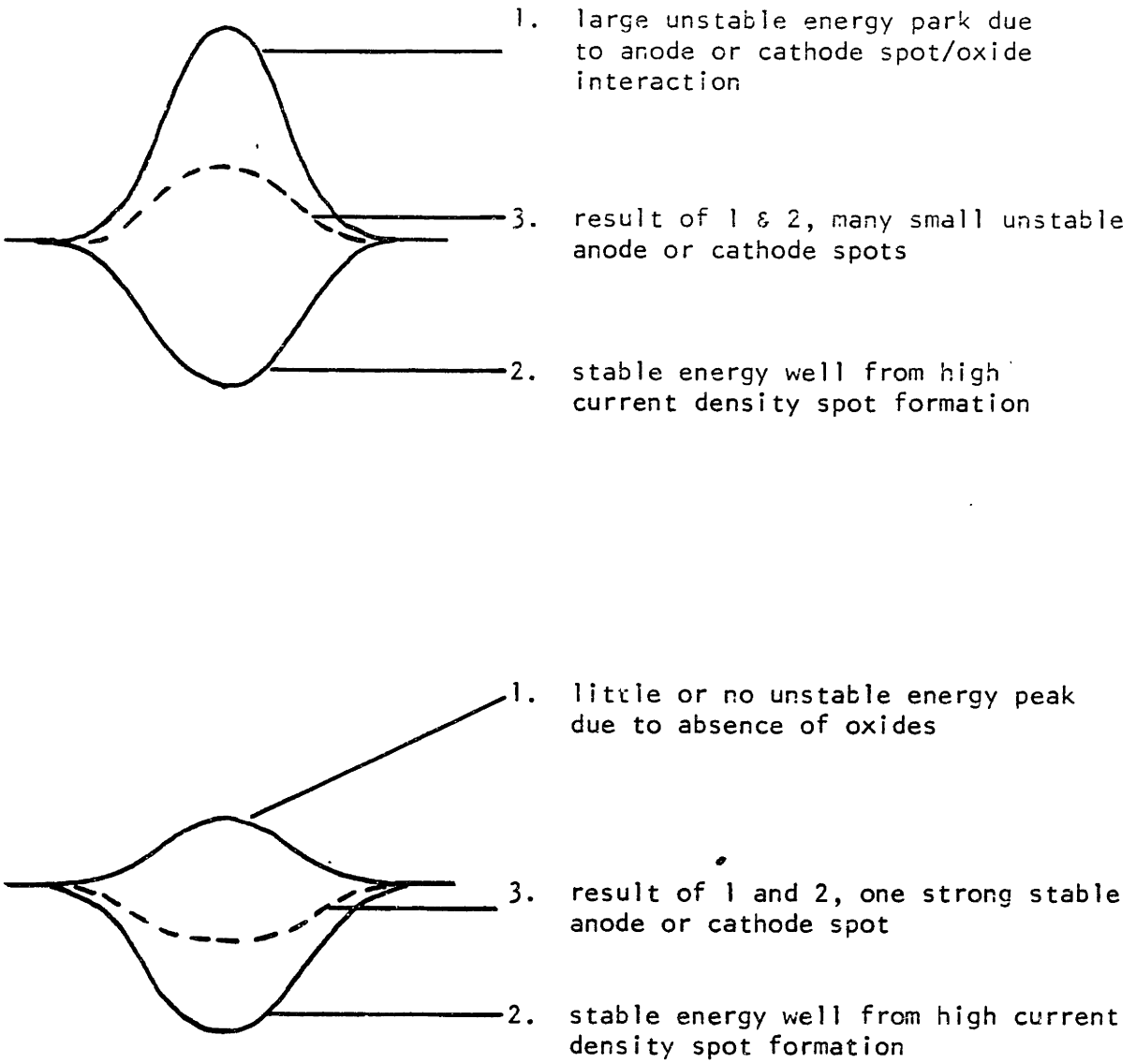

Figure 46: Driving force balance for stable (a) or unstable (b) plasma jet formation.

regions within the design space which would provide increased weld metal transfer control. The following sections will discuss the response of each dependent variable.

Droplet Transfer Size

At low pulsing frequency (15 Hz), droplet transfer size appears to reach a maximum in the low base current (100 A) high peak current (800 A) corner region of the experimental space (see Figure 47a). Apparently, short high current pulses at low base current do not provide sufficient energy to pinch off small droplets. At intermediate pulsing frequencies (150 Hz), a saddle of minimum droplet size occurs along the diagonal from I_b = 50 A, I_p = 300 A to I_b = 200 A, I_p = 1150 A (see Figure 47b). This indicates that large, short duration current pulses at high base current or small, long duration current pulses at low base current (approaching DC) will minimize droplet size. Finally, at high pulsing frequency (1500 Hz), droplet size appears to be minimized along a saddle aligned with the I_b = 200 A side of the experimental space (see Figure 47c). With respect to frequency, droplet sizes appear to be minimized at low frequencies (15 Hz). This may be due to the fact that low pulsing frequencies more closely match the natural frequency of droplet formation (see Section on Drop

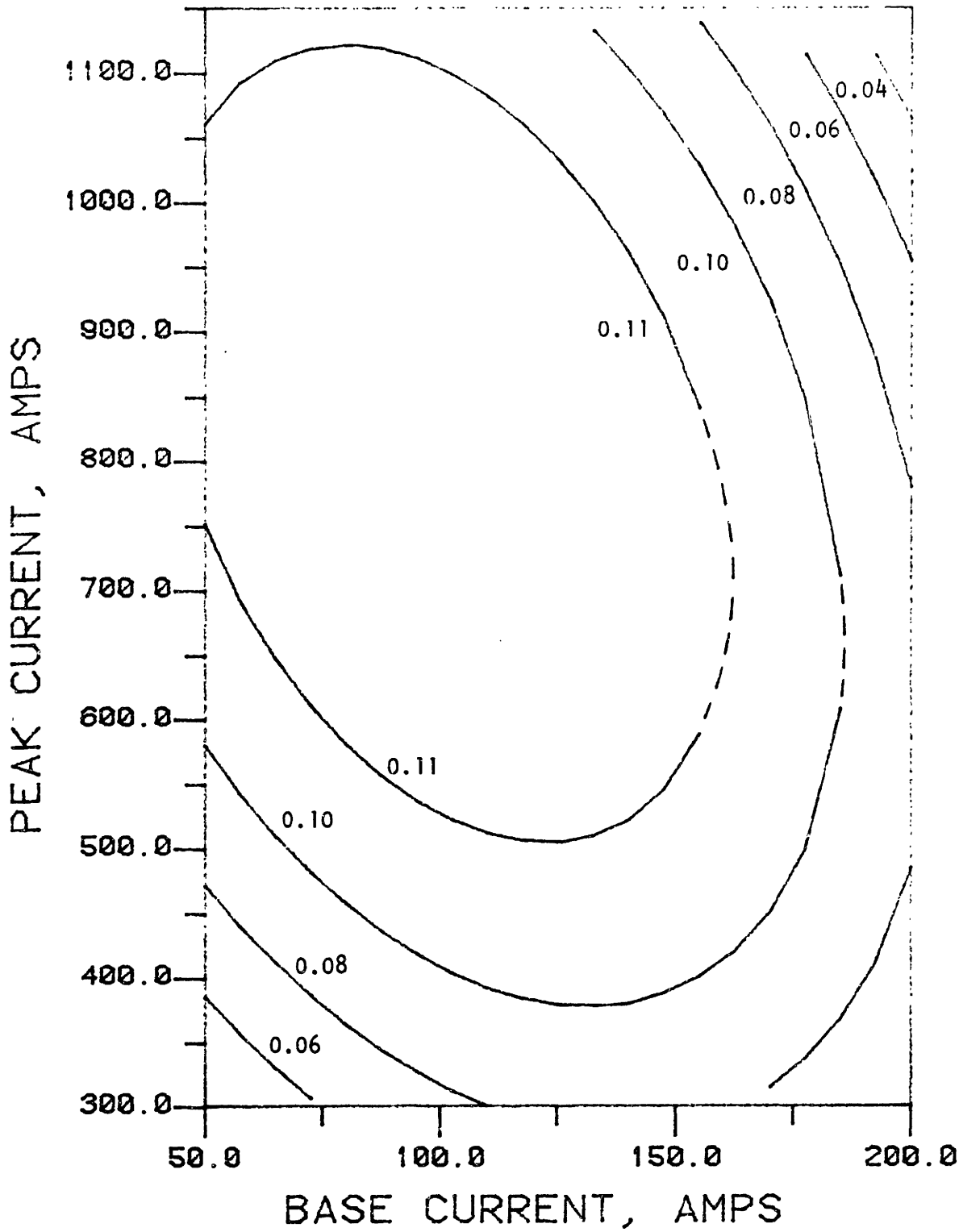

Figure 47a: Contours of constant droplet transfer size (inches) at 15 Hz
Standard deviation = 0.02866

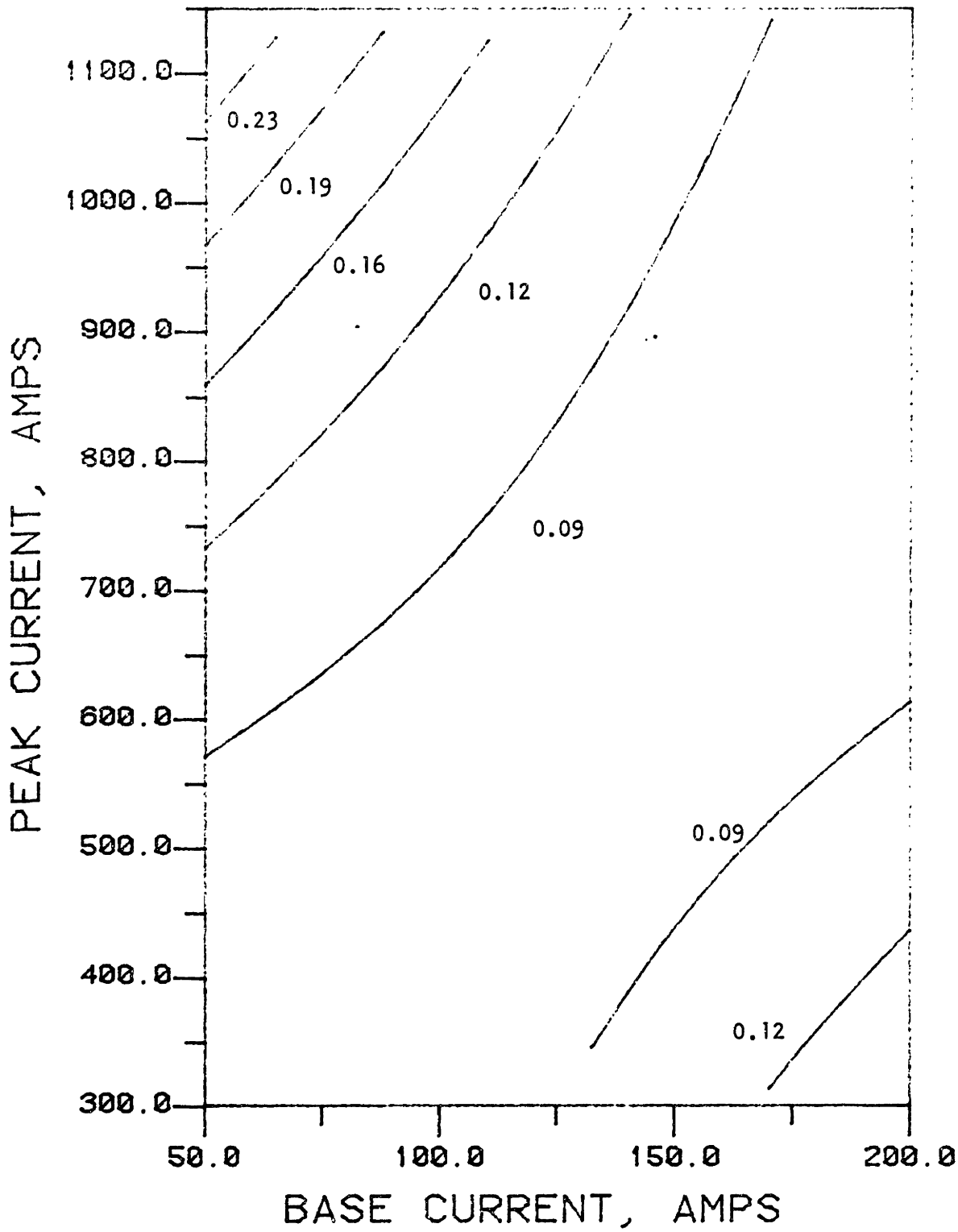

Figure 47b: Contours of constant droplet transfer size (inches) 150 Hz
Standard deviation = 0.08836

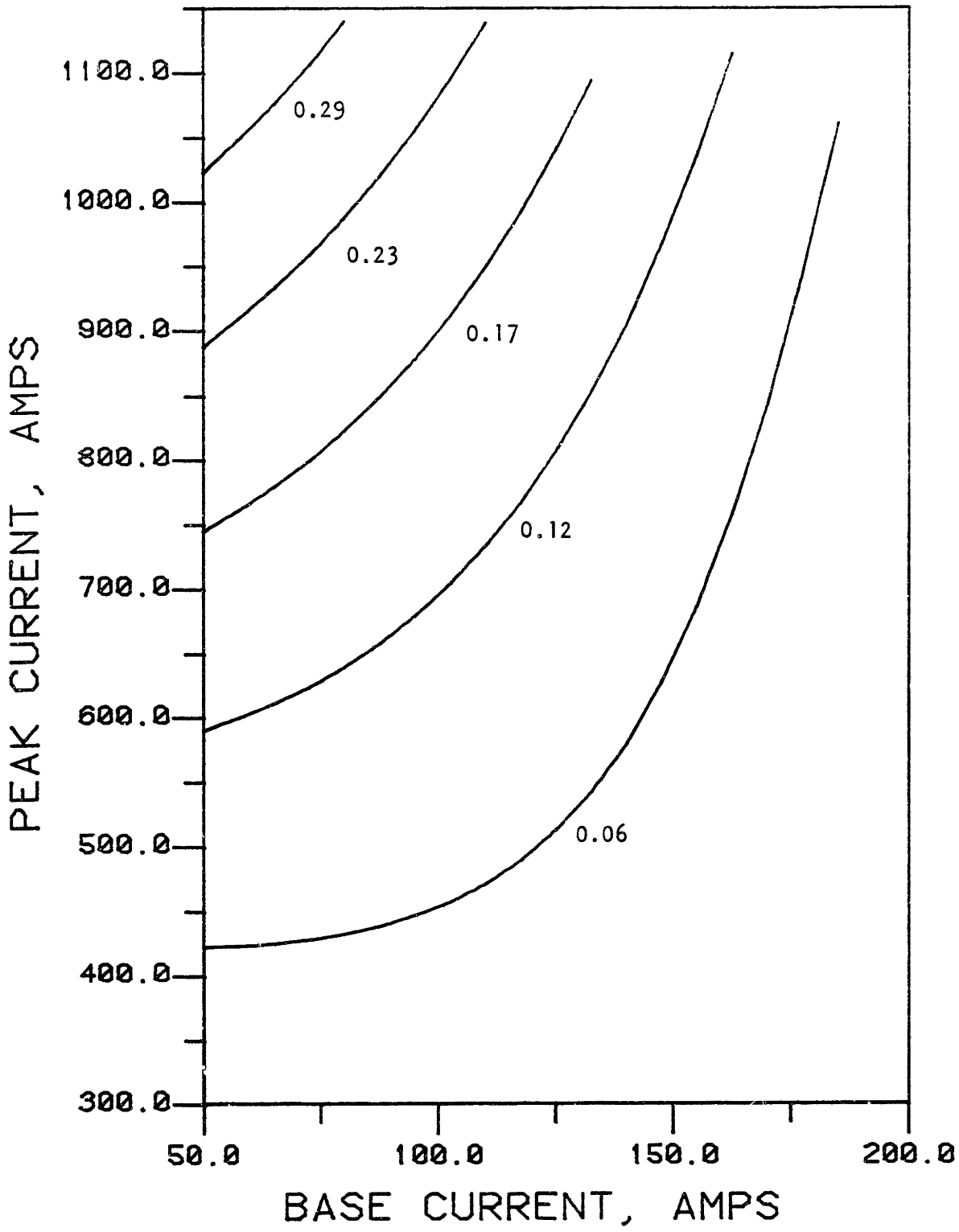

Figure 47c: Contours of constant droplet transfer size (inches) at 1500 Hz. Standard Deviation = 0.1312.

Transfer Frequency).

Droplet Spatter Size

At low pulsing frequency (15 Hz), droplet spatter size is maximized at about I_b = 150 A, I_p = 600 A near the center of the experimental space (see Figure 48a). At medium (150 Hz) and high (1500 Hz) pulsing frequencies, droplet spatter size is minimized in the region of medium base current (150 A) and high peak current (1150 A) (see Figure 48b, 48c). Droplet spatter size appears to increase slightly with increasing frequency.

Droplet Transfer Frequency

At low pulsing frequency (15 Hz), droplet transfer frequency is minimized at the center of the experimental space I_b = 125 A, I_p = 725 A (see Figure 49a). At intermediate pulsing frequency (150 Hz), droplet transfer frequency is maximized at the center of the experimental space I_b = 125 A, I_p = 725 A (see Figure 49b). Finally, at high pulsing frequency (1500 Hz), droplet transfer frequency is maximized at the low base current (50 A) and high peak current (1000 A) corner of the experimental space (see Figure 49c). Droplet transfer frequency appears to decrease slightly as pulsing frequency is increased. It should be noted that droplet transfer frequency extends from 5 to

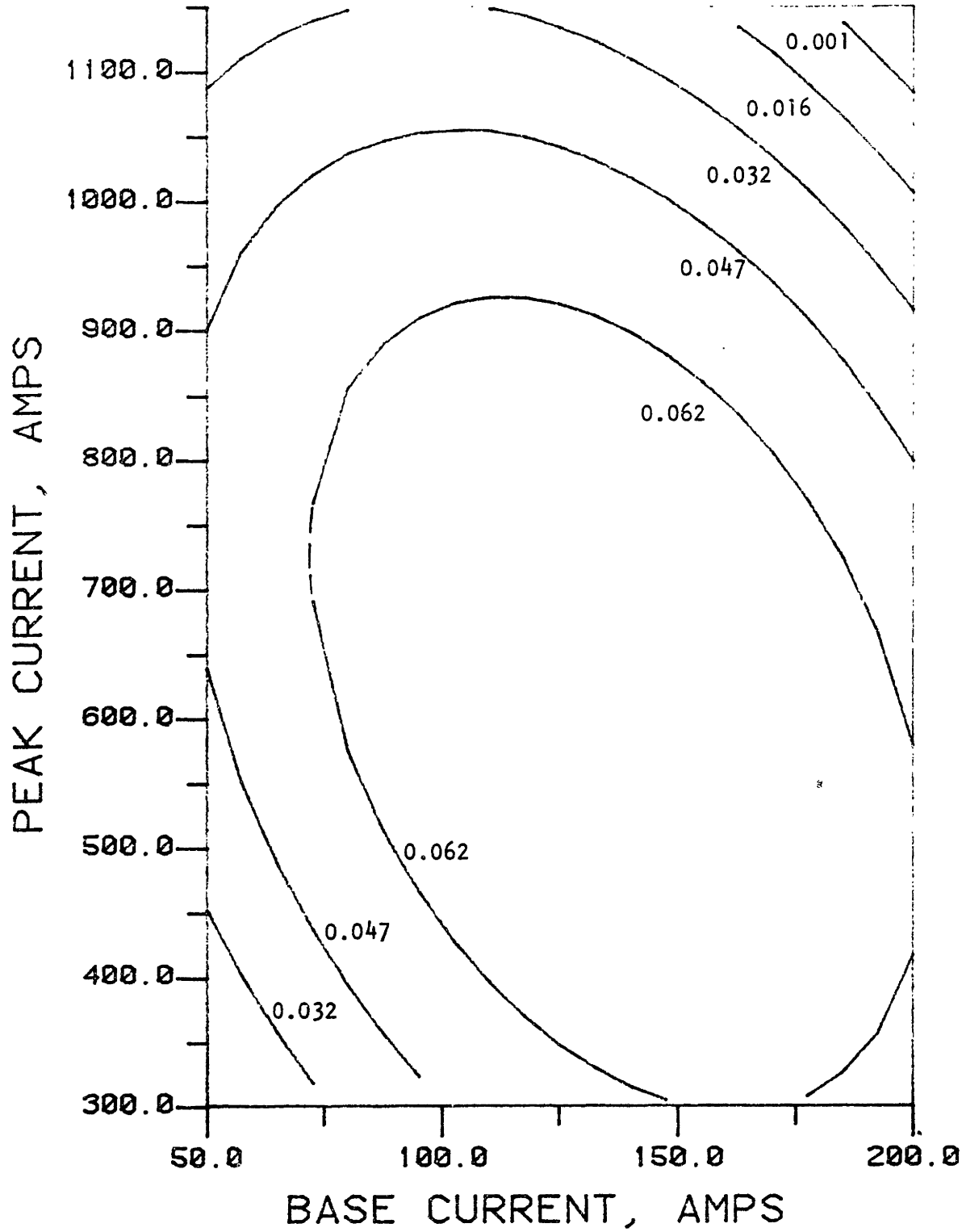

Figure 48a: Contours of constant droplet spatter size (inches) at 15 Hz. Standard deviation = 0.03302.

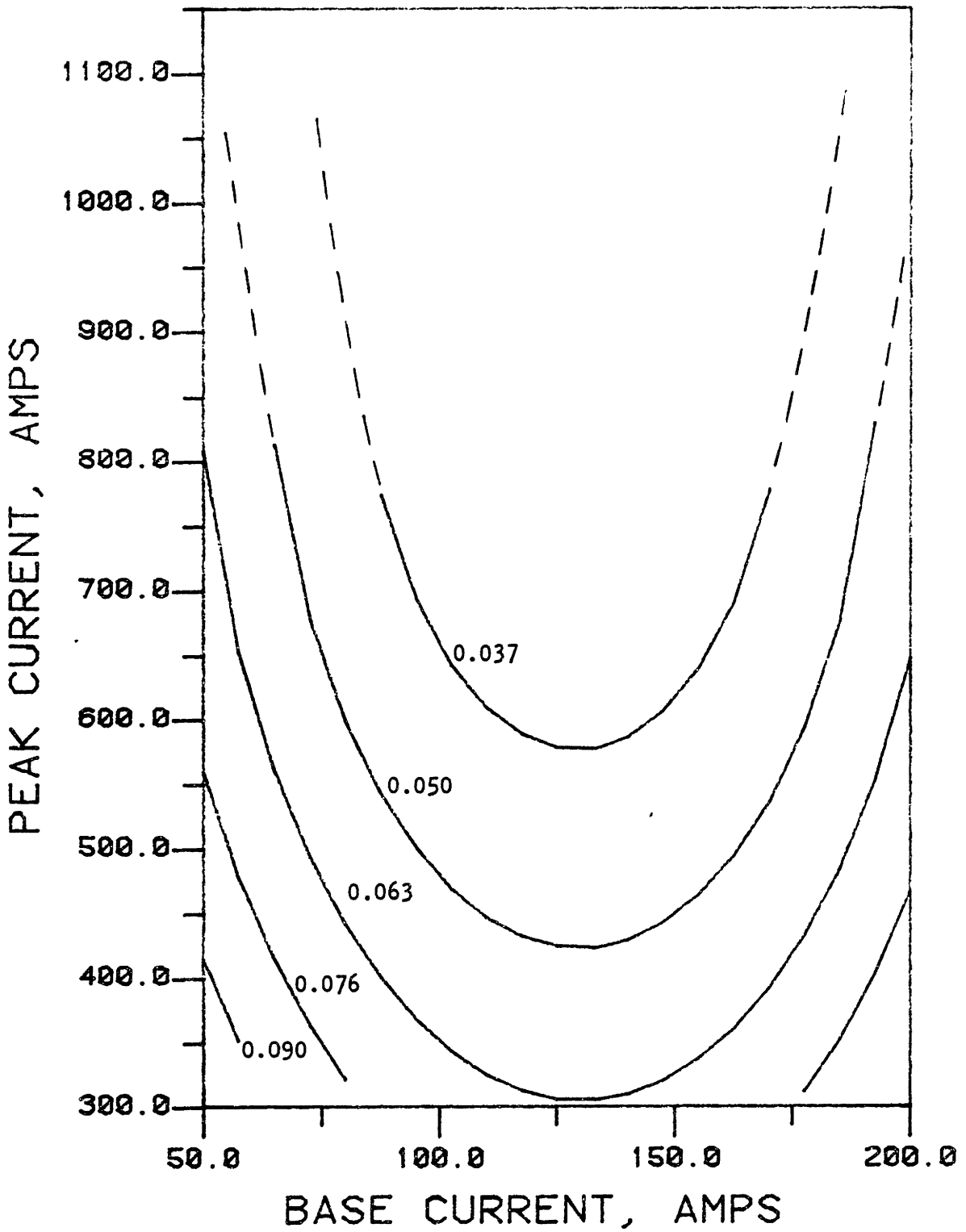

Figure 48b: Contours of constant droplet spatter size (inches) at 150 Hz. Standard deviation = 0.006394.

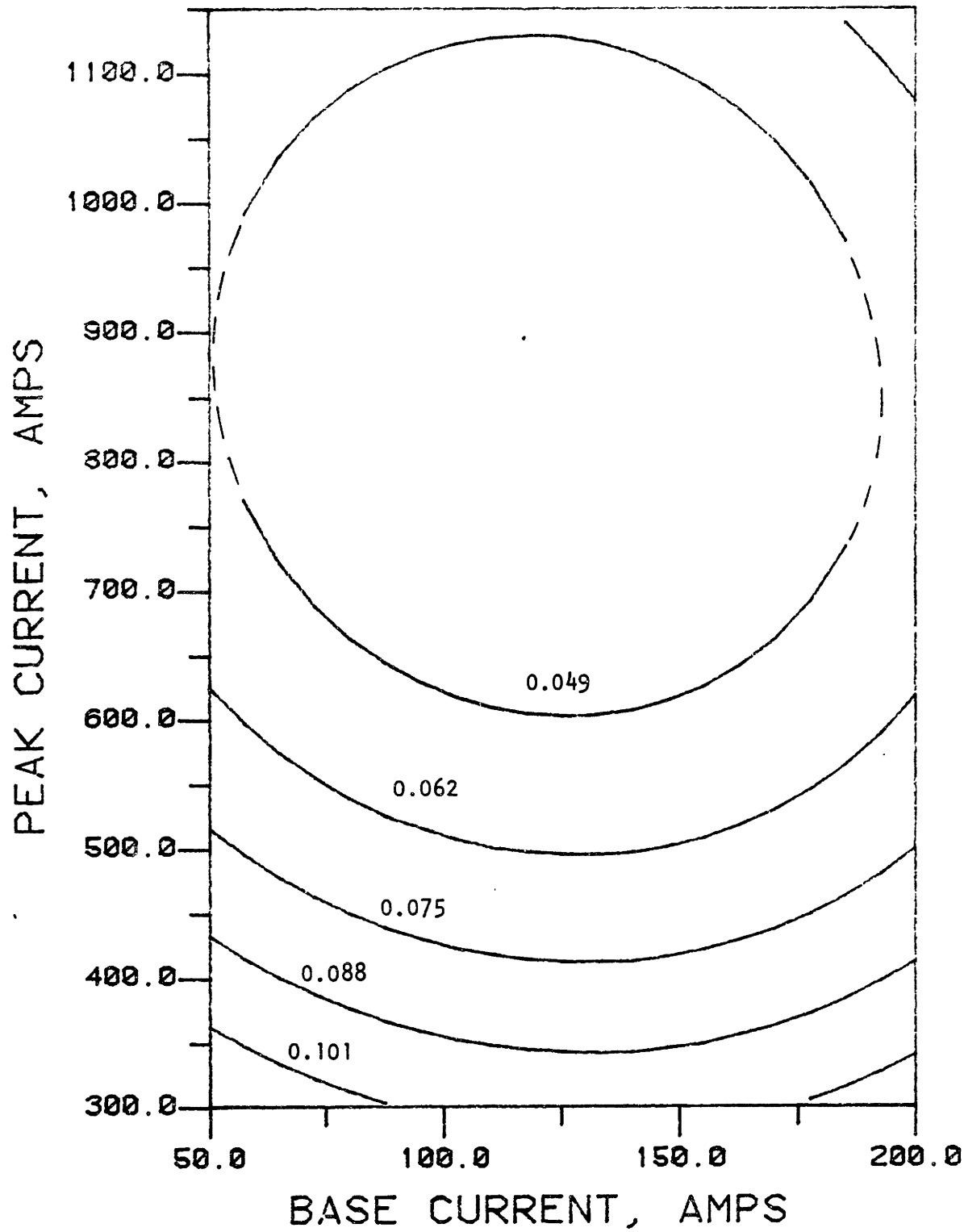

Figure 48c: Contours of constant droplet spatter size (inches) at 1500 Hz. Standard deviation = 0.01233.

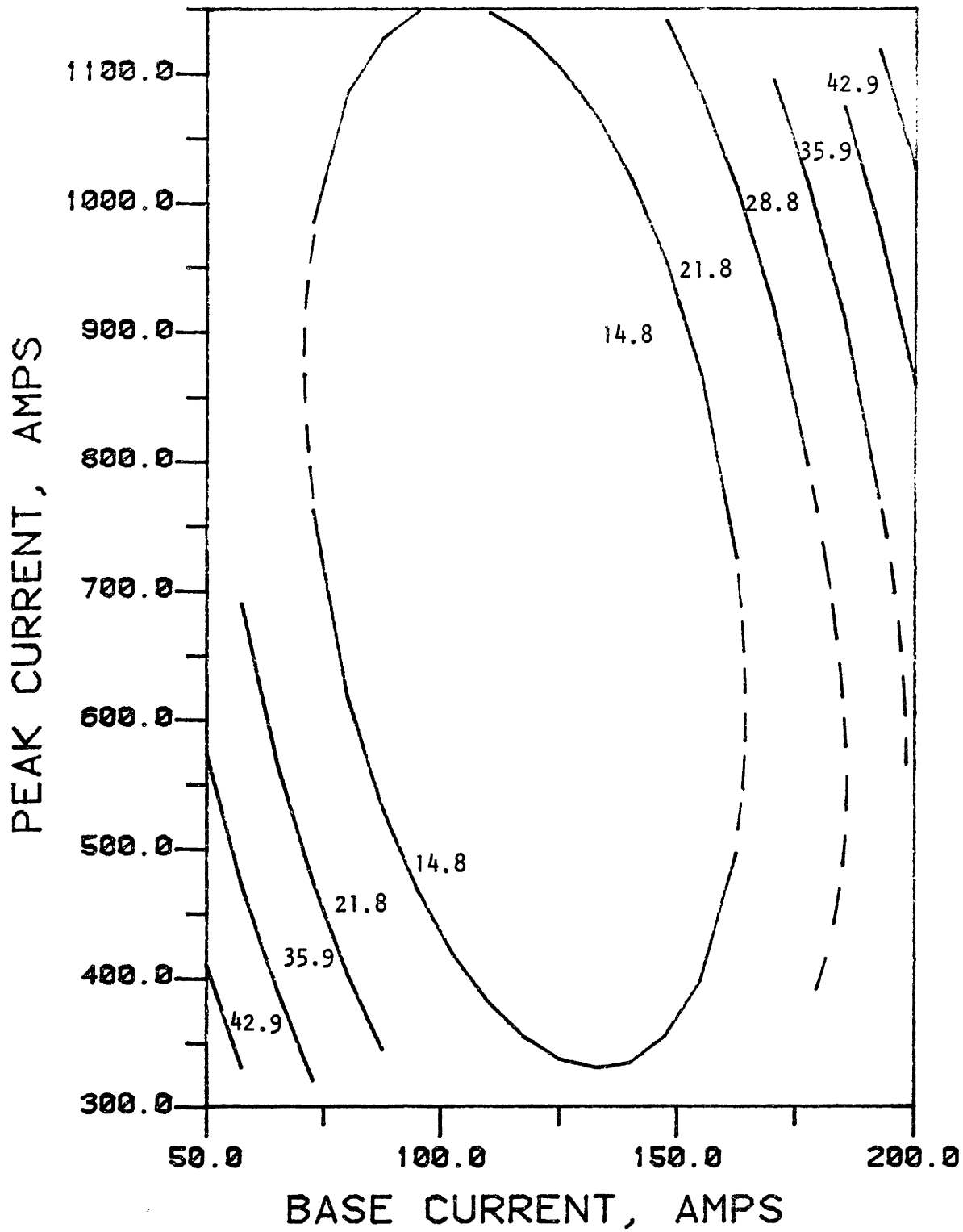

Figure 49a: Contours of constant droplet transfer frequency (Hz) at 15 Hz. Standard Deviation = 10.4.

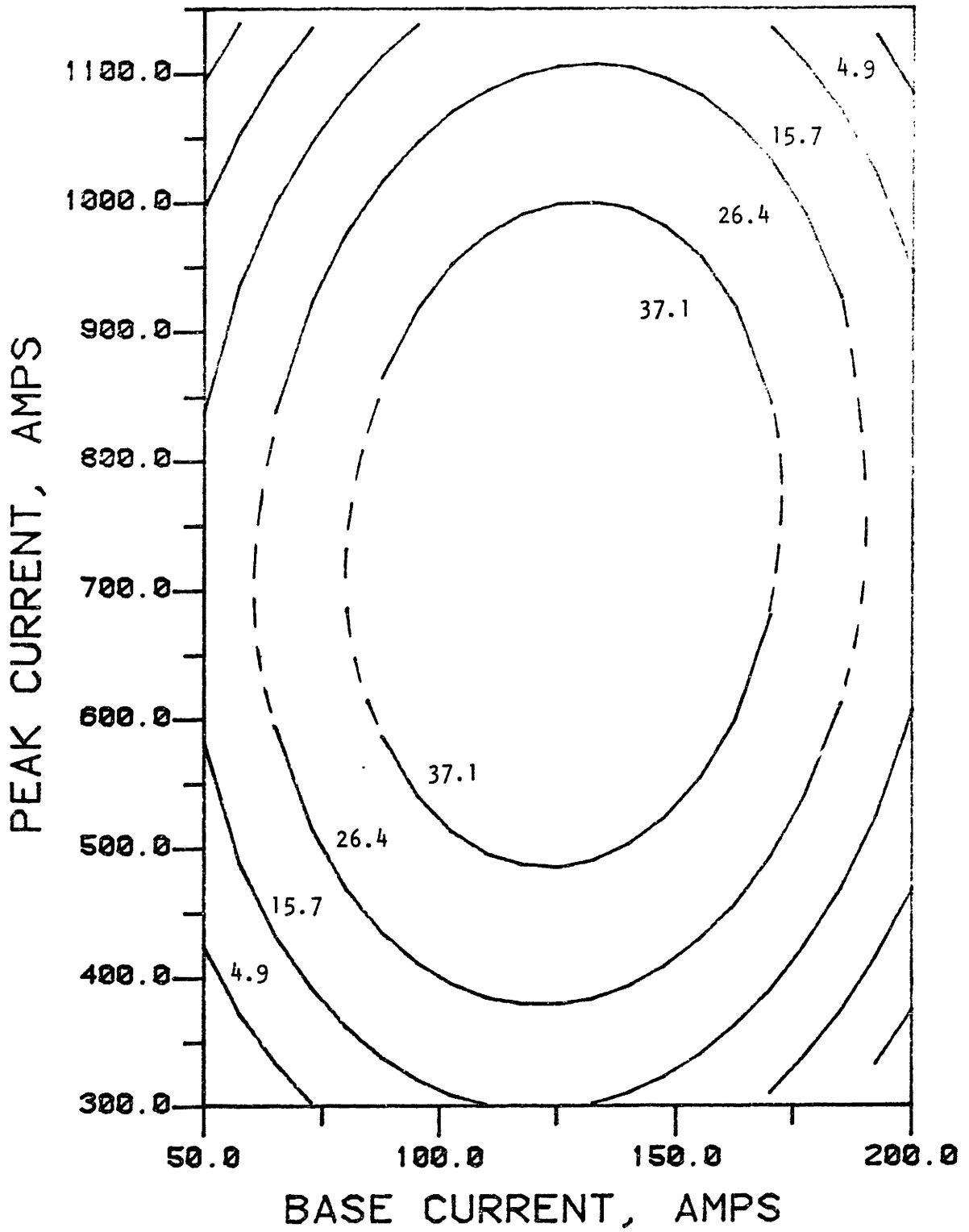

Figure 49b: Contours of constant droplet transfer frequency (Hz) at 150 Hz. Standard deviation = 12.5.

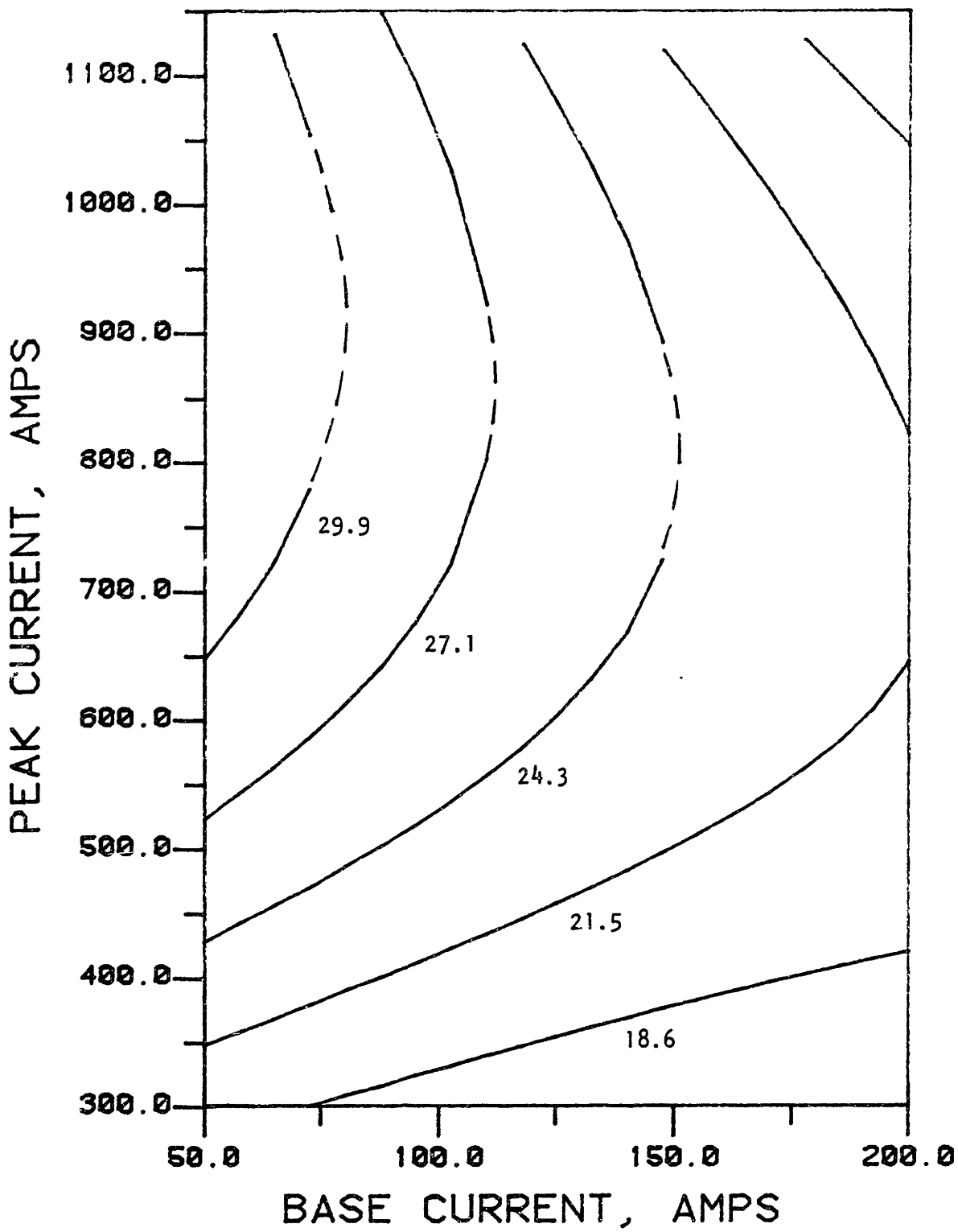

Figure 49c: Contours of constant droplet transfer frequency (Hz) at 1500 Hz. Standard deviation = 10.5.

40 Hz over the entire range of current pulsing frequencies. It appears that in order to achieve one-drop-per-pulse transfer, current pulsing frequencies on the order of 5 to 50 Hz should be evaluated in greater detail. As expected, droplet transfer frequency appears to be inversely proportional to droplet transfer size at a given pulsing frequency.

Wire Feed Rate

At low frequency (15 Hz), a saddle of maximum wire feed rate occurs at I_b = 125 A, I_p = 500 A (see Figure 50a). At intermediate frequency (150 Hz), maximum wire feed rate occurs at high base current over the range of peak current (see Figure 50b). Finally, at high frequency (1500 Hz), maximum wire feed rate occurs at the center of the experimental space, I_b = 125 A, I_p = 725 A (see Figure 50c). Wire fed rate appears to be a function of droplet transfer frequency and droplet transfer size at a given pulsing frequency as expected. The region of maximum wire feed rate apears to be near the center of the experimental space and toward high base current region in each case.

Weld Bead Width

At low frequency (15 Hz), maximum weld bead width occurs on a saddle located at low base current (50 A) near

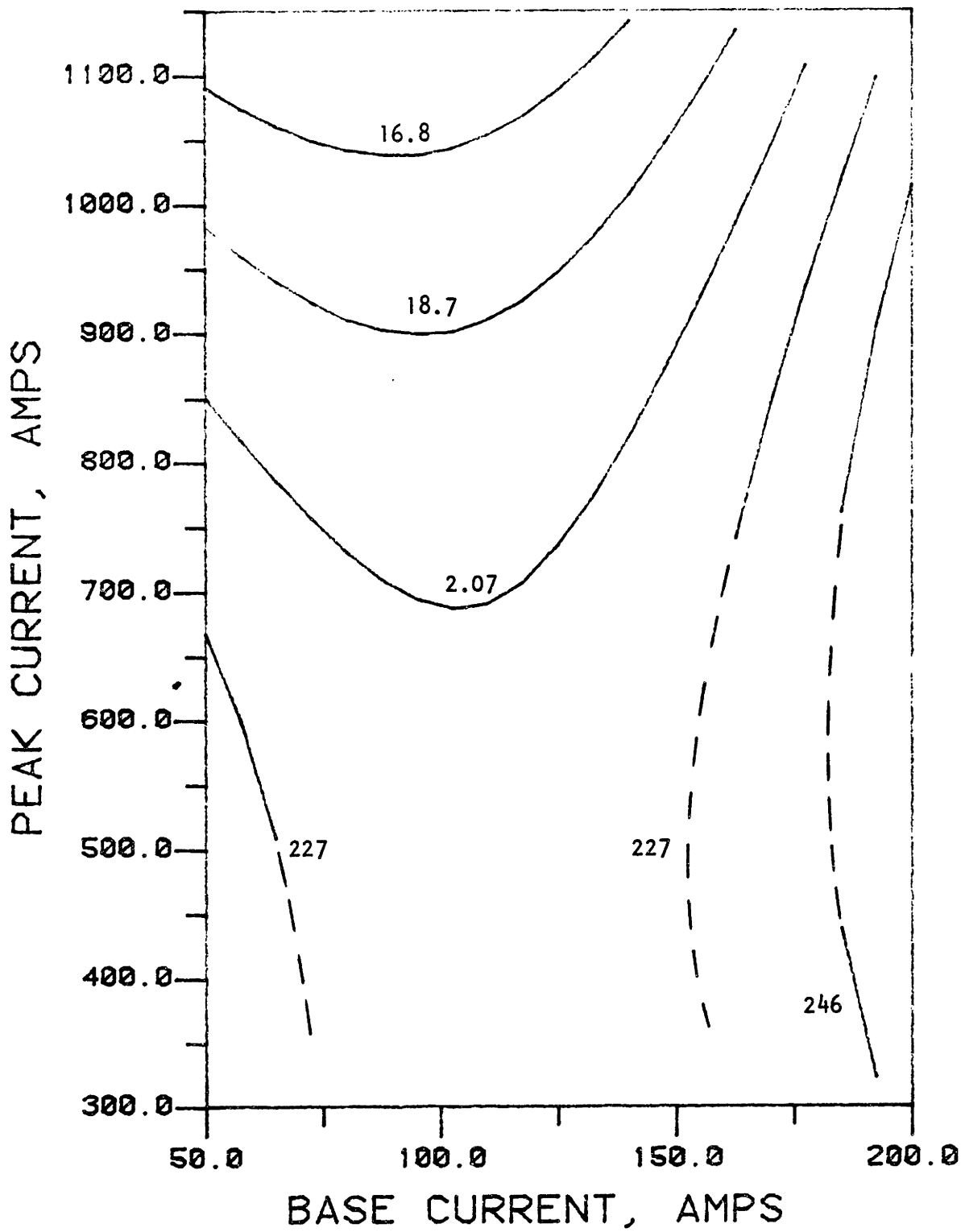

Figure 50a: Contours of constant wire feed rate (ipm) at 15 Hz. Standard deviation = 28.5.

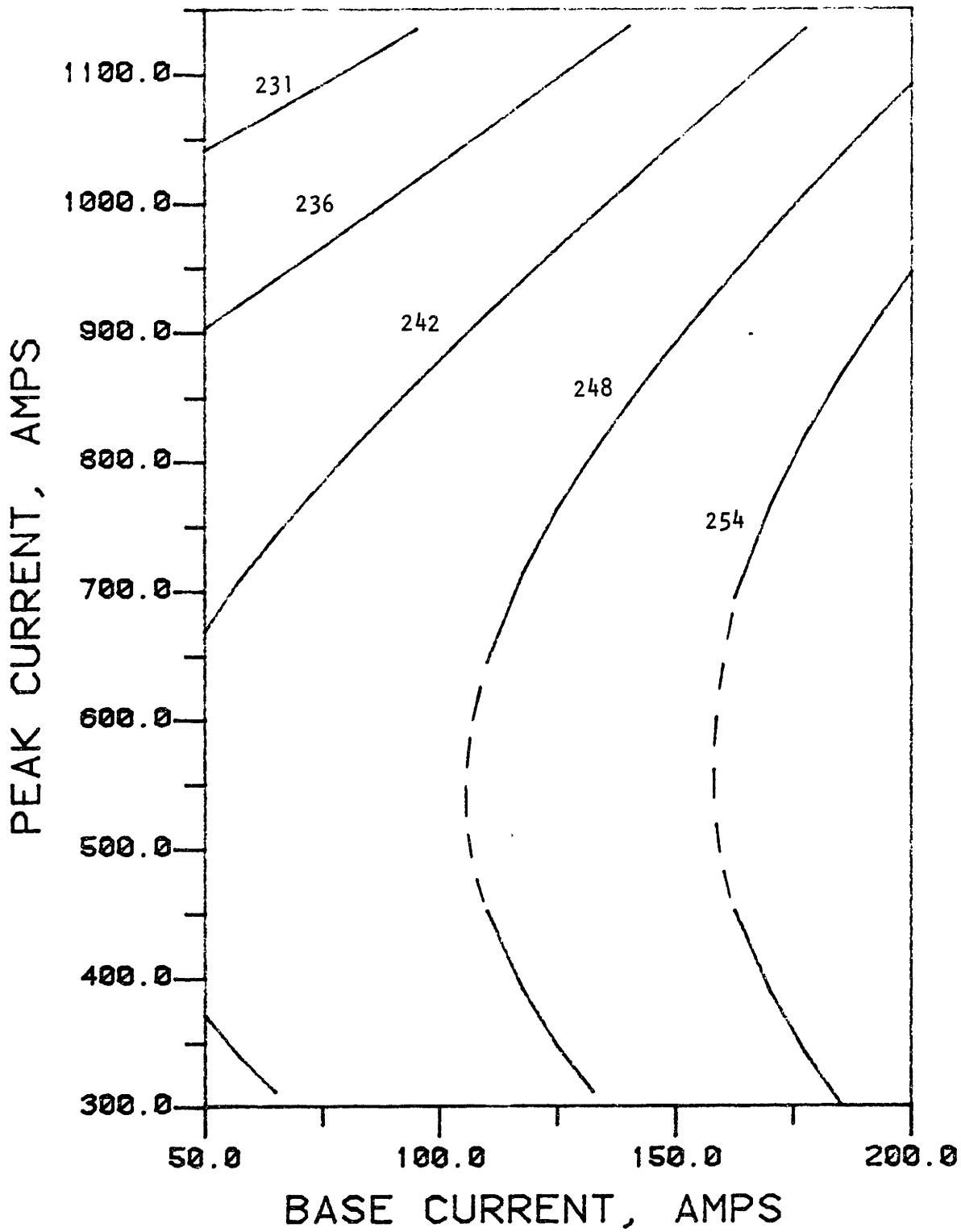

Figure 50b: Contours of constant wire feed rate (ipm) at 150 Hz. Standard deviation = 5.9.

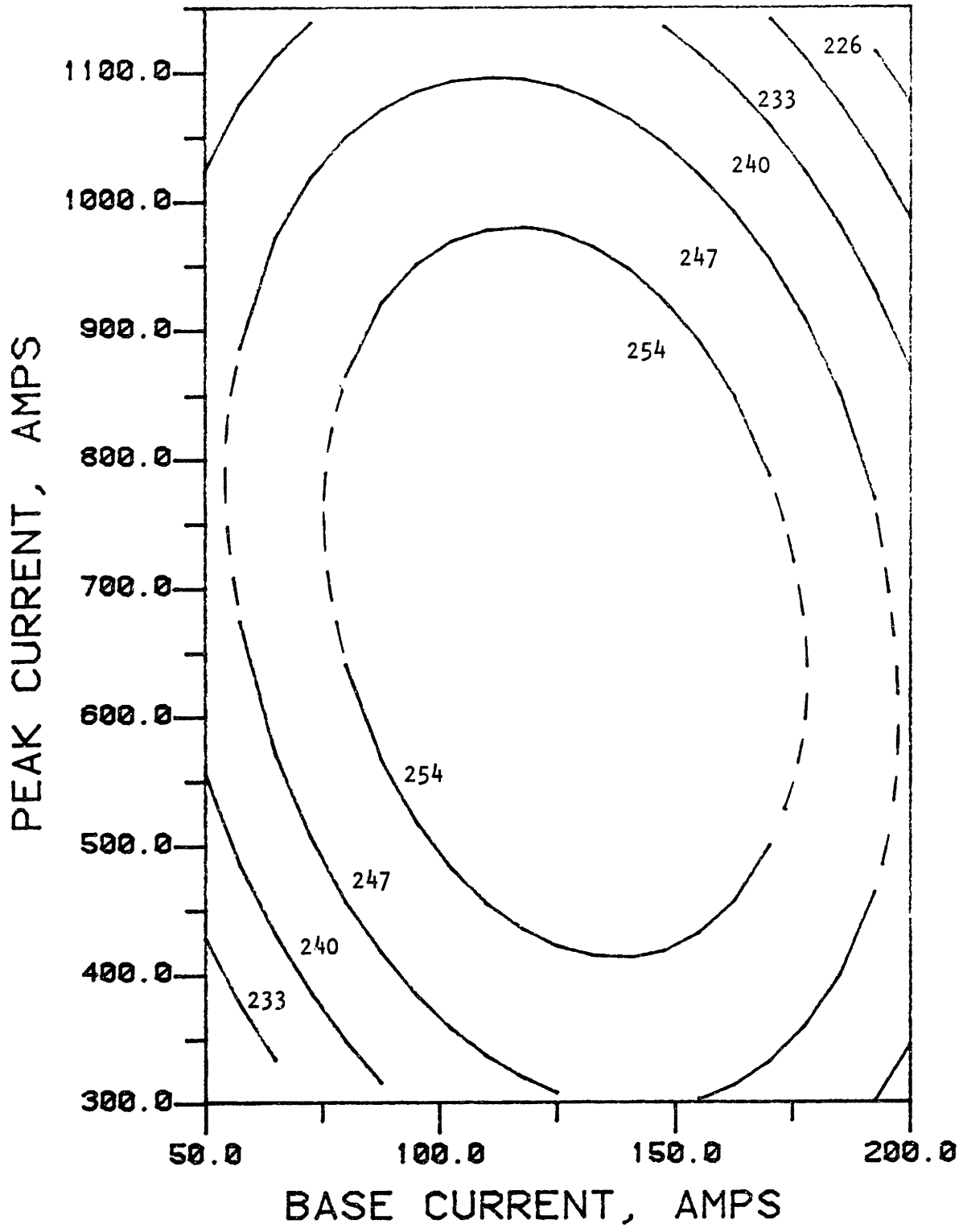

Figure 50c: Contours of constant wire feed rate (ipm) at 1500 Hz. Standard deviation = 9.5.

the center of the experimental space (see Figure 51a). At intermediate frequency (150 Hz), maximum weld bead width occurs in the low base current (50 A) and high peak current (1150 A) region of the experimental space (see Figure 51b). At high frequency (1500 Hz), maximum weld bead width occurs in the center region of the experimental space (see Figure 51c). Weld bead width does not appear to be a function of frequency but rather a function of base current and peak current.

Spatter Per Square Inch

At low frequency (15 Hz), the spatter occuring per square inch around the weld bead by point count was found to be a minimum at low base current (50 A) and high peak current (1150 A) (see Figure 52a). At intermediate frequencies (150 Hz), the spatter per square inch was a minimum again at low base current (100 A) and high peak current (900 A) (see Figure 52b). At high frequency (1500 Hz), the spatter per square inch was a maximum at high base current (150 A) over the range of peak current (see Figure 52c). The spatter per square inch at low and intermediate frequencies does not appear to be a function of frequency but rather a function of base current and peak current. At high frequency, consistently lower values of spatter per square inch were observed. This does not

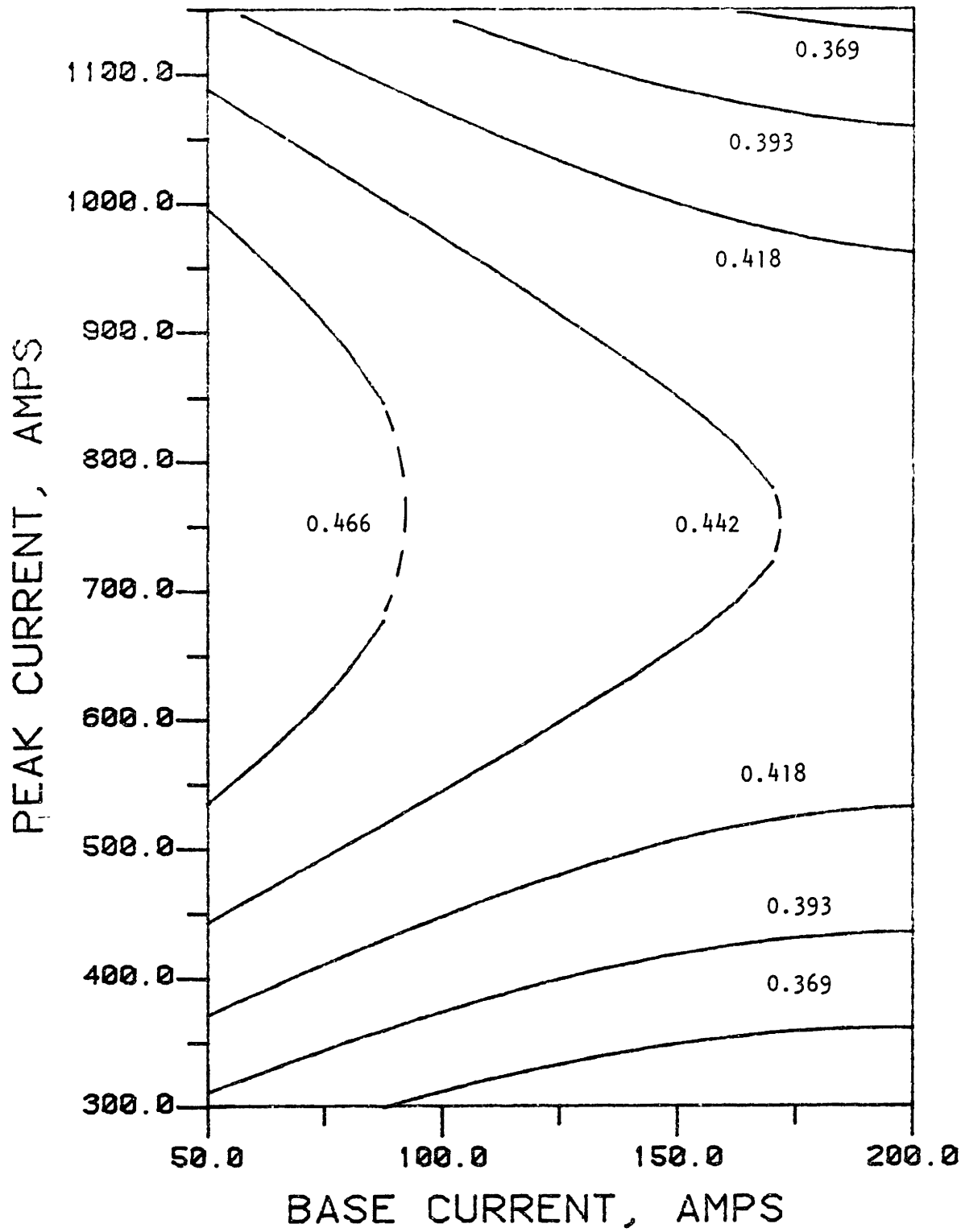

Figure 51a: Contours of constant weld bead width (inches) at 15 Hx. Standard deviation = 0.075

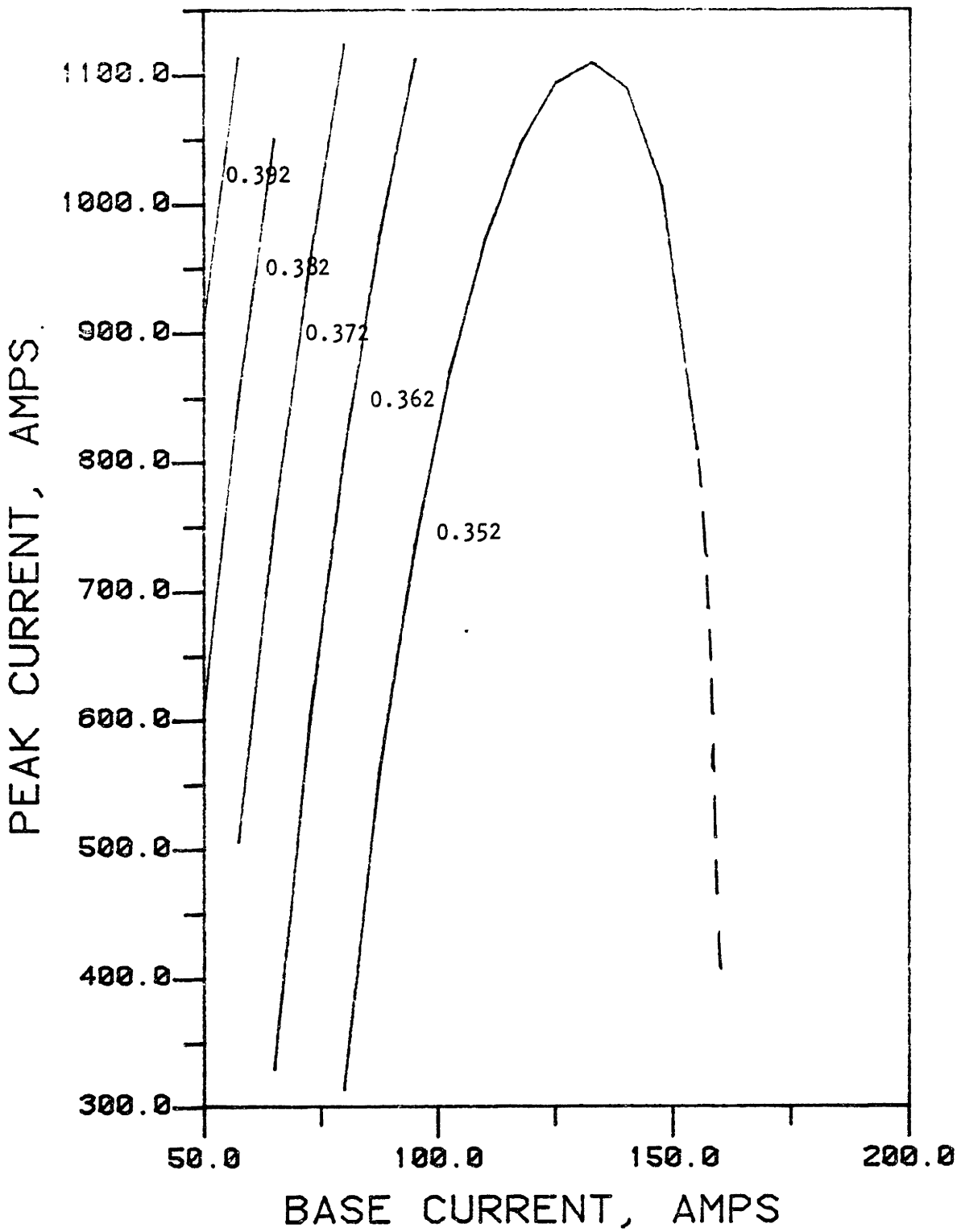

Figure 51b: Contours of constant weld bead width (inches) at 150 Hz. Standard deviation = 0.034

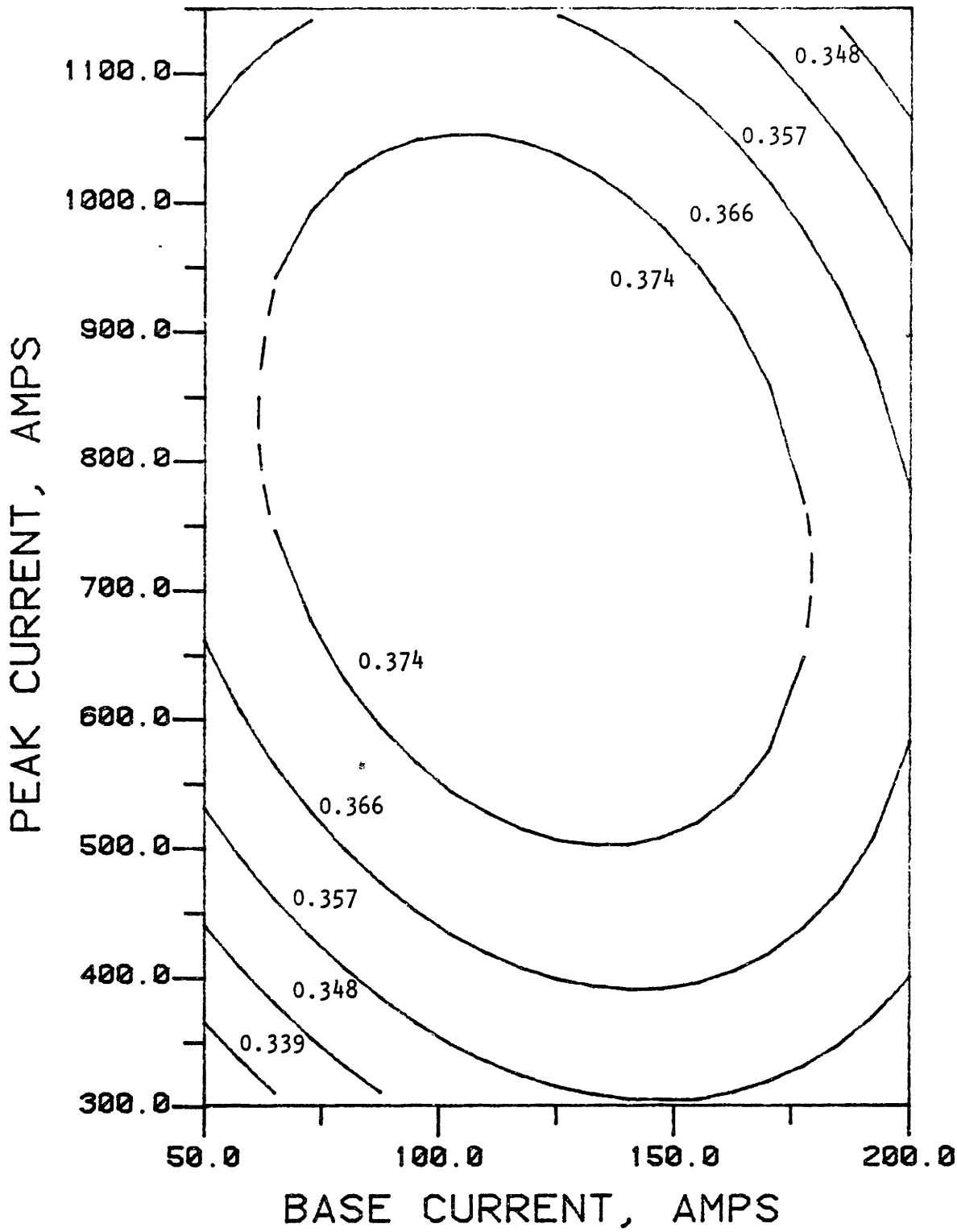

Figure 51c: Contours of constant weld bead width (inches) at 1500 Hz. Standard Deviation = 0.032

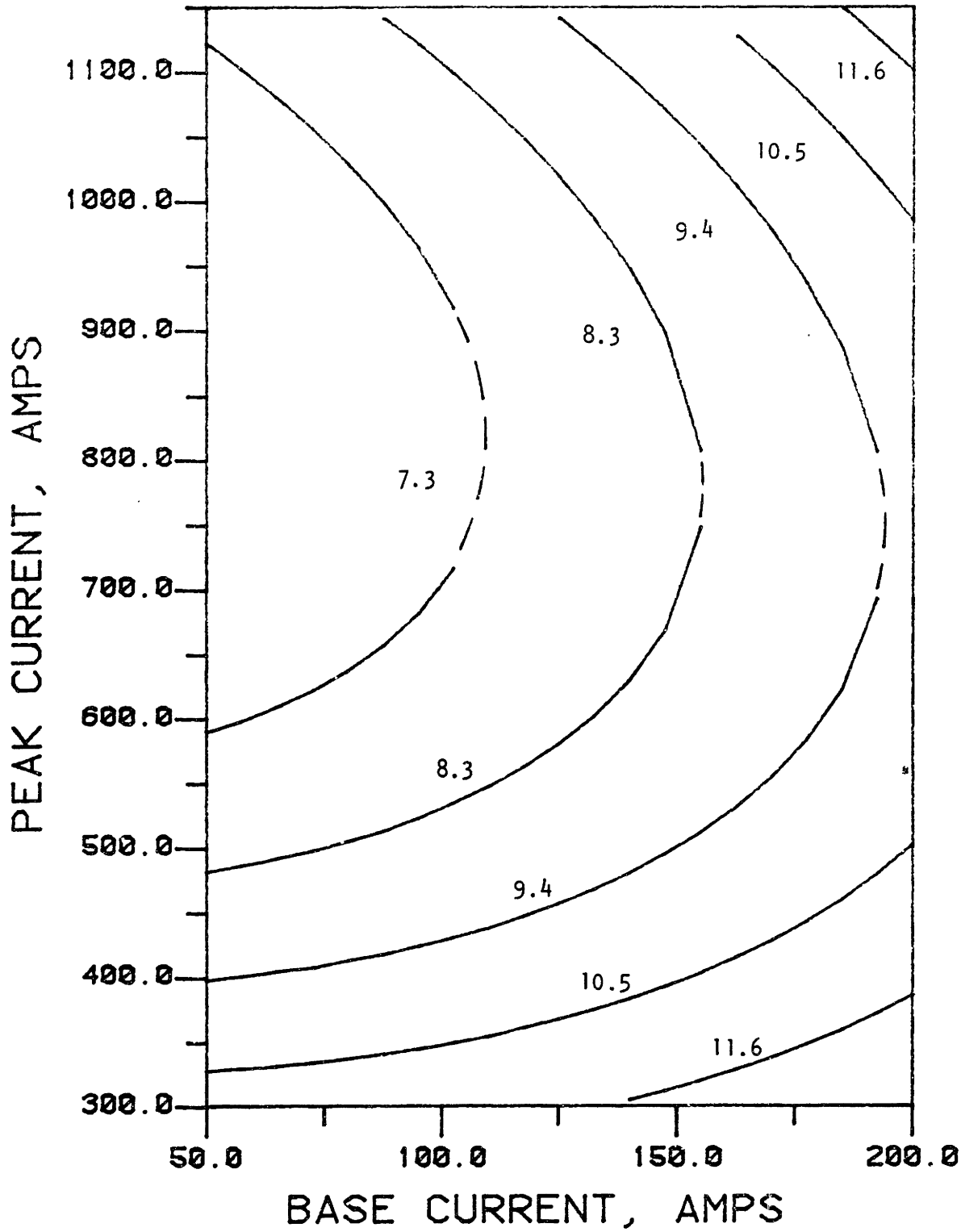

Figure 52a: Contours of constant spatter per square inch at 15 Hz. Standard deviation = 3.6

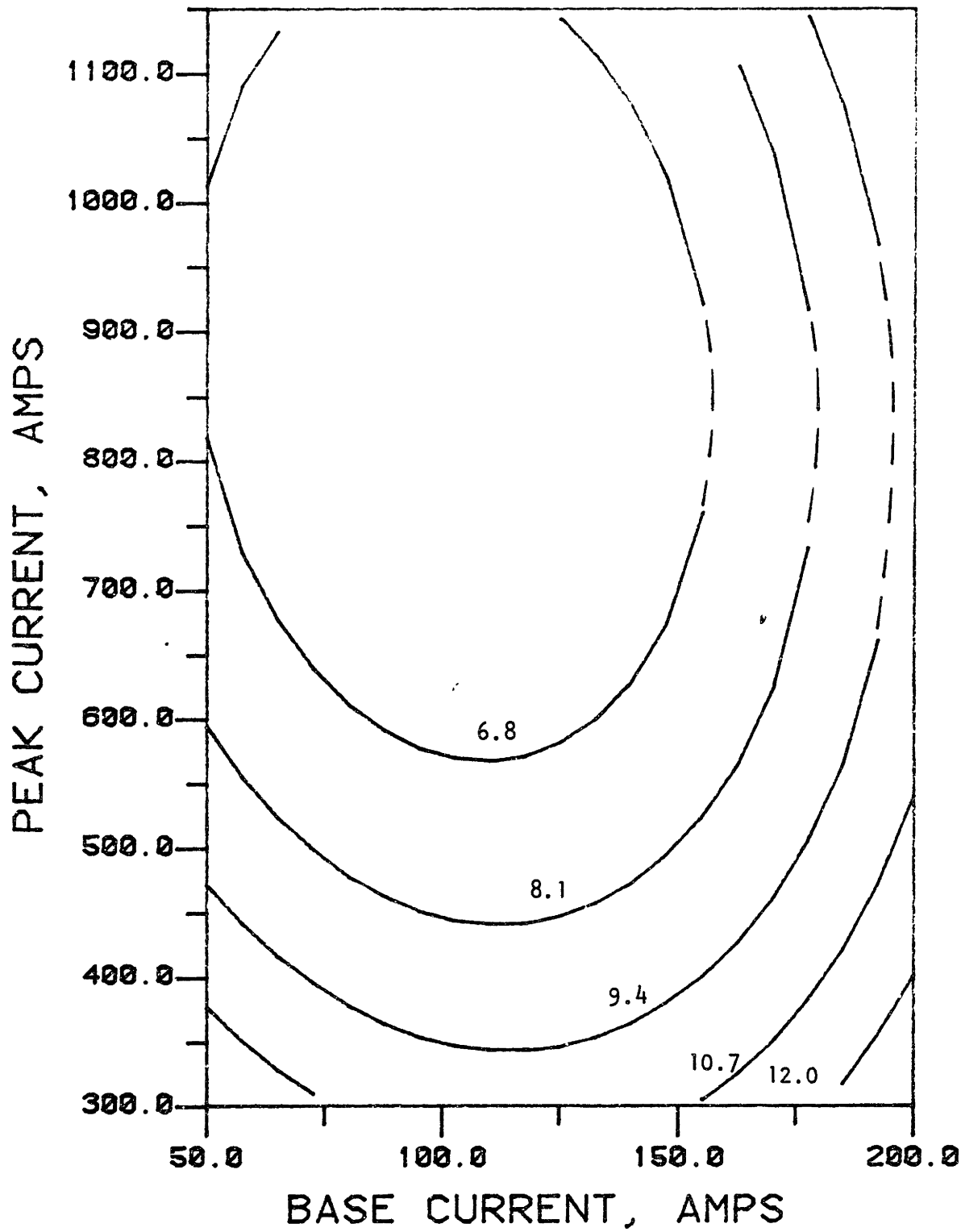

Figure 52b: Contours of constant spatter per square inch at 150 Hz. Standard deviation = 2.2

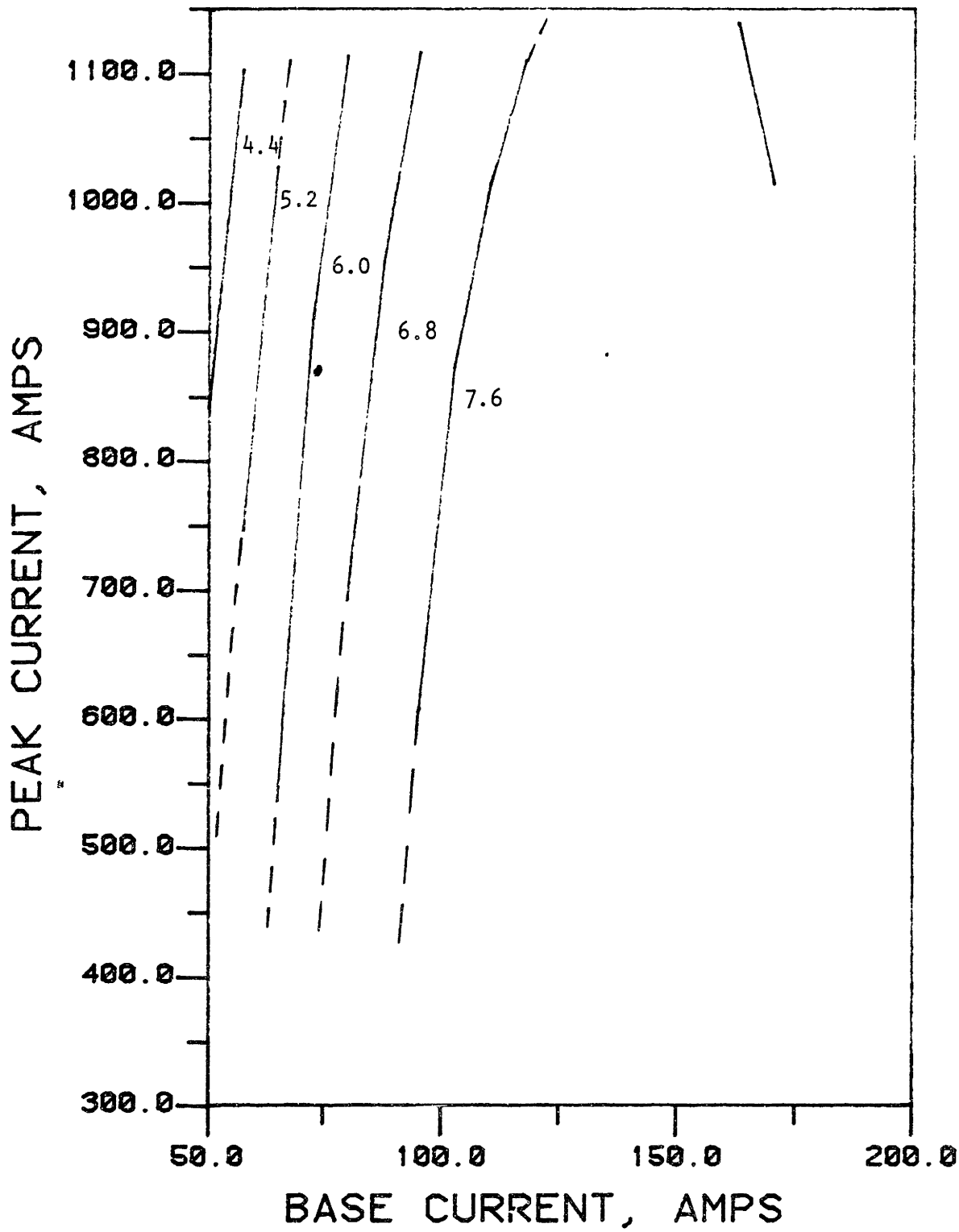

Figure 52c: Contours of constant spatter per square inch at 1500 Hz. Standard deviation = 2.0

necessarily indicate less spatter at higher frequency since spatter size is also larger at higher frequency.

The following general trends were observed based on the analysis of the response of each dependent variable:

1. Small drop sizes are achieved with high peak current pulses super-imposed on a high base current level for frequencies below 150 Hz. As the frequency is increased to 1500 Hz, the base current should be reduced to maintain small drop sizes. There appears to be a trade off in 1) base current, providing electrode tip melting, and 2) peak current, providing sufficient pinch force to detach a droplet of a given size.

2. Droplet spatter size appears to be minimized at low peak current levels. This result may be due to premature transition to peak current during droplet incorporation into the weld pool, providing sufficient pinch force to detach and eject the drop from the weld pool. If the droplet detachment frequency and current pulsing frequency can be synchronized so that peak current levels occur only during droplet detachment from the

electrode, this trend should not be present.

3. The frequency for spray transfer (droplets on the order of the same diameter as the electrode) appears to lie between 5 and 50 Hz for an average current of 250 Amps. This region of frequency should be evaluated in more detail for one-drop-per-pulse transfer. At higher average current, the frequency for spray transfer is probably higher, e.g., for an average current of 300 Amps, the spray transfer frequency is probably between 50 and 500 Hz.

4. Higher wire feed rates appear to occur in regions where base current is high or where the peak current is low but pulse duration is long to provide sufficient melting for fast droplet formation. At higher average current, much higher wire feed rates are expected, e.g., for an average current of 300 Amps, the wire feed fate is probably $\geq$300 ipm.

5. Weld bead widths appear to be greatest at low base current and high peak current. Overall, weld bead widths appear to be relatively equal allowing for

a range of width due to nonuniformity. It is expected that weld bead width will be a strong function of average current.

6. The spatter per square inch appears to be minimized at low peak current. This corresponds to the observation of small droplet spatter sizes at low peak current. As noted before, if the current pulse frequency and droplet detachment frequency are synchronized, this effect should not be present.

Based on the above observations, the region that appears to provide the optimum conditions for one-drop-per-pulse transfer lies between 5 and 50 Hz. In this frequency region, the high base current and peak current corner of the experimental space should offer the greatest control of weld metal transfer with minimal spatter formation.

Typical weld beads made at the frequencies of the design space centers, i.e., 15, 150 and 1500 Hz, at the center coordinates (I_b = 125 A, I_p = 725 A) are shown in Figure 53. Weld metal transfer characteristics observed at these center coordinates of the experimental spaces are shown in Figures 54 to 56. Almost all the modes of transfer

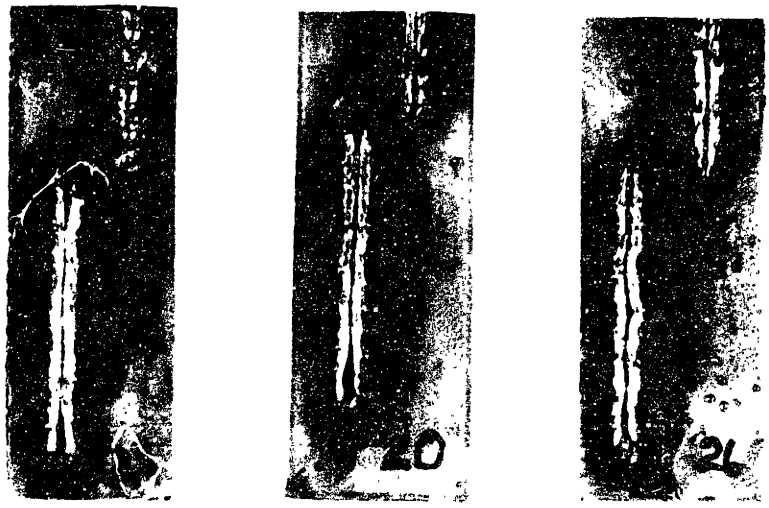

(a) (b) (c)

Figure 53: Titanium weld beads made with pulsing parameters at the center coordinates of the experimental space (I_b = 125 A, I_p = 725 A) at 15 Hz (a), 150 Hz (b) and 1500 Hz (c).

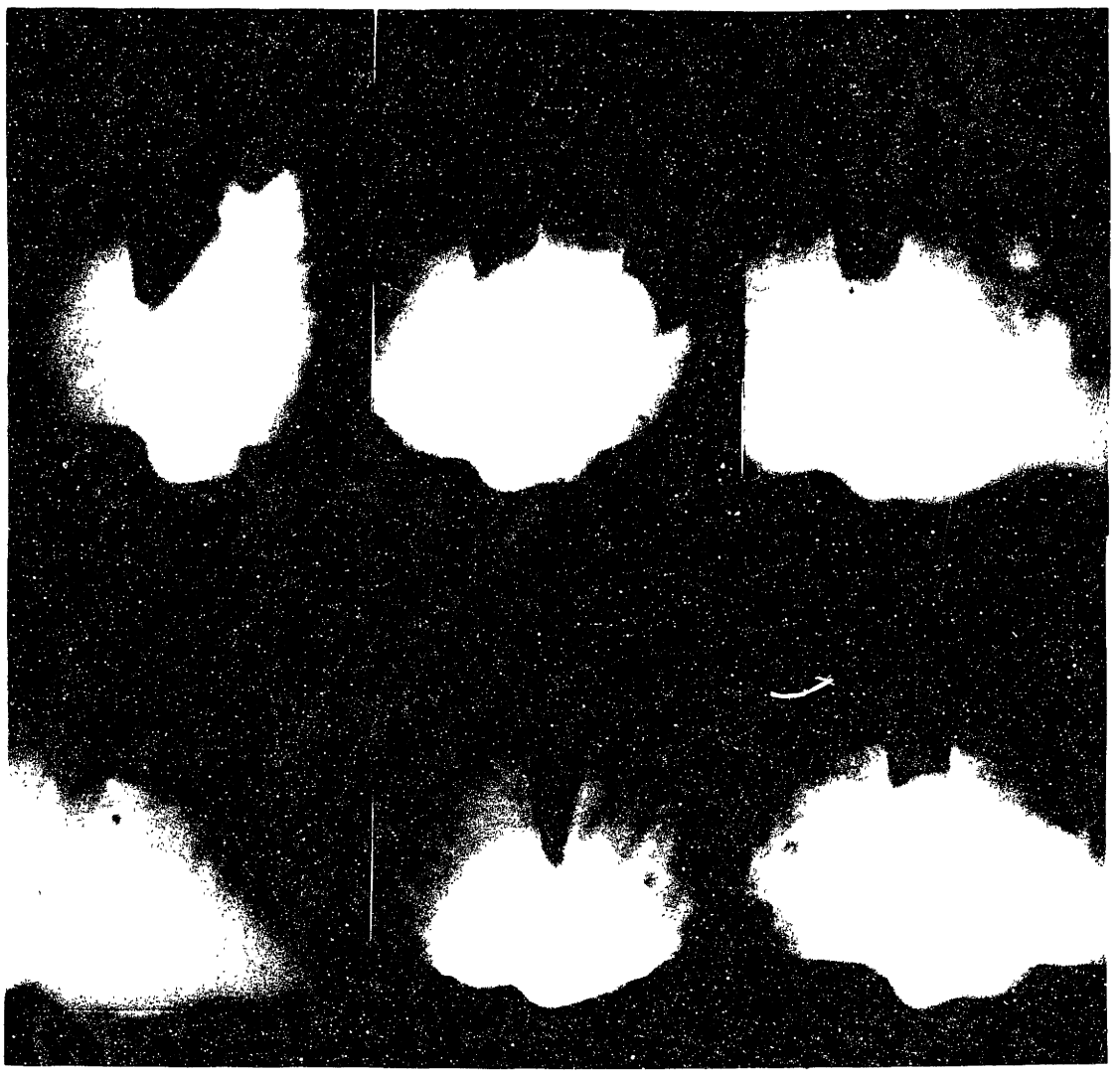

Figure 54: Titanium weld metal transfer with f = 15 Hz.
I_b = 125 A, I_p = 725 A, I_{av} = 250 A, V = 23.0, v_{wire} = 216 ipm
Avg droplet detach time = 7619 msec.
Avg droplet detach frequency = 13.0 Hz
Avg droplet diameter = 0.1260 in.
Avg spatter diameter = 0.0945 in.
Percent of transfer as spatter = 42.2
frame time = 0.167 msec.

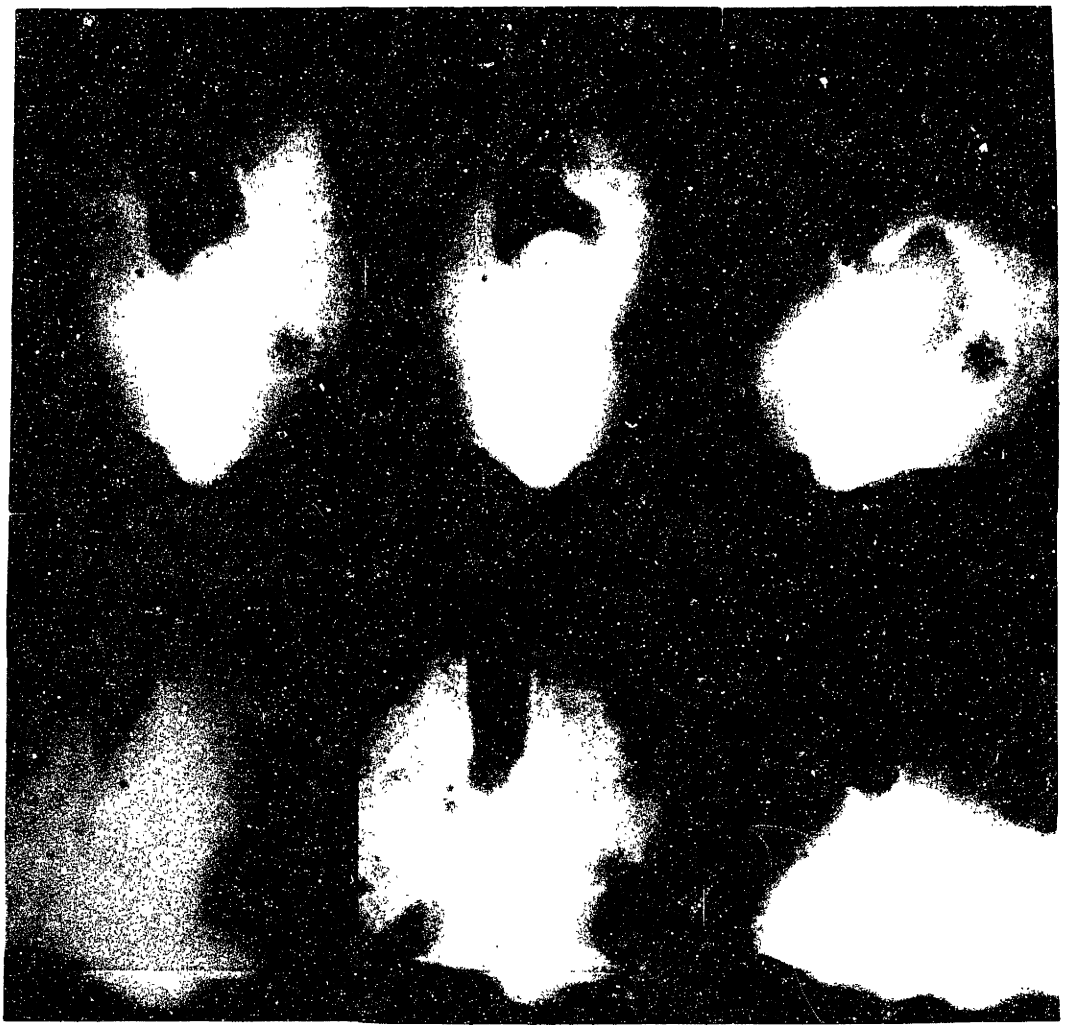

Figure 55: Titanium weld metal transfer with f = 150 Hz.
I_b = 125 A, I_p = 725 A, I_{av} = 250 A, V = 22.5 V, v_{wire} = 247 ip
Avg droplet detach time = 20.2 msec.
Avg droplet detach frequency = 49.5 Hz
Avg drop diameter = 0.0750 in.
Avg spatter diameter = 0.0300 in.
Percent of transfer as spatter = 6.4
frame time = .167 msec.

Figure 56: Titanium weld metal transfer with f = 1500 Hz.
I_b = 125 A, I_p = 725 A, I_{av} = 250 A, V = 23.0 V, v_{wire} = 260 ipm
Avg droplet detach time = 26.0 msec.
Avg droplet detach frequency = 38.5 Hz
Avg drop diameter = 0.0827 in.
Avg spatter diameter = 0.0578 in.
Percent of transfer as spatter = 34.1
Frame time = 0.167 msec.

defined in Figure 5 are observed in pulsed GMA welding of titanium.

8.3.3 Results of Welds Performed with a Commercial Pulsed Current Power Supply

During a visit by the author to Dimetrics, Inc., Diamond Springs, California, titanium GMA welding using the Metal Beam Power Source described in Section 4.2 was demonstrated. A 3/4-inch thick titanium (Ti-6Al-4V) plate and a 0.045 inch diameter electrode was used for this demonstration. Examples of weld beads from this demonstration are shown in Figure 57. Modulated pulsing frequencies from 100 to 700 Hz are represented in Figure 57a. Welds performed at 380 Hz are shown in Figure 57b. The use of the pulse width modulated current signal appears to eliminate spatter and provide a well shaped uniform bead. The 16.5 kHz pulsed current signal appears to stabilize the arc by eliminating stable plasma jet formation which normally results in unbalanced forces and uncontrolled weld metal transfer. Etched cross sections of the weld beads at each trial frequency are shown in Figure 58. The depth of penetration and weld bead shape appears to change with frequency of pulsing.

Based on the above observations, it appears beneficial to super-impose high frequency current pulsing on the lower

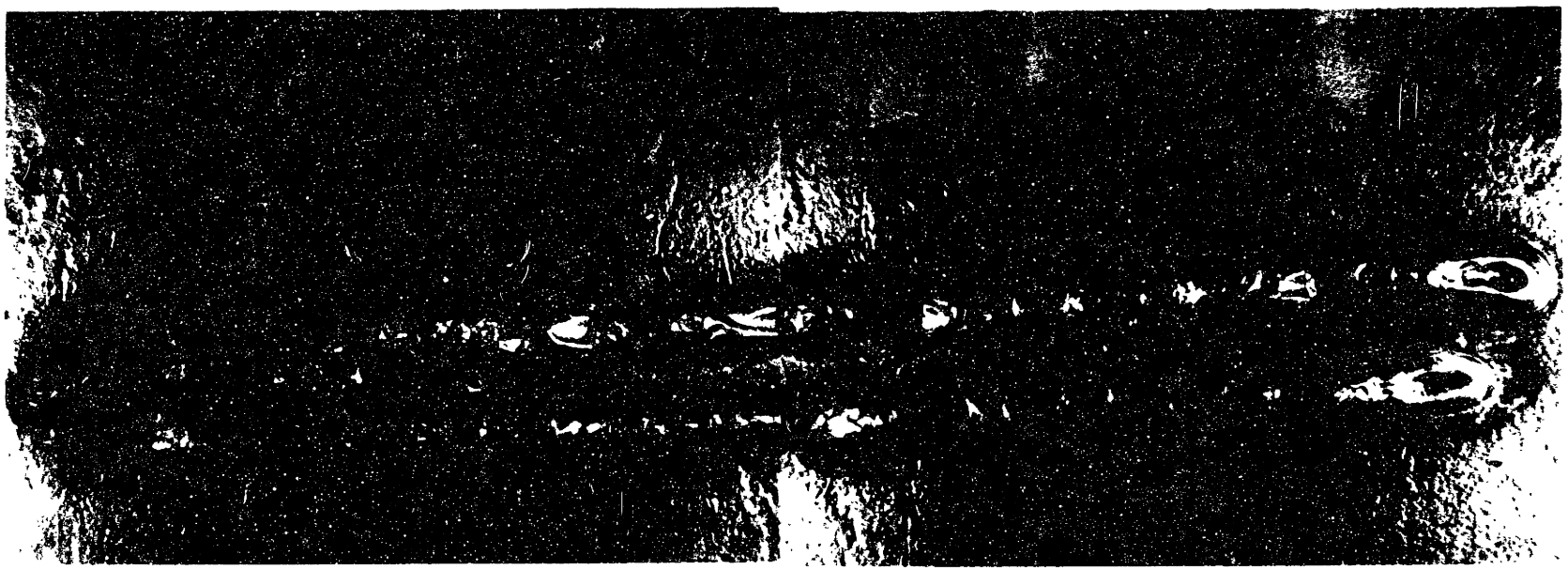

Figure 57: Weld beads made with Dimetrics Inc., Metal Beam Power Source. Pulsing frequencies are noted next to each weld bead.

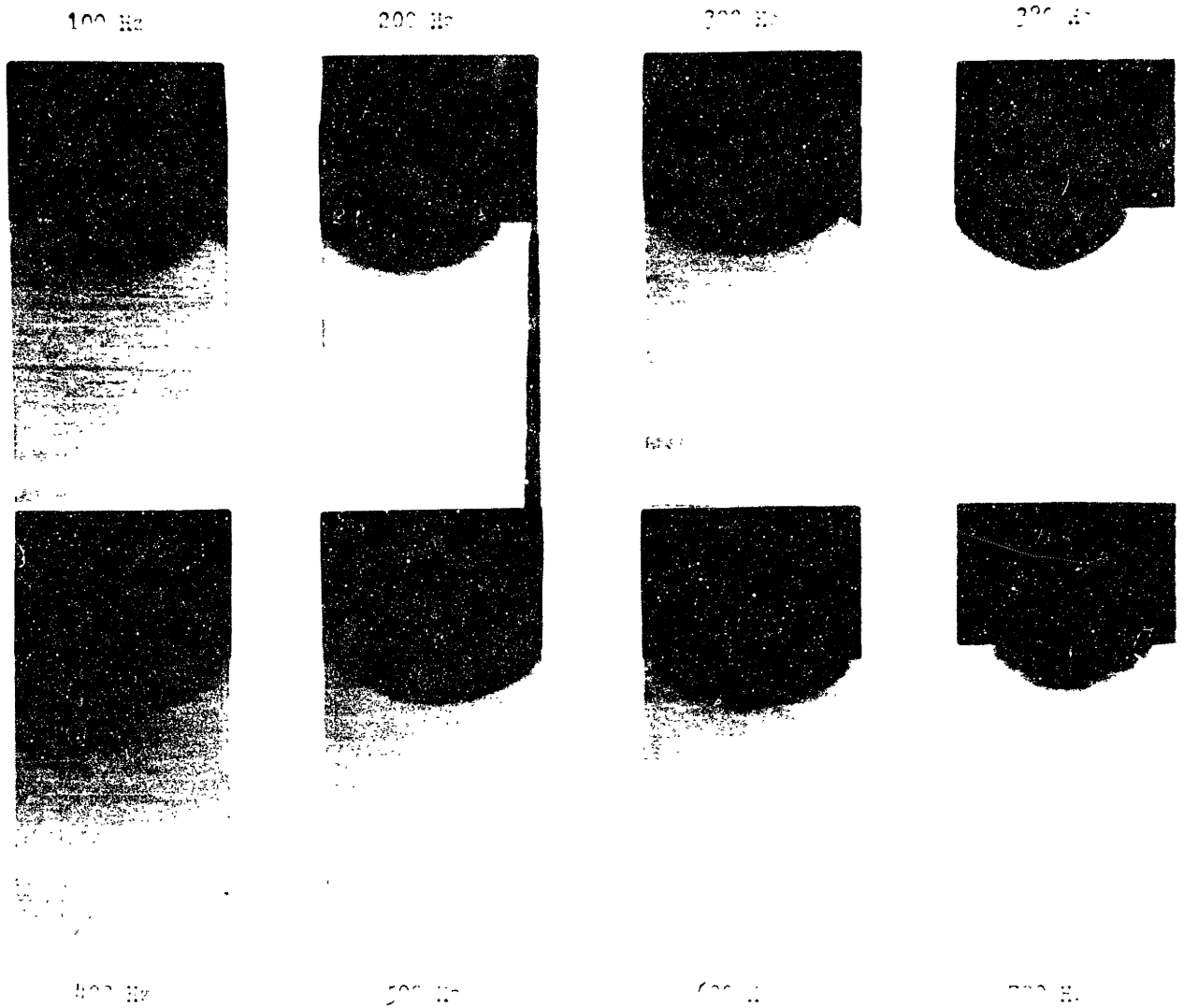

Figure 58: Weld bead cross sections at various frequencies from welds made with Dimetrics, Inc. Metal Beam Power Source.

frequency pulsing corresponding to droplet detachment frequencies. Further work in defining the optimum pulsed current parameters for titanium GMA welding should include an investigation of the stabilizing effect of high frequency 16.5 kHz pulsing on weld metal transfer.

8.4 Conclusions

The following conclusions were based on the results of the analysis of high speed movies of GMA welding of titanium and on obserations of a welding demonstration at Dimetrics, Inc., Diamond Springs, California. These conclusions should provide good direction for further research to determine optimum pulsed current parameters for controllable GMA welding of titanium.

1. With direct current in reverse polarity, stable anode and cathode spot plasma jets form causing unbalanced forces on transferring droplets. With direct current in straight polarity only the cathode jet is present and it exerts a reaction force on the droplet which repels it away from the weld pool. The stable plasma jets form as a result of the absence of a driving force to break the anode or cathode spot into many

small unstable spots as occurs with aluminum. The absence of this driving force may be due to the absence of islands of oxides on the molten titanium surface acting as efficient electron emitters.

2. The region that appears to provide optimum conditions for one-drop-per-pulse transfer at an average current of 250 Amps lies between 5 an 50 Hz. This frequency region appears to match the natural frequency of droplet detachment for spary transfer (droplet diameter equal or slightly larger than the electrode diameter) at 250 Amps average current. In this frequency region, the high base current and peak current corner of the experimental space should offer greatest control of weld metal transfer with minimal spatter formation. For higher average currents, higher pulsing frequency ranges should be evaluated.

3. High frequency pulsing (16.5 kHz) appears to offer unique weld metal transfer stabilization. This may be a result of the

breaking of the strong anode and cathode spots into smaller and weaker unstable spots resulting in weaker and more uniform plasma jet forces on weld metal transfer. The use of high frequency pulsing super-imposed on low frequency pulsing corresponding to the natural frequency for spray transfer should be evaluated for stabilization of weld metal transfer.

It is the opinion of the author of this thesis that modern pulsed current power supplies provide the necessary flexibility to tailor the current waveform for controlled metal transfer with all weldable materials including titanium. Based on results of the research performed for this thesis, it should only be a short time before a GMA pulsed current welding system is developed for controlled GMA welding of titanium.

9.0 OVERVIEW

The research performed for this thesis, like many research projects, exposed more new questions than it answered. Due to the limitations of time, the author regrets not having answered more of these questions. If interest in the development of pulsed current GMA welding systems continues, the following areas are considered by the author to be key items for research in the development of these systems.

1. The detachment of droplets is recorded in the voltage signal during GMA welding as a voltage spike. This voltage spike could provide a real time feedback to one or more welding parameters to help achieve and maintain one-drop-per-pulse transfer. The use of the droplet detachment voltage spike as a real time feedback signal in GMA welding should be evaluated.

2. A dynamic math model for weld metal transfer should be developed. The forces controlling weld metal transfer as a function of material type should be evaluated. In particular, the

driving forces described in Section 8.3.1 determining the nature of anode and cathode spot formation, and thus plasma jet formation, should be evaluated. In this regard, the effect of externally imposed oscillating magnetic fields on plasma jet formation and weld metal transfer should be evaluated to provide better understanding of the electromagnetic arc forces. This technique should also be evaluated for possible stabilization of weld metal transfer.

3. A heat transfer model for GMA welding should be developed to allow prediction of weld bead width and depth of penetration. A heat transfer model applying a superposition of a gaussian distribution heat source from Tsai's work at MIT on gas tungsten arc welding [60] with step heat input representing heat transferred to the weld pool by I^2R heating plus electron heating at the wire tip should be evaluated. This model provides a modified distributed heat source which can be used to define an operating parameter and ultimately

an estimation of weld bead size following Tsai's procedure for GTA welding.

Finally, it is important that both educational institutions such as MIT and industry share and cooperate in the development of pulsed current GMA welding systems so that the systems not only work in the laboratory but also in the field and in the shop as they are intended.

REFERENCES

1. Masusbuchi, K. and Terai, K., "Future Trends of Materials and Welding Technology for Marine Structures", a paper presented to the Society of Naval Architects and Marine Engineers, Philadelphia, PA, June 2-5, 1976, pp. 5-8 to 5-9.

2. Ford, J. M., Naval Research Reviews: NSRDC and the New ALVIN, NSRDC, Annapolis, MD, pp. 9-19.

3. Jackson, C. E., "The Structure of Arc Welding", a paper presented at the 17th Adams Lecture, Union Carbide Welding Products, pp. 4, 5, 17-22.

4. Houldcroft, P. T., Welding Processes, Cambridge University Press, 1967, pp. 15-17.

5. Waszink, J. H. and Graat, L. H. J., "Experimental Investigation of the Forces Acting on a Drop of Weld Metal", Welding Journal, April 1983, pp. 1085-1165.

6. Lochte-Holtgreven, W., "The Electric Arc Between Carbon and Iron Electrodes", Physics of the Welding Arc--A Symposium 1962, pp. 1-4.

7. Rykalain, N. N. et al., "Vaporized Electrode Material and Energy Balance in Welding Arcs", Physics of the Welding Arc--A Symposium 1962, pp. 46-49.

8. Cooksey, C. J. and Miller, D. R., "Metal Transfer in Gas-Shielded Arc Welding", Physics of the Welding Arc--A Symposium 1962, pp. 123-132.

9. Amson, J. C. and Salter, G. R., "An Analysis of the Gas-Shielded Consumable Metal Arc Welding System", Physics of the Welding Arc--A Symposium 1962, pp. 131-147.

10. Amson, J. C., "An Analysis of the Gas-Shielded Consumable Metal Arc Welding System", British Welding Journal, April 1962, pp. 232-249.

11. Wells, A. A., "A Momentum Principle for Arc Force", British Welding Journal, April 1962, pp. 227-231.

12. Greene, W. J. "An Analysis of Transfer in Gas-Shielded Welding Arc", Trans AIEE, July 1960, pp. 194-203.

13. Serdjuk, G. B., "Magnetic Forces in Arc Welding Metal Transfer", Physics of the Welding Arc--A Symposium 1962, pp. 173-180.

14. Houldcroft, P. T., "1977 Comfort A. Adams Lecture: Developing Precision Assembly by Welding", Welding Journal, August 1977, pp. 15-25.

15. Needham, J. C., "Control of Transfer in Aluminum Consumable Electrode Welding", Physics of the Welding Arc--A Symposium 1962, pp. 114-122.

16. Needham, J. C., "Pulse Controlled Consumable Electrode Welding Arcs", British Welding Journal, April 1965, pp. 191-197.

17. Reynolds, J., "New Process for Thin Gauge Aluminum", Welding Journal, July 1980, pp. 23-27.

18. Needham, J. C. and Carter, A. W., "Material Transfer Characteristic with Pulsed Current", British Welding Journal, May 1965, pp.229-241.

19. Lancaster, J. F., "Influence of Heat Flow on Metal Transfer in Metal/Inert Gas Welding of Aluminum", Physics of the Welding Arc--A Symposium 1962, pp. 170-174.

20. "What's the Best MIG Power Source for You?", Welding Engineer, April 1971, pp. 49-55.

21. Manz, A. F., The Welding Power Handbook, Union Carbide Corporation, Linde Division, 1973, pp. 125-145.

22. Hirschfield, J. A., "Practical Briefs: No. 8 of a Series on Welding Aluminum", Welding Journal, November 1974, pp. 709-711.

23. Stark, L. E., et al., "Welding of One-Inch Thick Ti-6Al-4V Plate", Welding Journal, September 1962, pp. 805-814.

24. "Selecting MIG Equipment for Aluminum", Welding Engineer, April 1971, pp. 56-60.

25. Salter, G. R. and Scott, M. H., "The Pulsed Inert Gas Metal-Arc Welding of One-Inch Thick Titanium 721 Alloy",

Welding Journal, April 1967, pp. 154s-167s.

26. Lesnewich, A., "MIG Welding with Pulsed Power", WRC Bulletin No. 170, February 1972, pp. 1-15.

27. Paton, B. E., Patopevskii, A. G., and Podola, N. V., "Programme Controlled Pulsating Arc Welding With a Consumable Electrode", Automatic Welding, 1964, No. 1, pp. 1-5.

28. Lenivkin, V. A., Klenov, G. I., and Baiduganov, Y. A., "Features of Weld Formation in Pulsed-Arc Welding with a Consumable Electrode", Weld Production, 1973, No. 2, pp. 49-52.

29. Dogget, E. H. and Zircher, W. E., "New Developments in Pulsed Spray Welding", Welding Journal, October 1970, pp. 780-787.

30. Owners Manual for Model Pulstar 450 Welding Power Supply, Miller Electric Manufacturing Company, Appleton, Wisconsin.

31. Owners Manual for Model PA-3A Pulsed-Arc Welding Power Supply, Airco, Union, New Jersey.

32. Ries, D. E., Personal Communication with Lockheed Missile and Space Company, Sunnyvale, California, September 27, 1982.

33. Ries, D. E., Personal Communication with Mare Island Naval Shipyard, Vallejo, California, September 29, 1982.

34. Paton, B. E., Sheiko, P. P., and Pashulya, P., "Automatic Control of Metal Transfer in Pulsed Arc Welding," Automatic Welding, 1971, No. 9, pp. 1-3.

35. Lapchinskii, V. P., Potapevskii, A. G. and Steblovskii, B. A., "The Argon Shielded Pulsed Arc Welding of Aluminum Alloys", Automtic Welding, 1975, No. 11, pp. 11-12.

36. Lenivkin, V. A., Eliserv, M. M., Kastanaev, V. M., and Klenov, G. I., "Optimizing Metal Transfer Characteristics in Pulsed MIG Welding", Automatic Welding, 1975, No. 11, pp. 11-12.

37. Lenivkin, V. A., et al., "The Determination of Regions of Controllable Metal Transfer in Pulsed Arc Welding with a Consumable Electrode", Weld Production, 1976,

No. 12, pp. 10-14.

38. Tenenbaum, F. Z. et al., "Characteristics of the Pulsed-Arc Consumable Electrode Welding of Alloy AMg6 in the Inclined and Vertical Positions", Weld Production, 1973, No. 6, pp. 33-37.

39. Buchinskii, V. N. and Potapevskii, A. G., "Selecting the Parameters of the Welding Conditions for Pulsed-Arc Welding with a Consumable Electrode", Automatic Welding, No. 6, pp. 15-18, 25.

40. Eagar, T. W., Personal Communication with Hitachi Mechanical Engineering Research Laboratory, October 1980.

41. Eagar, T. W., Personal Communication with M. Tomsic of Hobart Brothers, Troy, Ohio, June 28, 1982.

42. Shimada, W. and Ukai, J., "Effects of Pulsed Current Control on Welding Quality Improvement", IIW Doc XII-B-11-81.

43. Ries, D. E. Personal Communication with M. Kobayashi of Matsushita Electric Industrial Company, Japan, April 29, 1983.

44. Amin M. and Watkins, P. V. C., "Synergic Pulse MIG Welding", The Welding Institute, Cambridge, England, August 1977.

45. Ries, D. E., Personal Communication with H. Lesher, President of Dimetrics, Inc., Diamond Springs, California, September 28, 1983.

46. "Preliminary Specification, Metal Beam Power Source and Servo Controls", Nu-Weld Division of Dimetrics, Inc., Diamond Springs, California, May 3, 1982.

47. Manual for 600 ADC Current Regulator MI-33, Alexander Kusko, Inc., Needham Heights, Massachusetts, May 1981.

48. Galler, D., Kusko, A., and Converti, J., "A Fast Response Transistor Current Regulator for Welding Research", a paper presented at IEEE-IAS 1981 Annual Meeting, Philadelphia, Pennsylvania, October 5-9, 1981.

49. Wolfe, R. J. et al., "Out-of-Chamber Welding of Ti-7Al-2Cb-1Ta Alloy Plate", Welding Journal, October 1965, pp. 443s-457s.

50. Hardy, R. R., "Developments in Navy RDT&E Program on Welding Thick Alloy Titanium", Report 3930, Naval Ship Research and Development Center, Bethesda, Maryland, September 1973.

51. Gurevich, S. M., Podola, V. N., and Tetervak, A. F., "The Pulsed Arc Welding of AT3 Titanium Alloy", Automatic Welding, 1966, No. 5, pp. 72-73.

52. Needham, J. C., Cooksey, C. J., and Millner, D. R., "Metal Transfer in Arc Welding", British Welding Journal, February 1960, pp. 102, 114.

53. Mantel, W., "On the Physics of Welding Arcs", Physics of the Welding Arc--A Symposium 1962, pp. 213-223.

54. Pattee, H. E., Anno, J. N., and Randall, M. D., "Theoretical and Experimental Study of Cathodic Cleaning with the Plasma Arc", Welding Journal, April 1968, pp. 181s-192s.

55. Thornton, J. A. and Munz, W., "Sputtering", ASM Metals Handbook, Vol. , pp. 412, 416.

56. Martukanitz, R. P. and Michnuk, P. R., "Sources of Porosity in Gas Metal Arc Welding of Aluminum", Aluminum, May 1982, pp. 276-279.

57. Benninghoven, A., "Development in Secondary Ion Mass Spectroscopy and Applications to Surface Studies", Surface Science, 53, 1975, pp. 596-625.

58. Strategy of Experimentation, E. I. duPont de Nemours & Co., Applied Technology Division, Wilmington, Delaware, 19898.

59. Ryan, T. A. Joiner, B. L. and Ryan, B. F., MINITAB Student Handbook, Duxbury Press, 1976.

60. Tsai, N., Heat Distribution and Weld Bead Geometry in Arc Welding, MIT Thesis, April 1983.

61. Antler, M., "Tribology of Metal Coatings for Electrical Contacts", Thin Solids Films, Vol. 87, 1981.

62. Antler, M., "Processes of Metal Transfer and Wear", Wear, Vol. 7, 1964.

63. Rice, S. L., et al., "Research and Development on Wear

of Materials", Conference paper, University of Connecticut, August 1980.

64. Mison, A., et al., "An Experimental Study of Three Body Abrasive Wear", Conference paper, University of California.

65. Zum Gahr, K. H., "Formation of Wear Debris in Abrasion", Institute of Mateials of Ruhr University of Bochum, West Germany.

66. Zum Ghar, K. H., "Formation of Wear Debris by the Abrasion of Ductile Metals", Weaar, Vol 74.

67. Rabinowicz, E., "Friction and Wear of Materials," MIT, Wiley, 1965.

68. Belyi, V. A., et al., "Some Aspects of the Friction and Wear of Sliding Electrical Contacts", Wear, Vol. 77, April 1982.

APPENDIX

An Experimental Study of the Wear of Welding Contact Tips*

In automatic welding, the need to make the process more efficient and thereby reduce the overall cost has imposed higher requirements on the components of welding equipment, including the components of the nozzle. The expected life of the welding nozzle in automatic and semiautomatic machines is extremely short, especially when using titanium wire. Therefore, studying the sliding contact system made up of the wire and nozzle tip may provide answers which will greatly improve system performance.

In the hot wire GTA process, current is pased through a contact tip to the filler wire to electrically heat it before it is fed into the welding arc created by a tungsten electrode. In the GMA process, the filler wire acts as the welding electrode and welding current is passed through a contact tip to the wire as it is fed into the weld joint. In both cases, the wire slides through a copper contact tip at about 200 to 300 inches per minute for wire sizes from 0.035 to 0.0625 inches in diameter.

---

* Taken from a paper by D. E. Ries, G. L. Cava and R. L. Steinberg, MIT, December 1982.

Recently, problems have been encountered at the Mare Island Naval Shipyard with excessive wear rates of contact tips used to weld thick titanium plates for the Seacliff Resarch Submersible. This Appendix will discuss the possible wear mechanisms that may be contributing to the excessive contact tip wear with titanium and will compare relative tip wear experienced with HY-80 steel and Ti-6Al-4V wires. Possible solutions to reduce or eliminate tip wear will be discussed.

Wear Mechanisms in Electrical Sliding Contact

The most significant factor affecting the reliability of any type of electrical contact current carryng device is sliding wear. Although many types of wear have been found in sliding electrical contacts, the processes of greatest importance are adhesion, abrasion, and fretting.

The direction of metal transfer in sliding of unlubricated surfaces and its relation to wear are also of considerable importance. The mechanism of wear is dominated by a process called prow formation and is characterized by separation of the surface by a built-up lump of work hardened particles which grow by continuous plastic shearing of larger members.

Adhesive Wear

Adhesive wear occurs when surfaces experience metal transfer. Adhesive bonds are formed between touching asperities which are stronger than the cohesive strength of the metals. This results in removal of particles which may be lost from the surface to which they transfered [61].

There exist two regimes of adhesive wear, either mild or severe. The two regimes are separated by a narrow range of loads known as the transition load. Below the transition zone, wear debris is finely divided and above the transition zone the wear debris is coarse.

Electrical contacts that wear by the severe adhesive process invariably exhibit evidence of prow formation. Figure 59 [62] is a schematic representation of the prow formation process. At the onset of rubbing, a lump of metal which originates in the flat forms between the rider and the flat. As sliding continues, the lump continues to grow and projects forward, prow-like, against the flat. The prow consists of severely work hardened metal which gouges the flat. The ploughed solid becomes attached to the prow so that it grows in length. Various processes cause the prow to break off as it becomes very long. The most prominent is welding of the prow to the flat.

There are two theories explaining the prow-formation mechanism [62]. The theories differ chiefly in the way they

explain the initial formation of the prow on the smaller of the two surfaces engaged in sliding. The first theory states that adhesion at the contact between the surfaces will distort the rider and the flat in opposite directions as they move (Figure 60a) [62]. Shearing takes place in the larger member at an angle to the surface. This causes metal to emerge from the flat, Figure 60b [62], creating the prow that grows against its direction of movement. The second theory predicts that minute particles are transferred from one member to the other at the initiation of sliding. The number of particles will be greater on the smaller part and will be held firmly together on the rider to create a prow.

A strong similarity in the two theories is that the mechanisms for both require severe work hardening of the prow material. Without this, the hard lump which ploughs the opposite member could not persist on the surface.

There are at least five conditions which must be satisfied in order for the prow formation mechanism to operate [62]:

1. Prow formation probably occurs only at severe sliding rates.

2. In order for particles from the flat to adhere to the rider and to each other to form a prow, there

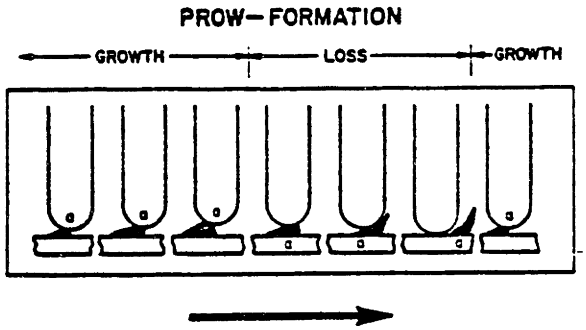

Figure 59: Schematic representation of prow formation. One of the processes by which rider loses prow, welding to flat, is shown. Letter "A" designates surface to which prow adheres [62].

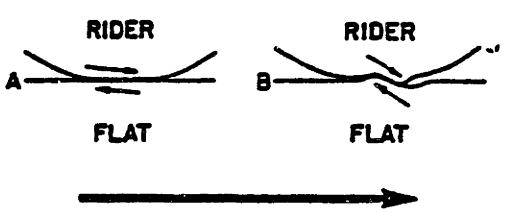

Figure 60: Schematic of one mechanism of prow initiation. A, initial contact; B, distortion of surfaces causes shearing to take place at an angle so that metal emerges from it to create a prow [62].

must be adhesion.

3. Metals do not form prows if they are sufficiently hard.

4. Annealing temperature of the rider specimen must be higher than that of the flat.

5. Transfer metal on the rider must be harder than the flat. For dissimilar metals, a harder rider on a soft flat will quickly convert to a sliding system of the soft metal and vice versa.

If the rider traverses the same track repeatedly, prow formation eventually ceases and is replaced by rider wear, a mechanism in which the small contact surface wears. This occurs primarily by transfer to the flat with some loose particle formation (in rider wear the flat gains mass rapidly). The transition from prow formation to rider wear is due to the accumulation of sufficient back-transfer prows on the flat. When the surface of the flat reaches the hardness of the prows, routing of the flat ceases and rider wear begins.

There are several additional ideas that should also be considered in the analysis of adhesive wear including:

1. There is a distinction between initial properties and those established in near surface zones during wear.

2. Surface properties differ from bulk properties, often quite significantly.

3. Both rider properties and flat properties must be considered.

In the analysis of wear tests in Reference 63 there was shown to exist characteristic subsurface deformation zones. The area that is furthest from the contact region (zone 1) consists of essentially undisturbed base metal. The intermediate region (zone 2), is plastically deformed, and the region containing the surface contact (zone 3) is usually homogeneous and very finely structured. The extent of cyclic stain accumulation is from zero at the zone 1-zone 2 interface to a maximum at the zone 2-zone 3 interface. Both disintegration and reorientation of crystal structure are usually observed as the zone 2-zone 3 interface is approached from the zone 2 side. In some cases there exists observable subsurface cracking in zone 2 in contact with a very thin zone 3, to suggest that delamination has occurred.

Abrasive Wear

Generally, abrasive wear of a surface is defined as material removal due to sliding contact with abrasive particles or a rough surface. Abrasive wear can be divided into two categories, two body and three body abrasive wear. Two body abrasive wear occurs when a rough surface or fixed abrasive particles slide across a surface to remove material. In three body abrasive wear, the particles are loose while sliding across the wearing surface. Three body abrasive wear can be further divided into two groups, closed or open three body abrasive wear. Closed three body abrasive wear occurs when loose abrasive particles are trapped between the two surfaces, while open three body wear occurs when the two surfaces are far apart or when only one surface is involved in the wear process [64].

The cause of abrasion is due to the displacement of material from surfaces in relative motion by the pressure of hard protuberances or hard particles, either between the surfaces or imbedded in them [65]. High elastic deformation causes cracking to occur below and in front of the abrasive particle. Wear debris is finally formed by shearing and/or crack formation and crack propagation. The ratio of the hardness of the abrasive particles to the hardness of the abraded material influences the wear rate. It has been

observed that abrasive wear rate decreases as hardness increases.

The mechanism of decohesion of wear debris is a function of type of abrasive particle, applied surface pressure and properties of the abraded material. There are three different mechanisms of decohesion of wear debris due to abrasion. They are microplowing, microcutting, and spalling [66]. In ductile materials, microplowing and microcutting are the dominant wear mechanisms.

Ductile materials are plastically deformed by microplowing action and only a small portion of the wear volume of wear grooves produced is immediately removed as debris from the worn surface. Pure microcutting results in volume loss equal to the volume of the wear grooves.

Theoretical and experimental work shows that decohesion of wear debris depends on the angle of attack between the leading face of the abrasive particles and the surface of the material. Material is detached by microcutting if the angle of attack exceeds a critical value which can be determined from the coefficient of friction.

Flow pressure together with work hardening determine the contact area between an abrasive particle and the materials to be worn. During abrasion, material work hardening is related to crystal defects caused by plastic deformation. The maximum flow pressure depends on the interaction of

dislocations with crystal defects, crystal structure, anisotropy and structural changes. The influence of texture has to be considered in crystal structures with a limited number of slip systems. Thin wear sheets elongated in the sliding direction are frequently formed during sliding between two surfaces and can be explained by delamination due to plastic deformation of surface layers, crack nucleation and crack propagation. Electron microscopy has shown that cellular dislocation structures developed in deformed surface layers of the worn materials [66]. Cell sizes are dependent upon the stressed properties of the material and promote the development of subsurface cracks.

Fretting

Fretting wear is the result of small amplitude oscillatory movement when mated contacts are subjected to vibration or other mechanical deflections. Wear debris accumulates between the contacts rather than being freely discharged because contact motion is limited. The wear debris from the base metal contain products of reaction with the environment such as oxides which may cause fretting corrosion. These oxide debris center around the periphery of the wear scar and substantially increases the contact resistance [67].

Effectiveness of Lubrication

The problem of improving the reliabiity of light current low speed sliding contacts and heavy current high speed sliding contacts is very complex [68].

Improvements in the wear resistance and in durability by applying hard coatings usually has a deleterious effect on the electromechanical characteristics of the contacts or increases the cost of the unit beyond reason when noble metals are used.

While lubricants have been used successfully in sliding contact, it is difficult to develop suitable lubricants for electrical contacts because their effect on current flow and wear behavior is not fully understood. The selection of lubricants for electrical sliding contacts depends on the working conditions and on the nature of the current flow. The friction and wear of light current low speed sliding contacts depends mainly on the lubricating action. For heavy current sliding contacts, the conductivity of the lubricant is important, especially at high speeds when hydrodynamic effects and electrical discharges occur. In the welding application, the lubricant may represent a contaminant which could adversely affect the quality of the weld. Titanium welds in particular are especially intolerant of any contamination, however minute.

Examination of Specimens and Calculations

Samples of worn hot wire GTA and GMA welding contact tips were obtained from Mare Island Naval Shipyard Welding Engineering Department. Tips are shown in Figure 61 with tip dimensions and wire sizes listed. All samples were machined to expose the contact tip channel at the tip and shank regions. Details of the sectioning are included in Figure 61.

Samples were then examined using a scanning electron microscope (SEM) for wear damage in the tip and shank regions. Energy dispersive analysis with x-rays (EDAX) was performed in the areas of interest to identify wear particles on the copper tip surface. Two samples included welding wire which had burned back and fused to the tip of the contact tube. These wires were carefully machined free of the contact tip and then examined for transferred wear particles under the SEM.

Typical SEM and EDAX analysis results of tip samples used for GMA welding of HY-80 steel and titanium are shown in Figures 62 to 76 at the end of this Appendix. Wear track width and transferred wear particle sizes were also recorded. Hardness tests were then performed on each sample near the tip region where the most severe wear occurred. Results of the hardness tests are included in Table 1.

Loads encountered in sliding the wire through the

SAMPLE TYPE A, B, C

MIG PROCESS

STEEL HY-80 WIRE

0.045 INCH DIAM

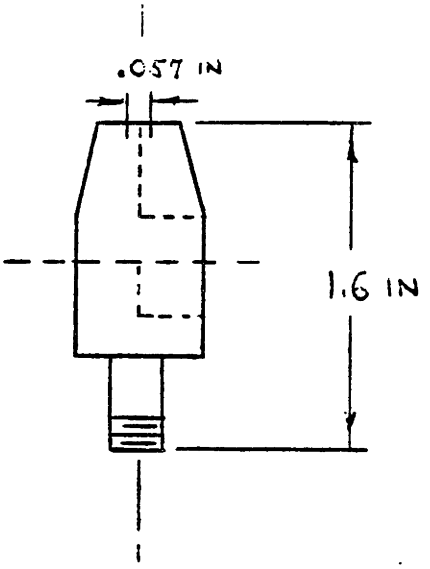

SAMPLE TYPE D

MIG PROCESS

STEEL HY-80 WIRE

1/16 INCH DIAM

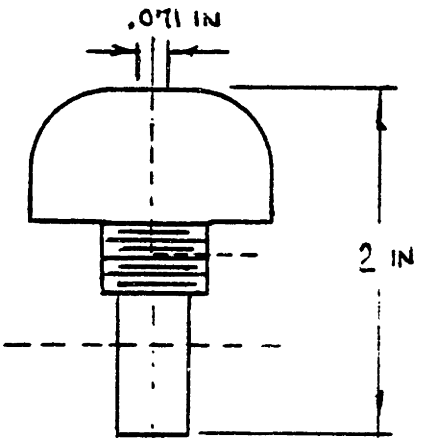

SAMPLE TYPE E

HOT WIRE TIG PROCESS

STEEL HY-80 WIRE

1/16 INCH DIAM

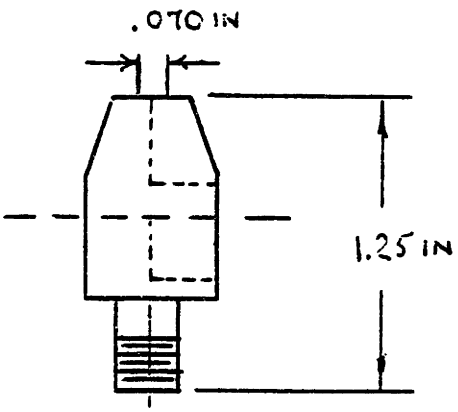

Figure 61: Contact tip dimensions and wire sizes.

SAMPLE TYPE F, G, H

HOT WIRE TIG PROCESS

TI-6AL-4V WIRE

1/16 INCH DIAM

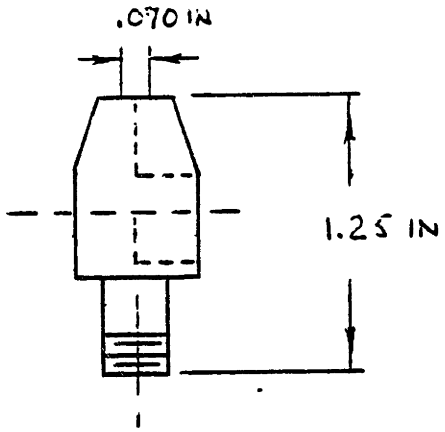

SAMPLE TYPE J, K

MIG PROCESS

TI-6AL-4V WIRE

1/16 INCH DIAM

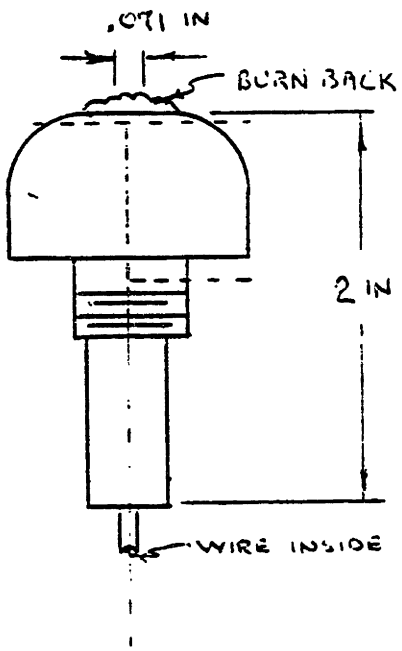

---------- Denotes lines of sectioning

Figure 61: Contact tip dimensions and wire sizes.

Table 1

SUMMARY OF CALCULATED AND MEASURED WEAR VALUES

SAMPLE ---->	A	B	C
HARDNESS, KG/MM^2	45.3	119.9	76.5
CALCULATED VALUES			
DV/DT (CU), MM^3/MIN	0.187	0.071	0.110
%RED. IF CU-BE USED	88.2	69.0	80.0
TIP LIFE (CU), MIN	<--------	39.7	-------->
TIP LIFE INCREASE, % IF CU-BE TIP USED	<--------	374.1	-------->
DMIN, MM	0.020	0.008	0.012
DAV, MM	0.061	0.023	0.036
DMAX, MM	0.183	0.069	0.110
D(ADHERENT), MM	0.058	0.022	0.035
L(ADHERENT), MM	0.099	0.037	0.059
LMIN, GRAMS	31.9	12.1	18.9
LACTUAL, GRAMS	<--------	2,497	-------->
MEASURED VALUES			
D (WEAR TRACK), MM	0.010 0.040	0.005 0.018	0.005 0.018
D (WEAR PARTICLE), MM	0.005 0.026	0.005 0.012	0.009 0.018
D (MELTED PARTICLE), MM	0.005 0.010	0.003 0.020	0.007 0.030

Table 1 (continued)

SAMPLE --------->	D	E	F
HARDNESS, KG/MM^2	93.5	100.7	89.0
	CALCULATED VALUES		
DV/DT (CU), MM^3/MIN	0.166	0.126	0.065
% RED IF CU-BE USED	75.3	88.1	76.1
TIP LIFE (CU), MIN	31.4	113.6	113.6
TIP LIFE INCREASE, % IF CU-BE TIP USED	308.6	265.9	265.9
DMIN, MM	0.010	0.006	0.007
DAV, MM	0.030	0.019	0.021
DMAX, MM	0.087	0.056	0.064
D(ADHERENT), MM	0.028	0.026	0.029
L(ADHERENT), MM	0.048	0.045	0.050
LMIN, GRAMS	15.5	9.8	11.1
LACTUAL, GRAMS	4,585	20,066.8	20,066.8
	MEASURED VALUES		
D (WEAR TRACK), MM	0.005 0.010	----- -----	0.004 0.026
D (WEAR PARTICLE), MM	0.003 0.005	----- -----	0.005 0.030
D (MELTED PARTICLE), MM	0.005 0.017	----- -----	0.003 0.010

Table 1 (continued)

SAMPLE ---------->	G	H	J	K
HARDNESS, KG/MM^2	111.0	117.0	90.6	56.4
	CALCULATED VALUES			
DV/DT (CU), MM^3/MIN	0.052	0.049	0.008	0.013
% RED IF CU-BE USED	71.1	69.4	75.0	84.6
TIP LIFE (CU), MIN	113.6	113.6	101.7	101.7
TIP LIFE INCREASE, % IF CU-BE TIP USED	265.9	265.9	419.8	419.8
DMIN, MM	0.006	0.005	0.007	0.011
DAV, MM	0.017	0.016	0.020	0.034
DMAX, MM	0.051	0.049	0.059	0.101
D(ADHERENT), MM	0.024	0.023	0.028	0.047
L(ADHERENT), MM	0.040	0.038	0.047	0.080
LMIN, GRAMS	8.9	8.5	10.3	17.5
LACTUAL, GRAMS	20066.8	20066.8	2524	2524
	MEASURED VALUES			
D(WEAR TRACK), MM	0.001 0.002	0.003 0.010	0.001 0.002	0.007 0.012
D(WEAR PARTICLE), MM	0.001 0.003	0.005 0.015	0.010 0.020	0.010 0.040
D(MELTED PARTICLE)	0.011 0.060	0.010 0.020	0.010 0.100	0.010 0.020
D(ADHERENT PARTICLE), MM	----- -----	----- -----	0.002 0.010	0.005 0.010

contact tip due to wire camber were calculated and wear rates were estimated for each sample using Archard's equation and measured hardness values as follows:

$$V = KLX/3P$$

where:

V = wear volume

K = wear coefficient

L = load

X = distance of sliding

P = hardness

A sumary of all calculated values of wear rate, tip life and wear particle size, as well as measured values of wear track and particle size, are included in Table 1. A summary of mechanical and physical properties of the materials in this study is included in Table 2. Wear rate and tip life values were also calculated for contact tips made of full hard (condition HT) copper beryllium alloy (Cu-Be) and these values are included in Table 1 with appropriate mechanical and physical properties in Table 2.

Conclusions Regarding Wear Mechanism

The following conclusions were made concerning the wear mechanism in copper welding contact tips based on

Table 2

MECHANICAL AND PHYSICAL PROPERTIES

MATERIAL --->	CU ETP	CU-BE	TI-6AL-4V	HY-80
SHEAR STRENGTH PSI	27 K			
ULTIMATE TENSILE STRENGTH, PSI	48 K	A, 75 K 135 K H, 100 K AT, 175 K HT, 195 K		
YIELD STRENGTH PSI	44 K		130 K	80 K
		AT, 130 K HT, 150 K		
HARDNESS, ROCKWELL	F87	A B45-85 H B88-103 AT C37	B90	D43
		HT C41		
HARDNESS, KG/MM^2	86	A 79-82 H89-128 AT 342 HT 382		
DENSITY, G/CM^3	8.89	8.23	4.43	
T(MP), °C	1065	1535		
RESISTIVITY, Ω cm	1.71	9.6-11.5	170-190	9.7-12.0
GAMMA, DYNE/CM		1100	1000	1200

calculations and SEM examinations of actual worn tips:

1. Adhesive wear in the form of plowing and delamination apears to control the wear of the tip in the regions away from the tip end. Abrasive wear due to extraneous particles like sand, and fretting wear do not appear to be controllinng factors in wear rate.

2. Melting of wear particles and spatter from the weld pool collect at the tip end region. These melted globules build up on the tip end and break off, causing severe material loss at the tip end. This material loss will increase tip resistance and thus increase I^2R heating, creating more melting of copper wear particles and softening of the tip. This condition probably leads to fast degradation of contact tip performance. It is noted that about 5% copper in titanium forms a low melting point eutectic ($800^{o}C$). This low melting point eutectic may form on titanium wire surfaces near the contact tip end contributing to liquid metal erosion of the tip end region.

3. Some tips appear softer at the tip end. This is

probably due to the annealing effect from arc heat and I^2R heating due to increased clearance at the tip end due to wear. Softer tips showed more severe wear in the SEM examinations.

4. Calculated wear particle size agrees well with observed wear particle size and wear track widths. Calculated sliding loads exceed the minimum sliding loads to produce wear particles by several orders of magnitude (see Table 1).

5. Estimated tip wear rates for steel wire are higher than for titanium wire. This is contrary to experience, which shows higher wear rates and shorter tip life for titanium wire. This may be due to the fact that with steel wire, wire rsistance is low and close to that of the copper tip (see Table 2), which may allow for greater wear and thus greater resistance due to wire/tip clearance. With titanium wire, wire resistance is much higher and thus smaller resistance due to the wire/tip clearance can be tolerated before I^2R heating causes wire feed instabilities and possible local melting or burn back at the tip end in GMA welding.

Possible Solutions

The following items are considered possible solutions for excessive weld contact tip wear:

1. Water cooling of welding contact tip should minimize tip softening due to annealing from I^2R heating and arc heat and reduce build up of melted particles at the tip end.

2. Use of copper beryllium alloy in the full hard condition (HT) will reduce wear rates by about 60 to 80% and increase tip life by about 200 to 400% (see Table 1). This precipitation hardened material is much harder than electrical grade copper and retains its strength and hardness at higher temperatures.

3. The use of better weld filler wire straighteners in the wire feed system should reduce wire camber and thus the load in the contact tip. This reduction in load should reduce wear rates in direct proportion to the load reduction, according to Archard's equation.

4. When possible, the use of soft solid film lubricants on the wire should reduce wear rates by covering over rough asperities on the wire that would normally cause plowing of the copper tip surface. This is not possible with titanium wire due to unacceptable effects of coating materials on weld mechanical properties. However, this should work with steel wire, as evidenced by the wide spread use of commercial copper coated steel wire.

5. The use of tungsten carbide inserts at the tip end should reduce excessive tip end wear due to tip annealing and wear particle formation. The cost of tips may then be balanced by reduced start/stop costs to change tips. Carbide tip inserts would cause wear of the wire, but this is of little consequence since it is consumed in the weld, and makes only one pass through the tip.

6. The use of coating mateials on contact tip surfaces which prevent the formation of low melting point eutectics, as can occur with titanium wire in copper tips, should reduce or eliminate the liquid metal erosion of the contact tip end. Silver does not form such a eutectic with titanium and can easily be plated on the copper contact tip surface.

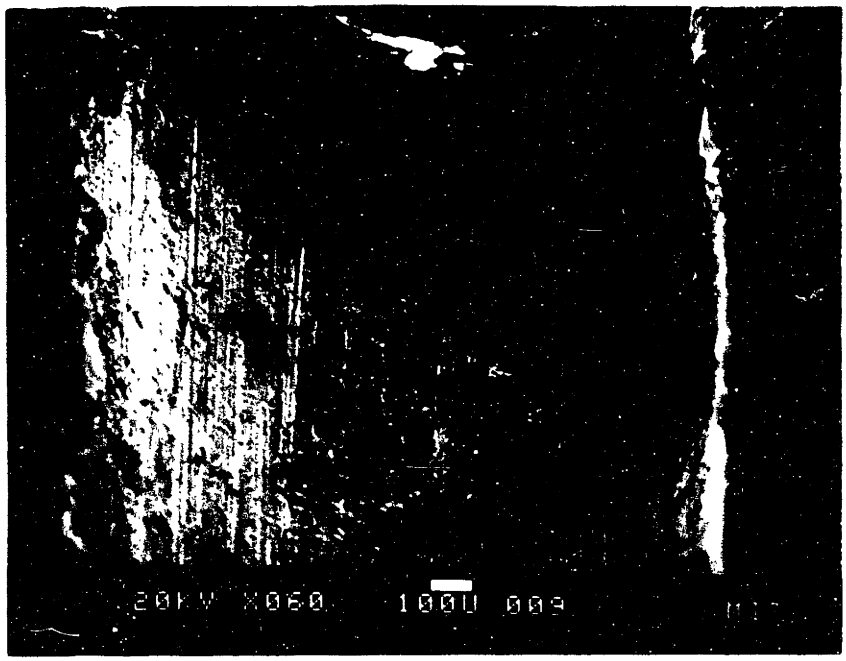

Figure 62: Tip region of sample A

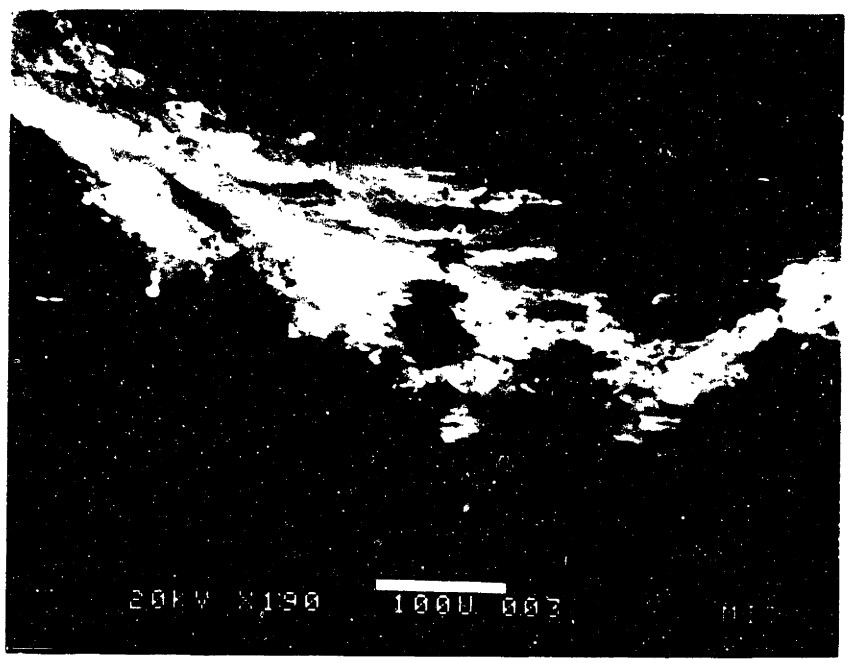

Figure 63: Tip region of sample A. Severe deterioration of tip end is shown including longitudinal crack. White areas are reflective, i.e., non-conductive material.

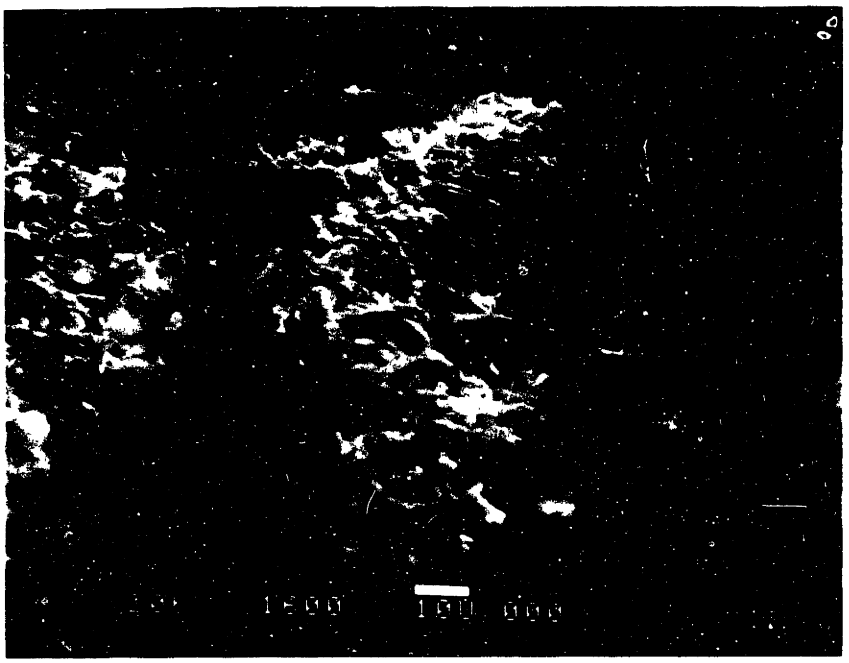

Figure 64: Root of longitudinal crack shown in Figure 63.

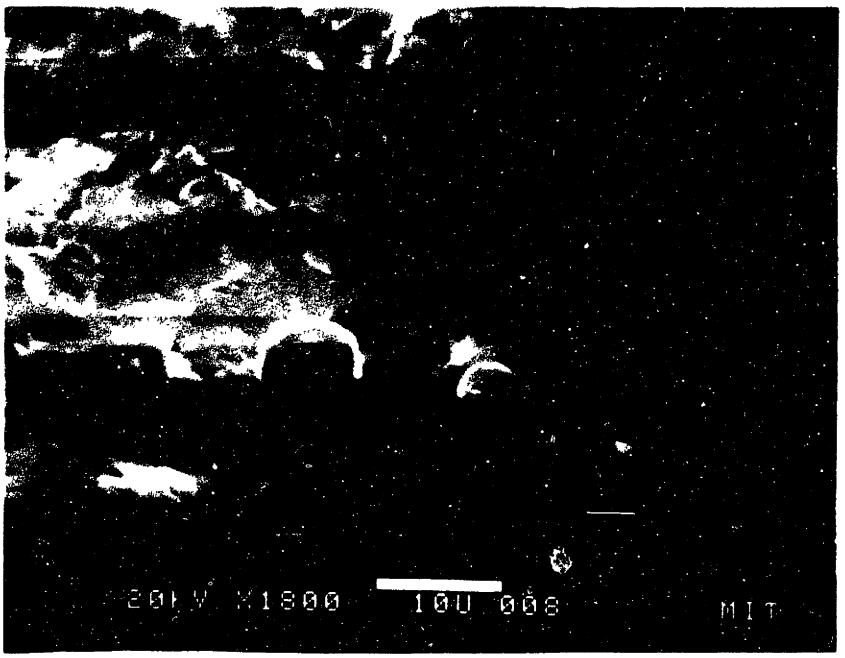

Figure 65: Tip end of sample A. Spherical particles are melted globules of iron.

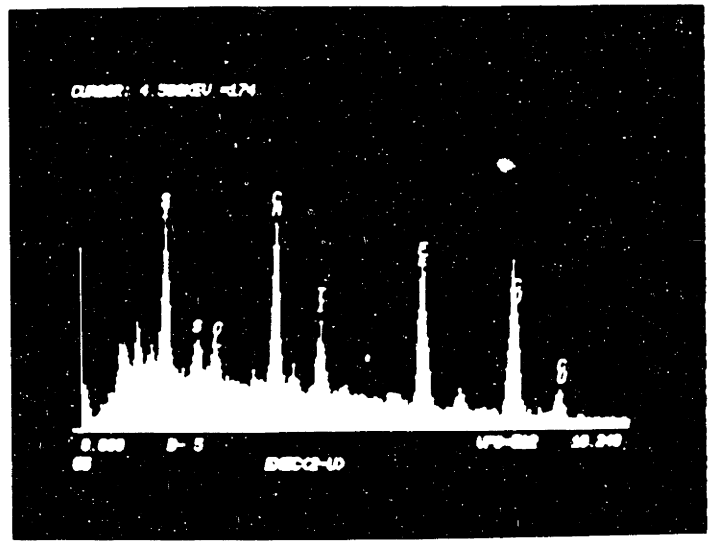

Figure 66: EDAX scan of Figure 65 identifies spherical particles as iron, reflective materials as oxides of silicon, calcium.

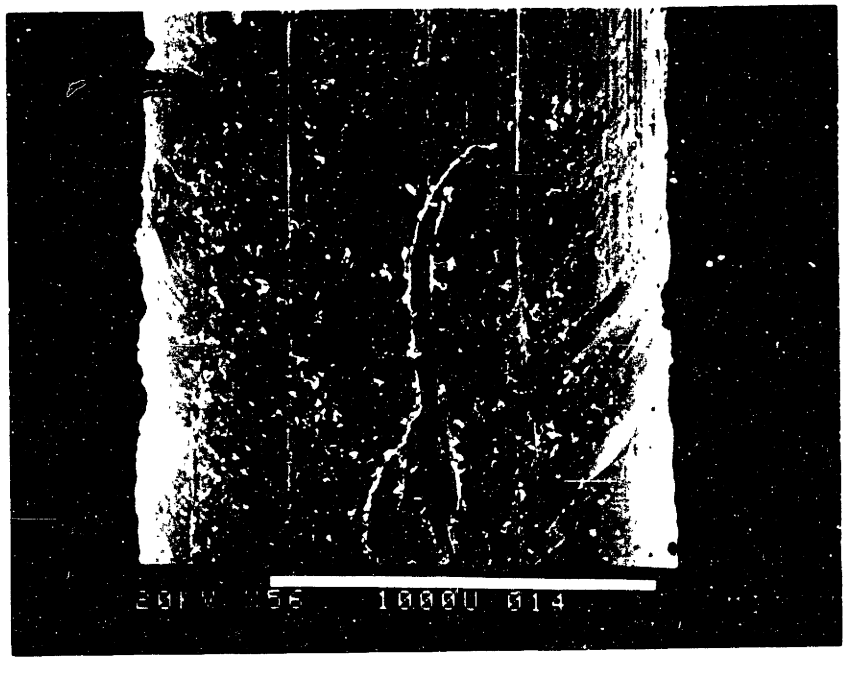

Figure 67: Shank end of sample A. Wear not as severe as ti[illegible] Large smeared copper particle.

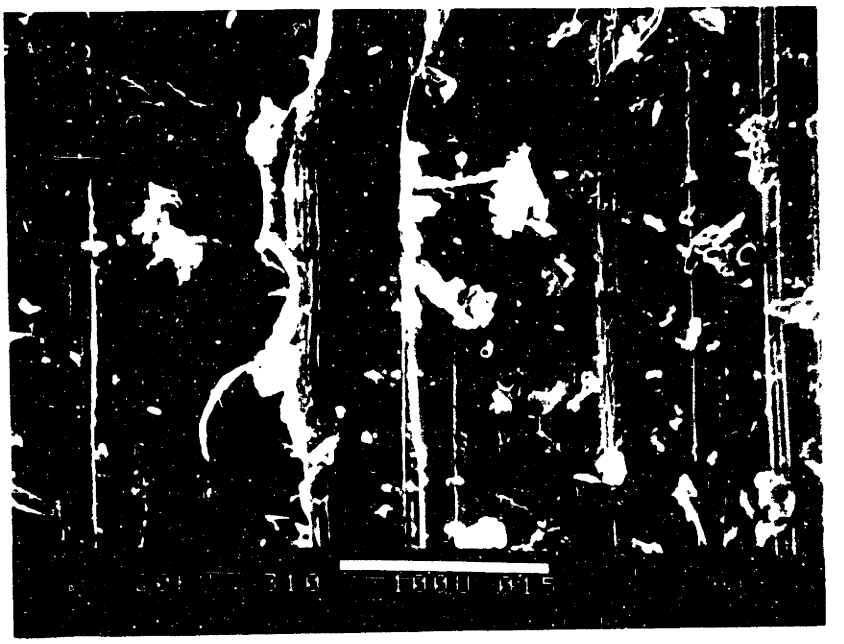

Figure 68: Shank end of sample A. Loose white particles are non-conductive oxides of silicon, calcium. Large smeared particle is copper, possibly a chip from manufacturing which broke loose and was dragged by the wire ar some time during use.

Figure 69: Copper particles on surface of titanium wire removed from Tip J.

Figure 70: Extremely high magnification (6000x) photo of particles found on titanium wire removed from Tip J.

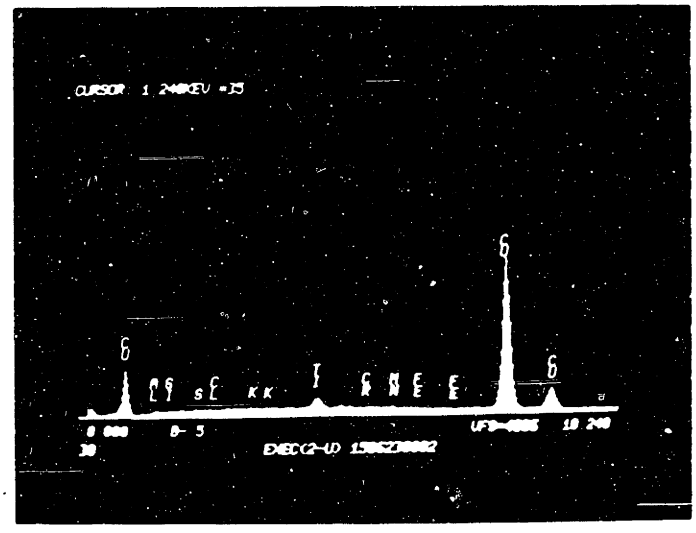

Figure 71: EDAX scan of particle shown in Figure 76 identifying as copper.

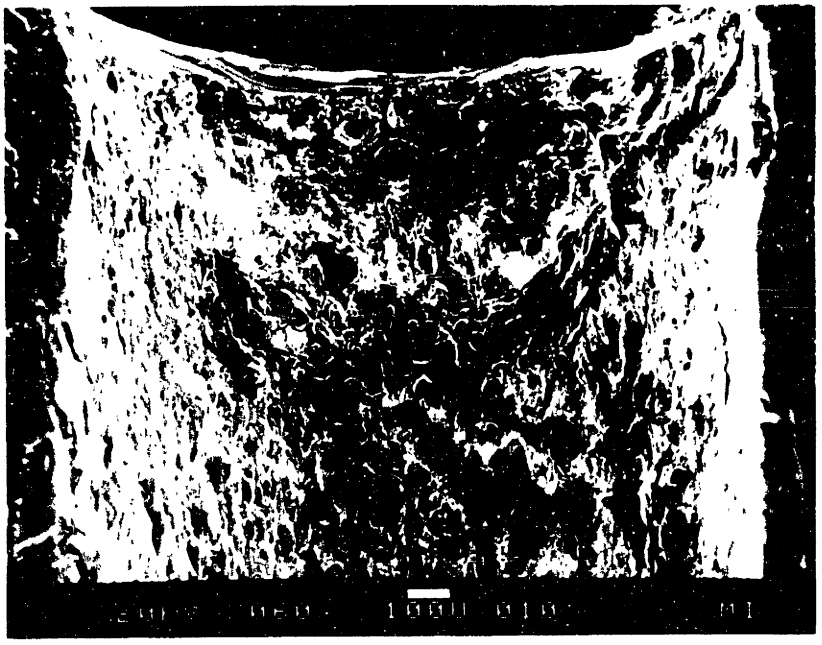

Figure 72: Tip of sample J, showing gross melting from wire burn back.

Figure 73: High power (1200x) photo of melted material at tip of sample J.

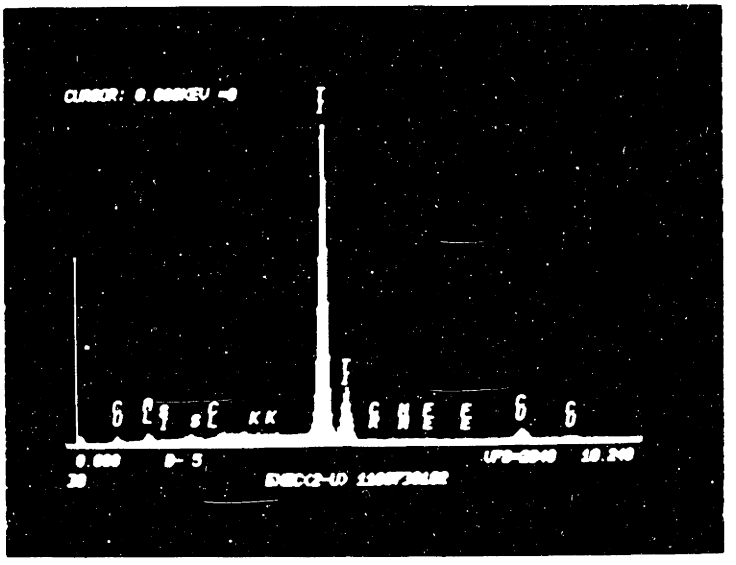

Figure . EDAX scan of melted material at tip of sample, identifying as titanium.

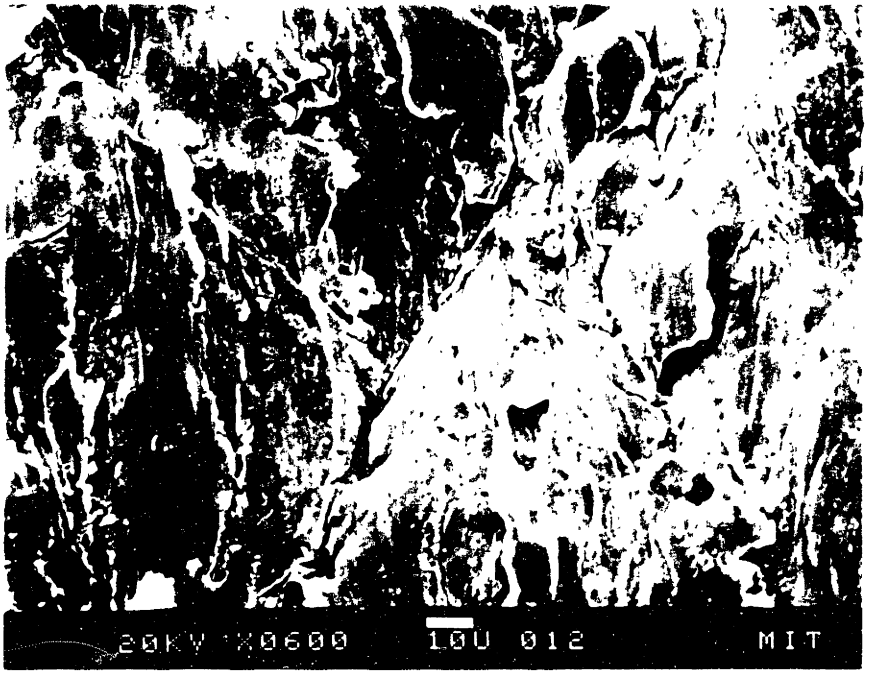

Figure 15 Droplets of titanium formed [illegible]

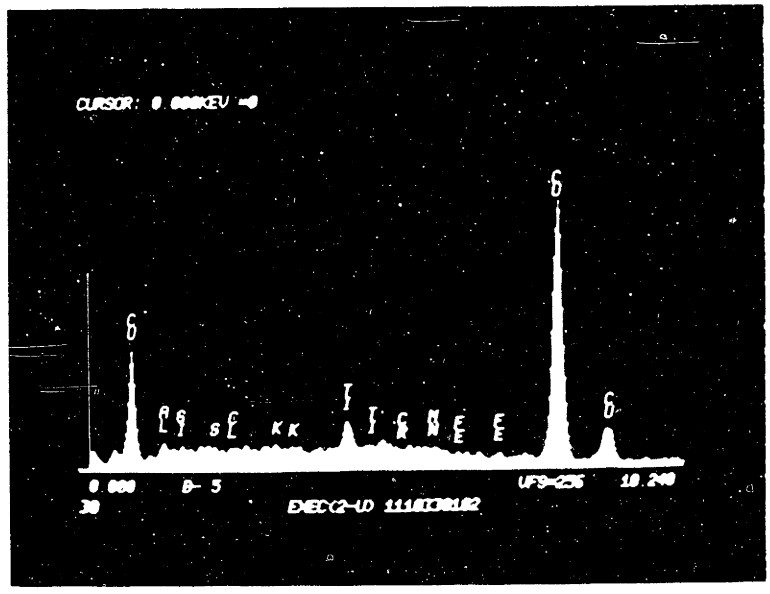

Figure 76: EXAX Scan of Figure 75.